

國立交通大學

生醫工程研究所

碩 士 論 文

The logo of National Central University (NCU) is a circular emblem with a gear-like border. Inside the circle, there is a stylized building and the year '1896' at the bottom. The text '腦部結構差異量化分析之
區塊多變量型態法' is overlaid on the logo.

腦部結構差異量化分析之
區塊多變量型態法

Parcellation-based Multivariate Morphometry for
Characterizing Differences of Brain Structures

研 究 生：林育宏

指 導 教 授：陳永昇 教授

中 華 民 國 九 十 八 年 六 月



腦部結構差異量化分析之區塊多變量型態法

Parcellation-based Multivariate Morphometry for Characterizing
Differences of Brain Structures

研究生：林育宏

Student：Yu-Hung Lin

指導教授：陳永昇

Advisor：Yong-Sheng Chen

國立交通大學
生醫工程研究所
碩士論文



Submitted to Institute of Biomedical Engineering

College of Computer Science

National Chiao Tung University

in partial Fulfillment of the Requirements

for the Degree of

Master

in

Computer Science

June 2009

Hsinchu, Taiwan, Republic of China

中華民國九十八年六月



摘要

磁振造影已經成為主要的醫療成像技術，用於了解腦部或是身體上的結構以及功能，它不僅廣泛應用於臨床診斷，而且在神經影像學研究。近年來，以體素為基礎的形態計量學 (voxel-based morphometry, VBM) 最常被使用於研究分析群體間大腦結構的差異性，以比較每一個體素的方式來找出其差異性。VBM 以統計的方式量化分析群組間的差異性，這個以體素為基礎的分析方法有能力上的限制，導致它無法偵測群組織間細微的變化。根據我們的經驗指出，同時地將所有的體素一起做分析會使區域間不相關的體素相互影響，這樣的分析方法是不恰當的。

本研究中我們提出了一個新的腦部結構分析方法，以區域為單位的多變量形態計量學方法，可用於偵測群組間腦部結構的差異性。與體素為基礎的分析方法相比較之下，我們提出的方法是同時考慮一個區域下所有的體素以多變量的方式來分析群組間腦部結構的差異性，而最重要的是我們將腦部結構區分成許多個小區域，藉此達到在相同區域下的所有體素有相同的關聯性。多變量的方法是採用線性鑑別度分析 (linear discriminant analysis, LDA) 是用來找出對於群組間結構差異性最具鑑別力的投影軸。位於該投影軸上的每一元素代表相對映體素具有的差異性鑑別能力。此鑑別能力可以視為用來評估影像群組間每一體素結構差異之程度等級 (significance level)。

我們的實驗方法包含了兩個部分，第一個部分是透過模擬一個區域的萎縮，用來驗證以區域為單位的多變量形態計量法的效能，另一個是應用在重性抑鬱障礙 (Major depressive disorder) 以及雙極性情感疾病 (Bipolar disorder) 的腦部結構分析。透過比較可以了解，以區域為單位的多變量形態計量法確實可偵測到群組間較細微的腦部結構差異。而此方法也比以體素為基礎的形態計量法更明顯地找出和病理上相關的腦部結構差異。

總結，我們提出了一個新的腦部結構分析方法，這個方法是以區域為單位的分析群組間的差異，而且所採用的多變量方法不會有資訊上的遺失，在分析時能更用更多的資訊更有效地分析腦部結構細微的差異性。



誌謝

感謝陳永昇老師和陳麗芬老師兩年的辛苦指導，老師在碩一時總是鼓勵我們認真的修課，希望我們不要因為研究進度而不認真修課，讓我們在碩一時學到了很多，在碩二的時候便要求我們認真的做研究，讓我們學習做研究的過程。還有每到寒暑假以及年終實驗室也會舉辦許許多多有趣的活動，不管是出遊還是尾牙大家都很開心的玩在一起，研究所這兩年有老師的指導我很珍惜。

也要感謝我身邊的朋友和實驗室同學，不論是一起打球、跑步、吃好料，唱歌還是一起上課、玩遊戲，有你們的陪伴，讓我度過了快樂的兩年。

最後要感謝我的家人還有我的女朋友，因為你們的照顧以及不時的給我信心，還有給了我許多寫作上的建議，以完成我的碩士論文順利畢業，我很感激，謝謝你們。



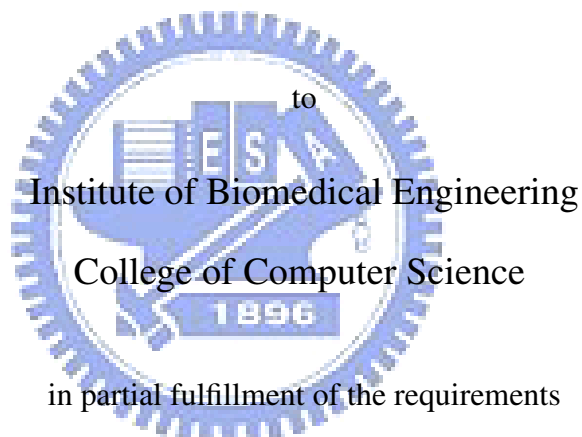


Parcellation-based Multivariate Morphometry for Characterizing Differences of Brain Structures

A thesis presented

by

Yu-Hung Lin



to
Institute of Biomedical Engineering
College of Computer Science

in partial fulfillment of the requirements

for the degree of

Master

in the subject of

Computer Science

National Chiao Tung University

Hsinchu, Taiwan

2009

**Parcellation-based Multivariate Morphometry for Characterizing Differences of
Brain Structures**

Copyright © 2009

by

Yu-Hung Lin



Abstract

Magnetic resonance imaging (MRI) has become primarily a medical imaging technique to visualize the structure and function of the body or brain. It is widely used not only in clinical diagnosis but also in neuroimaging research. In recent years, voxel-based morphometry (VBM) is one of the most popular technique for the analysis of structural brain discrepancy between different subject groups, in a voxel-wise manner. VBM analysis detects group differences by voxel-wise statistics comparisons which have limited power to identify subtle differences between two populations. And according to our experience, we figure out that when dealing with all features simultaneously, features in different regions of whole brain may be unrelated with each other it is incorrect that we take all features into consideration at one time.

In this work, we propose a parcellation-based multivariate morphometry method which can be used to detect the anatomical discrepancy in brain between two groups. Compared to the voxel-wise manner in VBM, the proposed method detects brain discrepancy in a multivariate manner by simultaneously taking all voxels within an area (or a region) in consideration. The most important idea is that we divide brain into several parts when analyzing such that all features in the same region may be correlated with each other. Linear discriminant analysis (LDA) is used to determine the most discriminant projection vector, also called a discriminant map separating two populations. Each parameter of the most discriminant vector represents the discrimination level of each voxel. That is, based on the discriminant map, each parameter stands for a significant level with each voxel.

To demonstrate the performance of the parcellation-based multivariate method, we carried out experiments by using the simulation data set and on a real medical data composed of MRI of subjects with major depressive disorder (MDD) and bipolar disorder (BD). The results with simulation data analysis have shown that the parcellation-based multivariate method has a better performance than VBM from the area under the ROC curve by comparing to VBM method. The results with real data analysis have also shown that our proposed method reveals several important findings.

In conclusion, we have proposed a parcellation-based multivariate method for characterizing group differences. And all voxels within the same region are simultaneously taken

into consideration. Moreover, our proposed method uses no feature reduction within analysis thus no information is lost. Our proposed method have shown that the parcellation-based multivariate morphometry analysis has a good performance on subtle and widely-distributed structural difference and it is more flexible within analysis.



Contents

List of Figures	xi
List of Tables	xiii
1 Introduction	1
1.1 Background	2
1.1.1 Brain Structures	2
1.1.2 Magnetic Resonance Imaging (MRI)	6
1.2 Morphometrics	8
1.3 Thesis Motivation	10
1.4 Related Works	11
1.5 Thesis Organization	13
2 Voxel-based Morphometry	15
2.1 Introduction	16
2.2 Optimized VBM Protocol	20
2.3 Implementation of VBM	24
2.4 Drawbacks of VBM	29
3 Parcellation-Based Multivariate Morphometry	31
3.1 Introduction	32
3.2 Framework of Parcellation-Based Multivariate Morphometry	33
3.3 Multivariate Analysis using a Modified LDA-Based Method	37
3.3.1 Conventional Linear Discriminant Analysis and Its Potential Problem	37
3.3.2 Discriminative Common Vector Method	40
3.3.3 The Problem of Combining The Unit Projection Vector	43
4 Experiment Results	45
4.1 Simulation Analysis	46
4.1.1 Simulation Data Generation	46
4.1.2 Accuracy Evaluation	47
4.1.3 Comparisons of Proposed Method and VBM	51

4.2	Real Data Analysis	54
4.2.1	Materials	54
4.2.2	MRI acquisition	54
4.2.3	Results and Comparisons of PBM and VBM	55
5	Discussion	83
5.1	Using the Parcellation-Based Approach	84
5.2	Different Size of Each Region	84
5.3	Limitations of the Atrophy Simulation Package	85
5.4	Why the Smoothing is Eliminated	86
6	Conclusions	89
	Bibliography	93



List of Figures

1.1	Brain structures	3
1.2	MR image	4
1.3	Brodmann map	5
1.4	MR scanner	7
2.1	Flowchart of standard VBM protocol	17
2.2	Concept of the spatial normalization	18
2.3	The segmentation	19
2.4	Flowchart of optimized VBM protocol	21
2.5	Concept of the modulation	23
2.6	Flowchart of VBM implementation	25
2.7	Bias correction	26
2.8	Brain extraction	27
2.9	Schematic scatterplots illustrating of significant bias of VBM	29
3.1	Schematic of the Anatomical Automatic Labeling template	34
3.2	Concept of the relation between projection vector with each standard bases	35
3.3	Flowchart of parcellation-based multivariate morphometry without prepro- cessing steps	38
4.1	The simulated atrophy images	48
4.2	Example of a ROC curve	51
4.3	ROC curves of PBM and VBM results with the atrophy scale from $1mm$ to $4mm$, $6mm$ and $8mm$	52
4.4	Concept of choosing a compatible threshold of PBM by t -test map of VBM analysis result.	56
4.5	Statistics t value within each region in MDD patients by PBM analysis method	57
4.6	Volumetric atrophy of gray matter in MDD patients by PBM analysis method	59
4.7	Volumetric atrophy of gray matter in MDD patients by VBM analysis method	63
4.8	Volumetric atrophy of gray matter in MDD patients by PBM and VBM analysis method	65

4.9	Statistics t value within each region in BD2 patients by PBM analysis method	66
4.10	Volumetric atrophy of gray matter in BD2 patients by PBM analysis method	68
4.11	Volumetric atrophy of gray matter in BD2 patients by VBM analysis method	71
4.12	Volumetric atrophy of gray matter in BD2 patients by PBM and VBM analysis method	73
4.13	Statistics t value within each region in BD1 patients by PBM analysis method	74
4.14	Volumetric atrophy of gray matter in BD1 patients by PBM analysis method	75
4.15	Volumetric atrophy of gray matter in BD1 patients by VBM analysis method	77
4.16	Volumetric atrophy of gray matter in BD1 patients by PBM and VBM analysis method	78



List of Tables

4.1	Definitions of TP, FP, TN, and FN	49
4.2	PAUC indices for ROC curves of parcellation-based multivariate morphometry (PBM) and VBM results with the simulation data	53
4.3	Clinical data of each groups	54
4.4	Statistics t value within each region in MDD patients by PBM analysis method	58
4.5	Atrophy of gray matter in MDD patients by PBM analysis method	60
4.6	Atrophy of gray matter in MDD patients by VBM analysis method	64
4.7	Statistics t value within each region in BD2 patients by PBM analysis method	67
4.8	Atrophy of gray matter in BD2 patients by PBM analysis method	69
4.9	Atrophy of gray matter in BD2 patients by VBM analysis method	72
4.10	Statistics t value within each region in BD1 patients by PBM analysis method	79
4.11	Atrophy of gray matter in BD1 patients by PBM analysis method	80
4.12	Atrophy of gray matter in BD1 patients by VBM analysis method	81



Chapter 1

Introduction



1.1 Background

1.1.1 Brain Structures

Human brain is the center of the human nervous system and can be extremely complex. It plays an important role in controlling human behavior, emotion and it regulates involuntary activities such as breathing and heartbeat, it also has been estimated to contain 50 ~ 100 billion neurons, of which about 10 billion are cortical pyramidal cells. The function of these pyramidal cells are signal transferring that is they communicate to each other by transferring signals via around 100 trillion synaptic connections. The weight of the brain is about 1.5 kilograms on average and the size is about 1130 cubic centimeters in man and 1260 cubic centimeters in woman.

Human brain consists of three main components: cerebrum, cerebellum and brain stem. These three components each have its different functions and characteristics, though the whole brain is highly cooperating with each other. Brain stem is under the cerebellum and connects the cerebrum spinal cord and cerebellum. This structure is responsible for basic vital life functions such as maintaining consciousness, heartbeat, breath, blood pressure, digestion, regulating the sleep cycle. Scientists say that this is the simplest part of human brains. Cerebellum is under cerebrum and behind brain stem, it is similar to the cerebrum in that it has two hemispheres and a highly folded surface or cortex. This structure is associated with regulation and coordination of movement, posture, and balance. Cerebrum or cortex is the largest part of the human brain, associated with higher brain function such as thought and action, it is divided into left and right cerebral hemispheres. Two cerebral hemispheres are connected by a very large nerve bundle called corpus callosum which communicates left and right cerebral hemisphere. According to sulci and gyri of cerebral hemispheres, cerebral cortex is segmented into four sections, the frontal lobe, the parietal lobe, the occipital lobe and the temporal lobe. The Frontal Lobe which is associated with reasoning, planning, movement, emotions, and problem solving. The parietal Lobe which is associated with movement, orientation, recognition, perception of stimuli. The Occipital Lobe which is associated with visual processing. The temporal Lobe which is associated

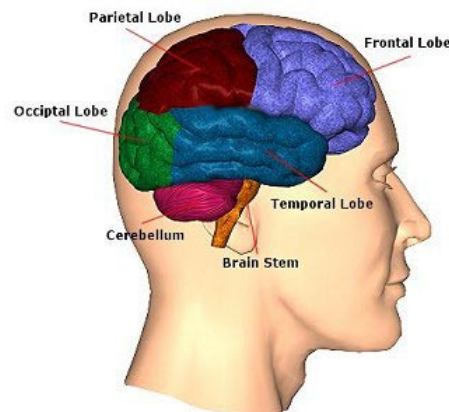


Figure 1.1: **Brain structures.** Main structures of human brain. There are three components: cerebrum, cerebellum, and brain stem. According to sulci and gyri of cerebral hemispheres, the cerebral cortex is segmented into four sections: the frontal lobe, parietal lobe, occipital lobe, and temporal lobe. Photo acquires from the website of Traumatic Brain Injury Resource Guide.

(Graphic source : <http://www.neuroskills.com/edu/brainfull.jpg>)

with perception and recognition of auditory stimuli, memory, and speech. We can see that each section has different function therefore the concept of brain structure is important for us to keep in mind. Fig. 1.1 shows main structures of human brain.

There are three types of brain tissues that can be generally segmented into gray matter (GM), white matter (WM) and cerebrospinal fluid (CSF). Fig. 1.2 is an MR image with gray and white matter labeled. These names simply derived from their appearance to the naked eye. Gray matter, which is known as the cortex, consists of the cell bodies of nerve cells and locates in exterior of brain. White matter, which is known as the medulla, transmitting the electrical signals that carry the messages between neurons and locates in interior of brain. Cerebrospinal fluid, which is the most dark of the three tissues and transparent fluid, fills ventricles and surrounds the brain and spinal cord. Therefore, it can absorb the shock and let the brain under the protection.

In 1909, regions of the cortex which is defined based on its cytoarchitecture or organization of cells is called Brodmann areas (BAs). Brodmann areas were originally defined

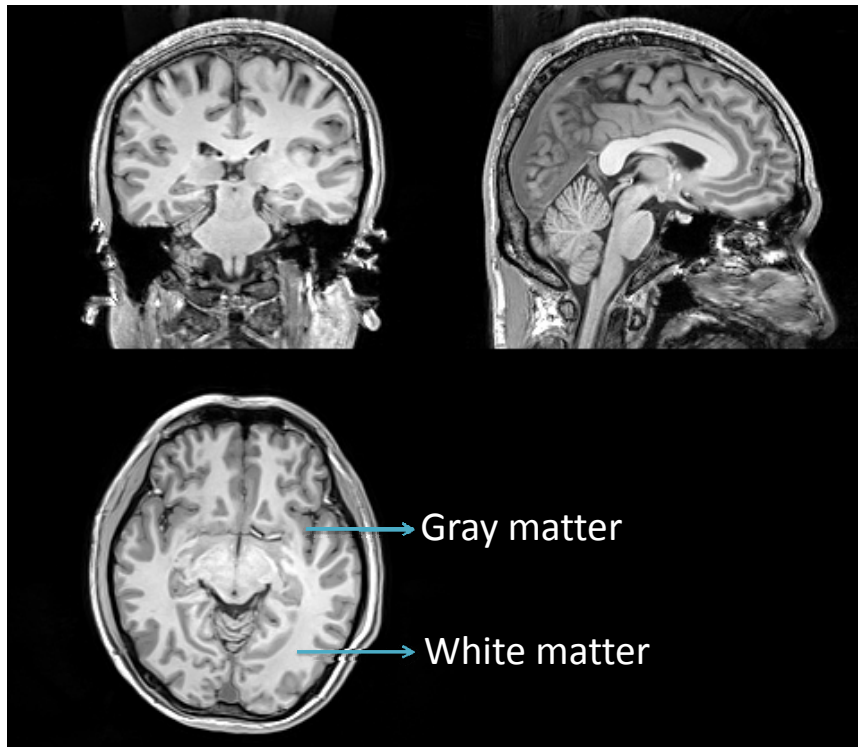


Figure 1.2: **MR image.** A 3.0 T Human brain magnetic resonance image which is labeling with Gray and White Matter part. These names simply derived from their appearance to the naked eye. It displays in sagittal axial and coronal view. The coronal view separates the body into anterior and posterior parts, sagittal view separates body into right and left parts and axial view separates the body into Superior and Inferior parts.

and numbered by Korbinian Brodmann based on the organization of neurons he observed in the cortex and he published his maps of cortical areas [1]. Each and every area is given a number from 1 to 52. Many of the areas have been correlated closely to diverse functions. For example, Brodmann areas 1, 2 and 3 in frontal lobe are the primary somatosensory cortex; BA 4 in frontal lobe is the primary motor cortex; BA 17 and BA 18 in occipital lobe is the primary visual cortex. Although the Brodmann areas have been discussed, debated, refined, and renamed exhaustively for a century, they have become the most widely known and commonly cited cytoarchitectural organization of the human cortex. Fig. 1.3 is Brodmann's maps. Although, we know Brodmann's map but we want to know the correct

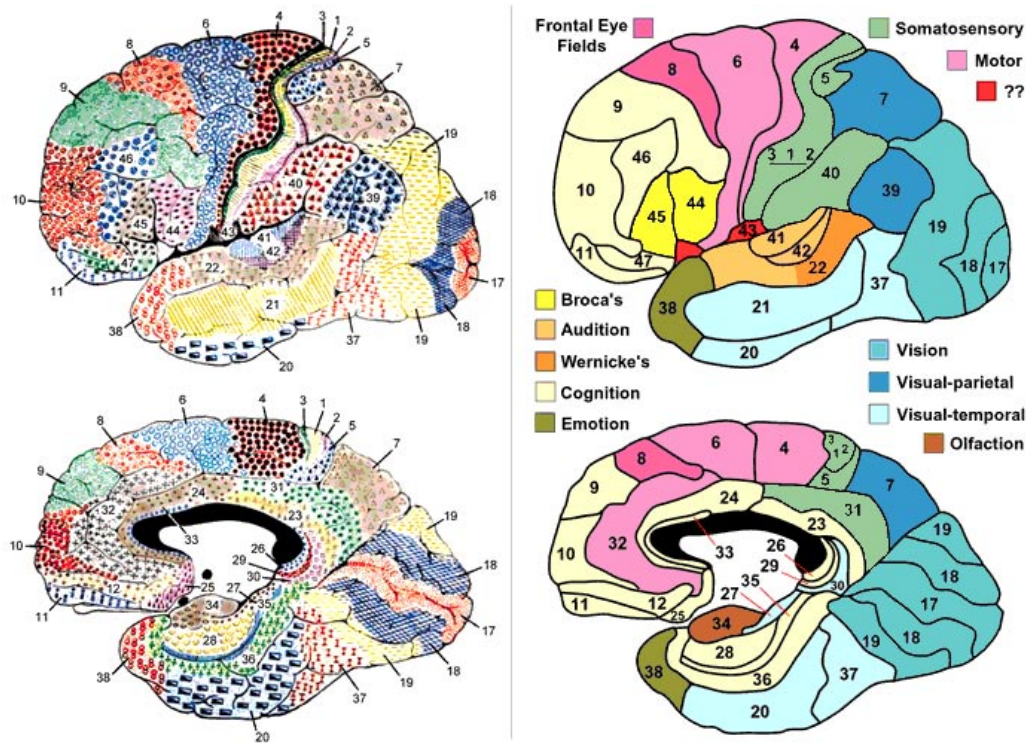


Figure 1.3: **Brodmann's map.** Brodmann's map was defined based on its cytoarchitecture and numbered by Korbinian Brodmann in 1909. It was divided into 52 discrete regions which was called Brodmann's areas (BAs). Photo acquires from the web site of Professor Mark Dubin University of Colorado.

(Graphic source: <http://spot.colorado.edu/~dubin/talks/brodmann/brodmann.html>)

Brodman area by using standardized x-y-z coordinates. Thus, an automated coordinate-based system to retrieve brain labels from Talairach Atlas called the Talairach Daemon is used [2]. It provided an 87 percent label match to Brodmann area labels BA 4 and BA 6 within a search range of 5 millimeters. The Talairach Atlas of human brain is defined by Talairach and Tournoux [3] in 1988. They defined a standard coordinate system on a European female brain aged 60 by anatomizing the brain to get the exact coordinate. Therefore, we can point out that a standardized x-y-z coordinates locates on which Brodmann area. It is useful for brain tissue location and becomes an invaluable tool in modern neuroimaging.

However, postmortem-studies were one of the few ways to study brain discrepancy and the relation between behavior and the brain. It have been used to further the understanding of the brain for centuries, until the first neuroimaging technique which is called pneumoencephalography (PEG) is shown. The pneumoencephalography, a procedure, was introduced by the American neurosurgeon Walter Dandy in 1919. With this neuroimaging technique, we can image the structure of the brain in vivo for clinical purposes or medical science. In the early 1970s, computerized axial tomography (CAT or CT scanning) was developed by Allan McLeod Cormack and Godfrey Newbold Hounsfield, and became available for diagnostic and research purposes because of the more detailed anatomic images of the brain. Thereafter, more and more imaging technique is developed such as single photon emission computed tomography (SPECT) and positron emission tomography (PET) and the structural imaging, magnetic resonance imaging like computer tomography (CT). In the next section, we will introduce magnetic resonance imaging (MRI).

1.1.2 Magnetic Resonance Imaging (MRI)

In recent years, magnetic resonance imaging (MRI) has become primarily a medical imaging technique to visualize the structure and function of the body or brain. It is also important for clinical diagnosis, medical treatment and further residential care. It was developed by Dr. Paul Lauterber in 1972 [4]. The major principle technique behind MRI is the development of nuclear magnetic resonance (NMR). In the past, magnetic resonance was used only for studying the chemical structure of substances. Until the 1970s NMR could be used to produce images of the body by Lauterbur's and Mansfield's great work. However, as the word nuclear was associated in the public mind with ionizing radiation exposure. It is generally now referred to simply as MRI.

There are three major components of an magnetic resonance imaging scanner : A static magnetic field, an RF transmitter and receiver, and three orthogonal, controllable magnetic gradients. Fig. 1.4 is a 3.0 T MR scanner. The image quality is directly proportional to the magnetic field strength. Higher magnetic fields increase signal-to-noise ratio, permitting higher resolution or faster scanning. However, The higher the magnetic field strength is,



Figure 1.4: **A MR scanner.** Photo acquires from the web site of Research Center for Integrative Neuroimaging and Neuroinformatics (RCINN) National Yang-Ming University. (Graphic source : <http://www.ym.edu.tw/rcinn/introduction.htm>)

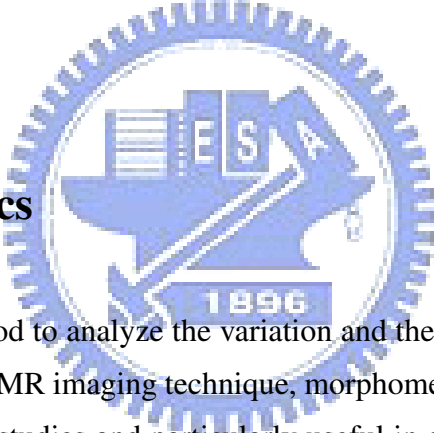
the better quality image we can acquire. A field strength of 1.0 - 1.5 T is a good compromise between cost and performance for general medical use. However, for certain specialist uses higher field strengths are desirable, with some hospitals now using 3.0 T scanners. Fig 1.2 is an MR image scanned by a 3.0 T MR scanner in National Yang-Ming University. With the rapid growth in MR imaging, it is a widely used technology in medical diagnosis, pathological study, and medical treatment. From head to foot, from cancer to cardiovascular vessel disease, from diagnosing to afterward following observations, it has already become an important imaging technique indispensable to modern medical centers.

There are many advantages of MR technology. First of all, it is noninvasive when detecting signals inside the body, so it is more safety for people under operations and diagnosis. Unlike computed tomography (CT), it uses non-ionizing radiation. Instead, it uses a powerful magnetic field to align the nuclear magnetization of hydrogen atoms in water molecules in the body. Which means MR imaging has no harm to patients who take the MR scan. Another advantage of MR imaging is that it provides much greater contrast between each different soft tissues of the body than CT does. It is especially useful in neurological (brain), musculoskeletal, cardiovascular, and oncological imaging and gives a great assistance in diagnosis of tumor or brain discrepancy in bipolar disorder (BD) or major depressive disorder (MDD). Another advantage of MR imaging is that it has no side-

effects which calls supplemental harm to patients. However, a disadvantage of MRI scanner is that the instrument is quite expensive. A new 1.5 tesla scanner approximately costs one million US dollars and two million US dollars for a new 3.0 tesla scanners. Constructing a MRI suite can cost a hundred thousand US dollars.

In human brain diagnosis and its researches, more and more studies are using CT, 2-D MR image or even higher resolution MR images. Because of the great contrast between different soft tissues of the brain, we can more easily distinguish gray matter, white matter and cerebrospinal fluid from brain. Due to the improvement of image resolution and development of the image processing tools and computers could handle numerous and complex operations, a number of unbiased whole brain morphometric analysis methods were proposed to characterize brain discrepancy.

1.2 Morphometrics



Morphometrics is a method to analyze the variation and the change in size or shape of organisms or brain. With the MR imaging technique, morphometric analysis are now commonly performed on in-vivo studies and particularly useful in analyzing the fossil record. It gives a quantitative element to describe the discrepancy of objects and allows more rigorous comparisons. In morphometric analysis, we can describe complex shapes or variation in size, and use the numerical comparison between different objects. Furthermore, statistical analysis can highlight areas where change is concentrated and quantify the level of significance. The morphometric analysis of brain images originally requires manually defining a number of regions of interest (ROI). It means that the method is based on an defined region of interests and analysis each object in this pre-defined ROI to perform the statistical differences on the volumes in each object [5].

However, the method has many potential drawbacks and limitations, including the demand of subject is always high, subjectivity, lacking of reproducibility. Quite a few lim-

itations are that it is impossible to know which area in brain might be atrophy or enlarge by diseases or a surgical trauma, we could not know the relations between diseases and the area which has been analyzed by the method in advance. Although several regions are known related to the disease, the measurement may include other surrounding regions blur the results and reduces statistical power. Therefore, since a priori knowledge of regions of interest for the disease is quite important, and according to sufficient previous studies, we can make up to the deficiency of priori knowledge.

More and more complex automatically/semiautomatically morphometric methods include the techniques of spatial normalization and tissue segmentation are proposed to analyze shape transformation or brain structure discrepancy. These methods can be divided into two categories: The first category uses the deformation fields computed by spatial normalization to compare the differences, which are to detect the differences in shape of the brain. The other category uses the normalized images to make comparisons, that is to detect the differences in brain tissue under an identical space.

The first category of morphometric method includes methods that measure the spatial transformation, which is analyzed by the deformation field deformed from templates of brain to each individual subject in the study. Several methods have been proposed, such as deformation-based morphometry (DBM) [6, 7] and tensor-based morphometry (TBM) [8,9]. These approaches are the most direct way of measuring brain shape. But the method is based on the perfect registration between the template and the subject. Otherwise, a bad registration with small errors may reduce the accuracy of the method.

The other category of morphometric method includes the well-known method: voxel-based morphometry (VBM) [10, 11]. It uses a spatial transformation to normalize images into an identical space. Due to the use of the normalized images, the overall shape differences between subjects can be removed. It means that each subjects registered to the template will be in the same template space and in the same shape, and we can make comparisons of brain tissue in normalized images. The method have been commonly used in several studies within the past decade.

1.3 Thesis Motivation

In this thesis, we use an multivariat approach method. The preprocessing of this approach is the same with the second category of morphometric method named voxel-based morphometry (VBM). The method uses normalized images to detect differences of brain structure. Although VBM is one of the most popular morphometric method and has been used in several studies, there are some limitations in this technique which causes VBM can not detect the differences of brain structure in a certain case: VBM detect group differences in a voxel-by-voxel manner at a time. A voxel-wise method means it consider every voxel independently to detect group differences by a statistic test, and when detecting one voxel, the neighbor voxels will be out of consideration. This voxel-wise method is simple and ease to detect every voxel independently. However, the images of the brain are shown in a 3D volume space, in the spatial point of view, the method is defectively in detecting group differences in voxel-by-voxel manner. The neighbor voxels, nearby brain tissues, should also be taken into consideration simultaneously [12].

Furthermore, in the previous section, the regions of the brain structure are always correlated to diverse functions. For example: the frontal lobe is associated with reasoning, the parietal lobe is associated with movement, the occipital lobe is associated with visual processing, the temporal lobe is associated with perception and recognition of auditory stimuli. That is we should not consider the regions voxel-by-voxel but regions with brain structures.

In order to overcome these limitations, in this work, we proposed another method by using a parcellation-based analysis approach, called the parcellation-based multivariate morphometry (PBM) to conquer this limitation of uni-variate analysis and of whole-brain analysis. This multivariate morphometry method can take the voxles in a region into consideration simultaneously. In this method, a high dimensional classification technique is used and detects the most hyper-plane to separates groups. The most discriminative hyper-plane not only minimize the scatter within groups, but also maximize the scatter between groups. It can separate the different groups and characterizing the discrepancy in the regions. Also,

we divide the brain into several regions in an anatomical way. The regions which are correlated to diverse functions can be separated by the discriminative vector.

1.4 Related Works

Several Multivariate classification techniques applied to these studies typically consist of three components, feature extraction, feature dimensionality reduction and feature-based classification. Feature extraction and feature-based classification are important when feature dimensionality reduction is the next. First of all, feature extraction, When effectual features have been extract, the feature-based classification or other analysis can be completed by using several classification techniques in machine learning. Otherwise a noneffective feature will be redundant and needless for analysis. Feature dimensionality reduction is applying a mapping of the multidimensional space into a space of fewer dimensions. This means that the original feature space is transformed by applying a linear transformation such as principal components (PCA) analysis method, which is main linear technique for dimensionality reduction. PCA performs a linear mapping of the data to a lower dimensional space. Finally, in the field of machine learning, the goal of classification is to group subjects that have similar feature values, into groups. A linear classifier achieves this by making a classification decision based on the value of the linear combination of the features, a linear discrimination analysis technique or support vector machines (SVM)-based classifier can be used. A number of multivariate statistical classifiers have been adopted to several studies not only for classification but also for characterization of brain discrepancy.

In 2002, Pettey and Geeadopted [13] proposed a multivariate linear discriminant method to characterize discrepancy of segmented MR images of the corpus callosum. At first, all segmented MR images were normalized to a male subject, and obtain for each subject a vector field or deformation field which tells us the displacement of the voxel needed to place into the correct position of the template. Finally, the quantity wishes to examine is the determinant of the jacobian of this transformation. In the pointwise statistics analysis,

they measured how different the determinant of the jacobian is between the two populations. In the multivariate analysis, they chose to keep the first few principal components of the image features, to deal with the small sample size problems. Subsequently, they find the linear combination which best discriminates between the populations by applying linear discriminant analysis. The only segmented image features were used to analysis in this study.

In 2004, Lao et al. [14] proposed a support vector machine (SVM) approach method based on whole brain images. The procedures are described in the following steps: First of all, the raw images are smooth with a 3D Gaussian filter and then downsampled by a factor of 4 in each dimension. Secondly, the smoothed downsampled images are segmented by using a method based on Markov random fields with inhomogeneity correction. The smoothed, downsampled and segmented images are normalized. Thirdly, they use the data of many subjects to train an SVM classifier. In the last stage, they applied the train SVM classifier to a new subject which is not including in the training set. There are two main problems in this study. One is the nonlinearity of the classifier, the other is the dimensionality reduction before pattern classification. A nonlinear support vector classifier is used, which means the group differences depend on the morphology itself. The nonlinear SVM method can only classify the morphology data, it can not be summarized with a single image. Besides, the dimensionality reduction, which may be needed for dealing with a very high-dimensionality data. Due to this feature selection process, the original brain can not be reconstructed.

In 2007, Thomaz et al. [15], present a general multivariate linear framework. This is the first multivariate statistical analysis of the human brain in Alzheimer's disease (AD) which uses the whole features simultaneously rather than segmented images. The goal is to identify and analyze the most discriminating hyper-plane separating two groups. The feature selection of the images are projected from the original space to a lower dimensional spaces by the use of Principal Component Analysis (PCA) method. Subsequently, a linear discriminant method called Maximum uncertainty Linear Discriminant Analysis (MLDA) is adopted to find the most discriminant hyper-plane on the PCA subspace.

It is similar to the previous work of our group [16]. Our goal is as well as to find a most discriminant vector to separate two populations by using a modified linear discriminant analysis method. Before the analysis of the whole brain images, we adopted a 3D wavelet transformation on the whole brain images in advance to increase spatial correlations between each voxels. Once we found the most discriminant hyper-plane, we perform the inverse 3D wavelet transformation to get the discriminant map in the original space. However, from our previous experiences, the voxel-based analysis somehow is defective without the consideration of nearby voxels. And in the previous work, we can figure out that the used of a modified linear discriminant method can deal with plenty of features simultaneously. But in the whole brain analysis features may be redundant. It is superior to other multivariate methods owing to no tissue information is missing with the feature reduction processes during the multivariate analysis. Some brain regions may or may not assist the detection of group differences and some regions with a great significant level may be unimportant. A region-based approach is quite important for analyzing anatomical structure. Therefore we use a parcellation-based multivariate method to analyze brain structures and detect group differences.



1.5 Thesis Organization

In the following chapters, we will introduce the voxel-based morphometry (VBM), parcellation-based multivariate morphometry (PBM), experiment results, discussion and conclusion. In chapter 2, we will introduce what VBM is, the optimized VBM protocol, the implementation of VBM and then its drawbacks. In chapter 3, we come up our idea of multivariate morphometry analysis and a framework of parcellation-based multivariate morphometry analysis. Chapter 4 is the experiment results with simulation data which is used to estimate the performance between two morphometry method. Then we have a discussion about the method and experiment results in chapter 5 and the conclusion in chapter 6.



Chapter 2

Voxel-based Morphometry



2.1 Introduction

Voxel-based morphometry (VBM) is a technique that detects the group differences in brain anatomy through a voxel-wise comparison of spatial normalized MR images [11]. That is to identify differences in relative voxels of brain structures. It is not a region of interest but whole-brain method to characterize volume and tissue concentration differences in brain structural MR images, it is also an unbiased statistical method which is a commonly used tool in the identification of characteristic differences of brain structures. By using the statistical approach of so-called statistical parametric mapping (SPM), the normalized images were statistically tested using the general linear model based on the Gaussian field theory.

In traditional morphometry method, it is based on the pre-defined regions of interest (ROI) then analyze the images with this pre-defined ROI. However, this is time consuming to define ROIs, especially when there are a large amount of subjects. And every single manual error in defining ROIs will cause small differences in volume.

VBM is increasingly applied to detect group differences in brain among various types of patient group and control groups. In recent years, it is shown that lots of the disease are correlated with the abnormal brain tissue. The method provides an analysis of inter group differences in brain tissue or volume on the voxel-wise basis in a standardized space. The results of VBM studies characterizing group differences in some disease are consistent with the result of previous studies, such as bipolar disorder (BD) [17, 18] or major depressive disorder (MDD) [18, 19].

In general, the procedures of VBM analysis can be divided into two parts which are the preprocessing and the voxel-based parametric statistical analysis. Simply the procedures of the preprocessing involve spatial normalization, segmentation, and smoothing [10]. Finally, a voxel-wise statistical inference is applied to these preprocessed images. The standard VBM procedure involves four steps describe in order figure 2.1 is a standard VBM protocol.

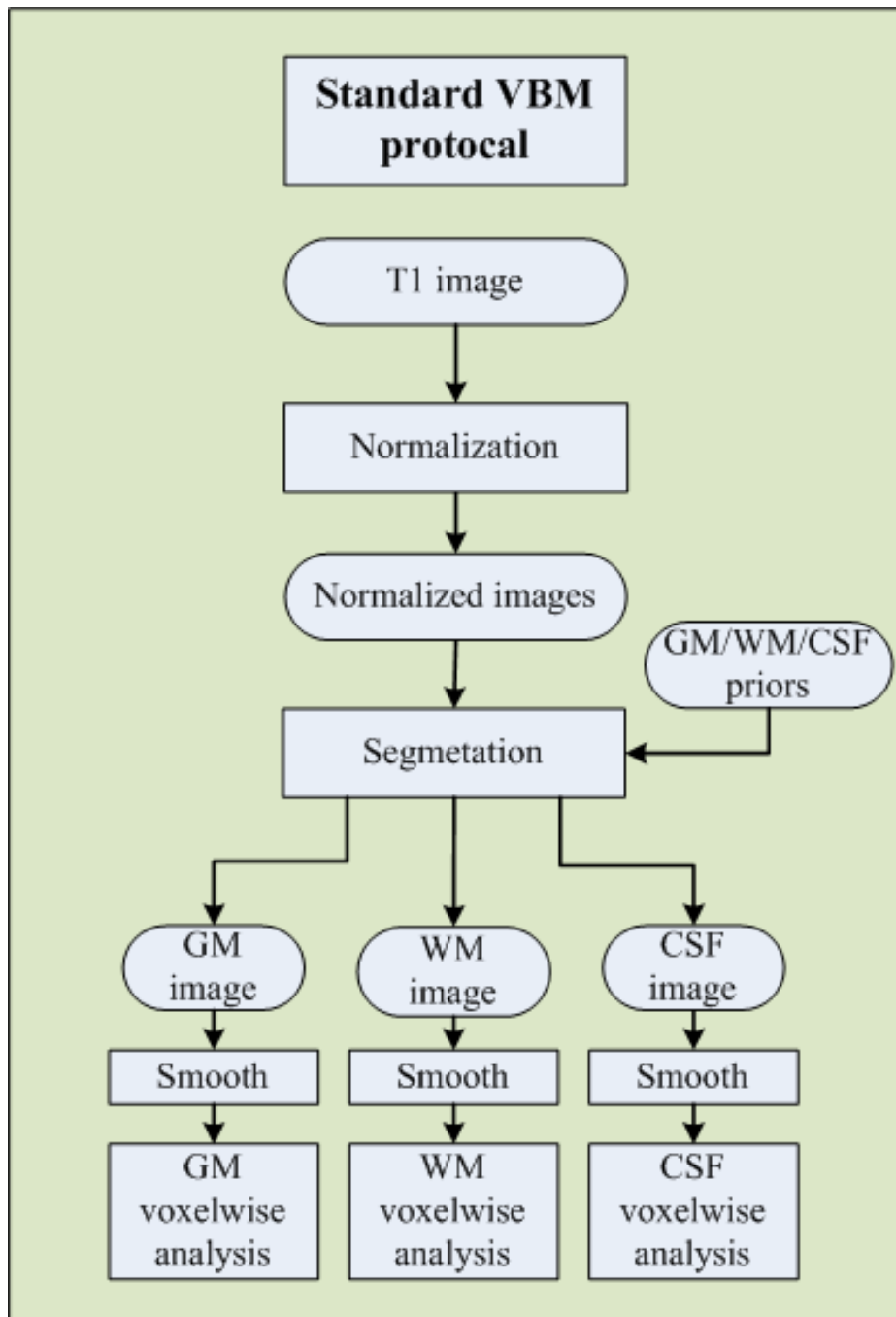


Figure 2.1: **Flowchart of standard VBM protocol.** Raw images are first normalized to a standard space with a template. Secondly, GM, WM and CSF are segmented from the normalized images. Thirdly, the normalized and segmented images are smoothed with an isotropic Gaussian kernel to make the data close to normal distribution. Finally, a voxelwise statistical inference is applied to those normalized, segmented and smoothed data.

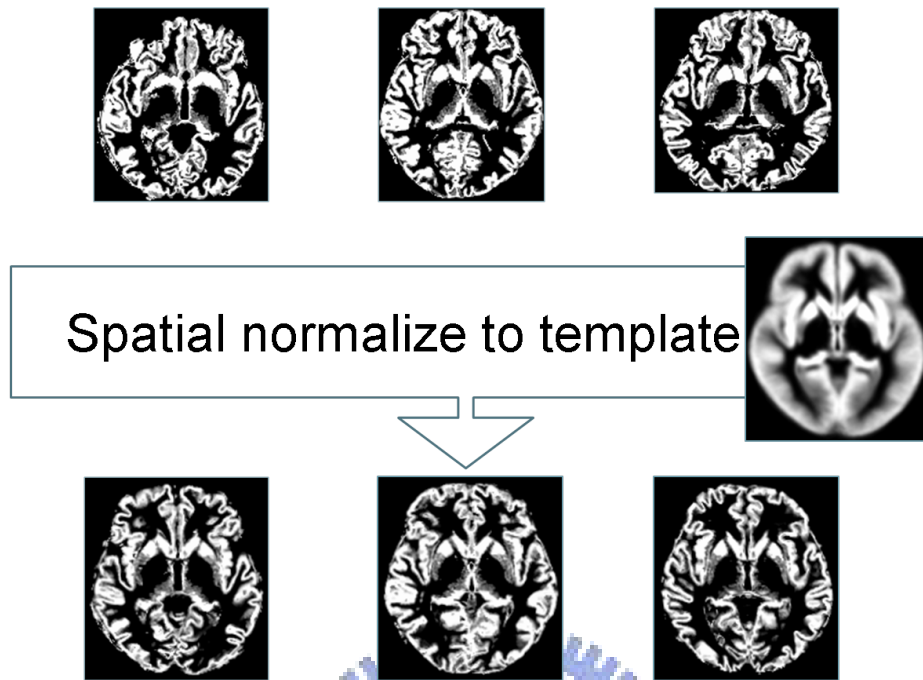


Figure 2.2: **Concept of the spatial normalization.** The spatial normalization is to correct the differences of shape and size between each subjects. All images in native space must be normalized to a template where the standard space is. After normalization, all voxels in the same standard space represent same tissues in each subjects.

1. Spatially normalization of all images to the same stereotactic space

As shown in the figure 2.2, the spatial normalization registers brain images of different subjects into the same stereotactic space which is called template space. It is impossible to compare each voxel of different MR images in native space because of different sizes, shapes and the diversity of the scanning position. After spatial normalization, all normalized brain images are in an identical space. One certain voxel in different brain images should represent the same brain tissue. It is important that the more accurate registration we used, the fewer the choice of the template image bias the final solution.

2. GM, WM and CSF extraction from the normalized images

As shown in the figure 2.3, in the segmentation, the spatially normalized images are next segmented into gray matter (GM), white matter (WM) and cerebrospinal fluid

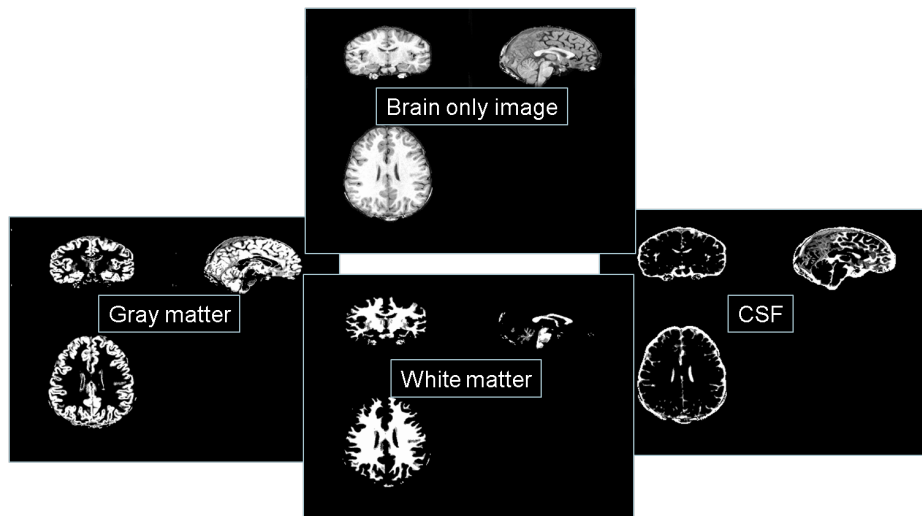


Figure 2.3: **The segmentation.** The figure shows an example of segmentation result. A brain only image is segmented into different tissue classes which are gray matter (GM) image, white matter (WM) image and cerebrospinal fluid (CSF) image.

(CSF). After segmentation, we could obtain brain tissues and perform the statistical analysis on these tissues. In consequence of the spatial normalization and segmentation, the voxel at the same position represents the same brain tissue.

3. Smoothing

In smoothing, the segmented gray and white matter images are now smoothed by convolving with an isotropic Gaussian kernel. The size of the smoothing kernel should be comparable to the size of the expected regional differences between the groups of brains, but most studies have employed a 12 millimeter FWHM kernel. It makes the data more normally distributed and reduces the registration error which is resulted from spatial normalization. It also ensures that each voxel in the images contains the average amount of gray or white matter tissue around the voxel.

4. Voxel-based statistical analysis for localization

As a result of the smoothing step, a VBM analysis involves a voxel-wise statistical analysis by comparing the normalized and smoothed GM or/and WM images of different groups of subjects. Standard parametric statistical procedures (t tests) are used

to test the hypotheses at each and every voxel, to measure the group difference is to find out the area or voxels reach the significant level in statistic two sample t test. The results comprise the level of group differences and if reaching the significant level, we can say that there is a difference between the groups at this voxel. Eventually, A voxel-wise statistical parametric map (SPM) comprises the result of many statistical tests.

There are various ways to implement voxel-based morphometric methods. The purpose of different implementation is to maximize the ability of making inferences in group differences. For example, another method applied the procedure in the order: segmentation first, normalization, smoothing and statistical analysis which is called RAVENS [5] method. In the next section, we will introduce another improvement method based on the standard VBM called optimized VBM [10].

2.2 Optimized VBM Protocol

There are several studies reveal potential problems of the standard VBM. One of those studies discusses about the imperfect registration effects on VBM. An imperfect registration may cause the segmentation error because of brain tissue is in the different space, and it leads into an incorrect comparison between normal control and patient subject [20]. It is owing to the implementation of segmentation. In the segmentation method, a mixture model technique is used, and the model contains the distributions of the voxel intensity of brain tissues (GM, WM, CSF). A priori probability map contains a priori knowledge of the distribution of the brain tissues in normalized space is used to improve the segmentation of brain tissues. Furthermore, if the VBM analysis is focus on the brain tissues such as gray matter or white matter, the segmented image will be normalize into template space which may cause that, the better segmented images used the better accuracy of the registration. In conclusion, the registration and segmentation influences each other, an optimized VBM protocol is proposed by Good et al. [10].

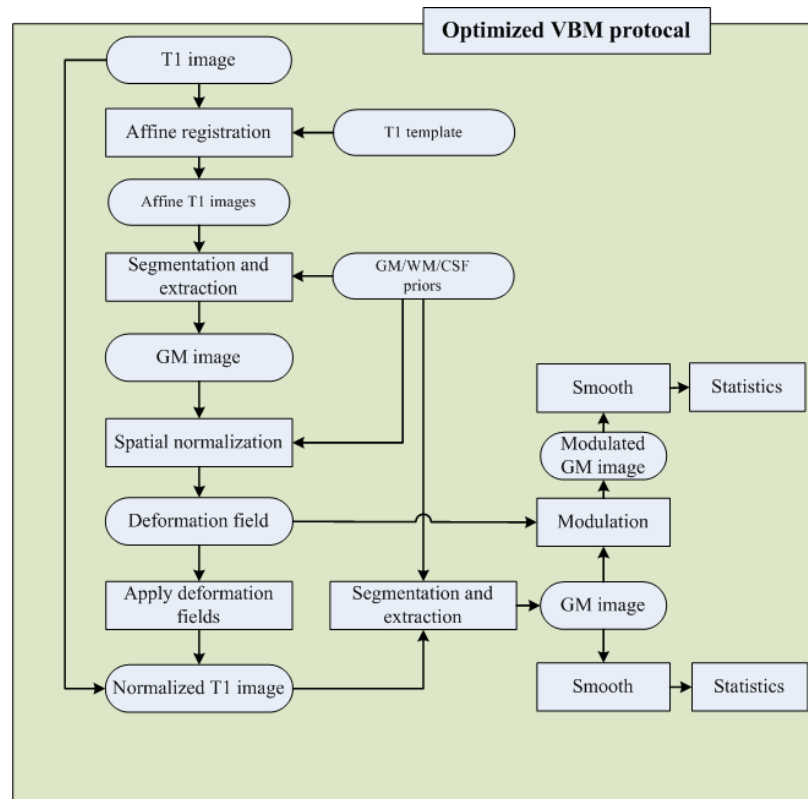


Figure 2.4: **Flowchart of optimized VBM protocol.** Optimized VBM protocol consists of the following seven steps: (1) creation of GM, WM and T1 template, (2) segmentation and extraction of affine-registered brain images, (3) normalization of GM/WM/CSF images into the GM/WM/CSF template, (4) normalization of whole brain T1 images with optimized normalization parameters, (5) segmentation and extraction of normalized T1 images, (6) modulation, and (7) smoothing.

The optimized VBM protocol [10] for characterizing group differences of gray or white matter is list below in order, and Fig 2.4 is the flowchart of optimized VBM protocol.

1. Creation of GM, WM, CSF and T1 template

Customized template is created by averaging all the normalized smoothed gray/white matter subjects from the standard VBM protocol. the optimized template is created to minimize any potential bias for spatial normalization. All T1 images are normalized to a template, segmented into GM, WM and CSF images and then smoothed with an 12 millimeter full-width at half-maximum (FWHM) isotropic Gaussian kernel.

Each normalized, segmented and smoothed T1/GM/WM/CSF images are averaged to create T1/GM/WM/CSF templates respectively.

2. Segmentation and extraction of affine-registered brain images

This is a fully automated method to remove scalp tissue, skull and non-brain tissues. At first, all T1 images in native space are segmented into GM, WM and CSF images. Then a series of morphological operations is applied to these segmented images to remove unconnected non-brain voxels. Finally the gray and white matter are extracted in native space.

3. Normalization of GM/WM/CSF images into the GM/WM/CSF template

In this step, the segmented GM/WM/CSF images in native space are normalized to the customized GM/WM/CSF template individually in stereotactic space. Thus we can obtain the optimal deformation fields.

4. Normalization of whole brain T1 images with optimized normalization parameters

The optimal deformation fields obtained in the previous step are now reapplied to the raw whole brain T1 images in native space. Therefore we can obtain the raw T1 images which are in the same space with the gray/white matter template.

5. Segmentation and extraction of normalized whole brain images

In order to get a preferable segmentation, the optimally normalized whole brain T1 images are now in the stereotactic space. Then segmented into gray, white matter and CSF. A series of morphological operations is applied again to these segmented images to remove unconnected non-brain voxels. Finally, the optimally normalized and segmented GM/WM/CSF images are got in stereotactic space.

6. Correction for volume changes which is also called modulation step (optional)

Due to the nonlinear spatial normalization, volumes of certain brain areas may be enlarged or atrophy. In order to preserve the volume of a certain region within a voxel, a correction for volume changes, usually called as modulation. A multiplying voxel values in the segmented images by the Jacobian determinants which is obtained in

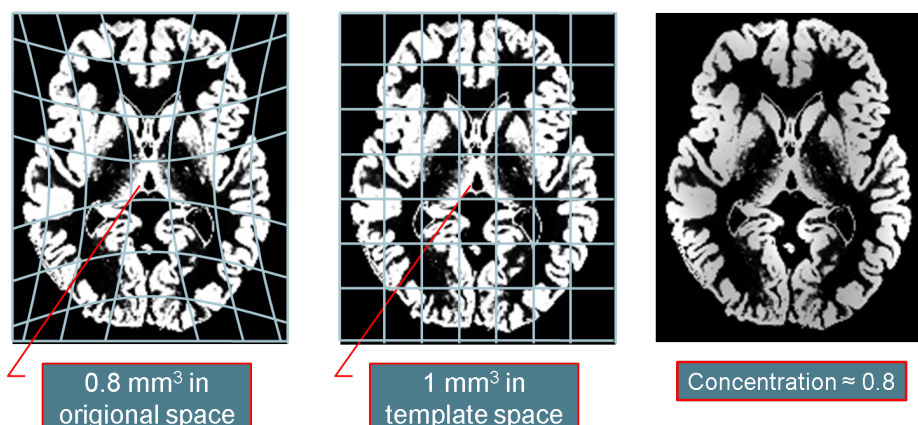


Figure 2.5: **Concept of the modulation.** The figure illustrates the modulation of a normalized segmented image. Due to the spatial normalization, after images are normalized into a standard space, volumes of certain brain areas may be enlarge or atrophy. The result of modulation are used to correct for volume changes. For example, the pixel in the native space is 1 millimeter square. after normalization, the pixel becomes 3 millimeter square in standard space. It means, the concentration should be divided by 3 to preserve total volumes in each pixels.

the spatial normalization step. Figure 2.5 is a concept of the modulation.

7. Smoothing

It is same with the standard VBM method, the optimally normalized segmented and modulated images of different tissues are smoothed using an isotropic Gaussian kernel. Smoothing makes the population more normally distributed and reduces the registration error. The choice of the smoothing kernel is related to the expected differences. An 8 millimeter or 12 millimeter FWHM smoothing kernel is often used in VBM method.

8. Statistical analysis

As the standard VBM method, a voxel-wise statistical analysis is performed on those optimally normalized, segmented, modulated and smoothed images to characterize regionally discrepancy between different groups. The use of two-sample t test is to calculate the significance of group differences at every voxel. The t -test map is a 3D volume, the voxel dimension and voxel size which are the same with every MR

images. Thus we can make inferences in group differences by each voxel which is stored in t test map reaches a significance level.

The optimized VBM protocol provides a more preferable normalization and segmentation. And features of the optimized VBM are first creating a separated grey and white matter templates, and second a fully automatic brain extraction technique. It also adopts a modulation step to preserve volume change during spatial normalization.

2.3 Implementation of VBM

In order to maximize the ability of making inferences in group differences, an imperfect registration and a bad segmentation result will reduce the ability of the VBM, which implies that each of steps in VBM is important and each bad results may affect the VBM studies badly. Therefore we should be careful when implementing every single step and make sure that the performance of tools we used is the best. Several tools are used in VBM studies such as brain extraction, segmentation and spatial normalization. Following is the implementation of VBM by our group.

The implementation of VBM in this work is illustrated in figure 2.6. It is similar with standard VBM protocol but in different order of the normalization and the segmentation step, due to the characteristic of the segmentation tool which can segment images in the native space instead of a standard space. Moreover the bias correction is done at first to correct the inhomogeneity of the magnetic field which may cause the image tissues become difficult to differentiate.

1. Bias correction with N3

An artifact often seen in MRI is for the signal intensity to vary smoothly across an image, which is referred to as RF inhomogeneity or intensity non-uniformity. It is

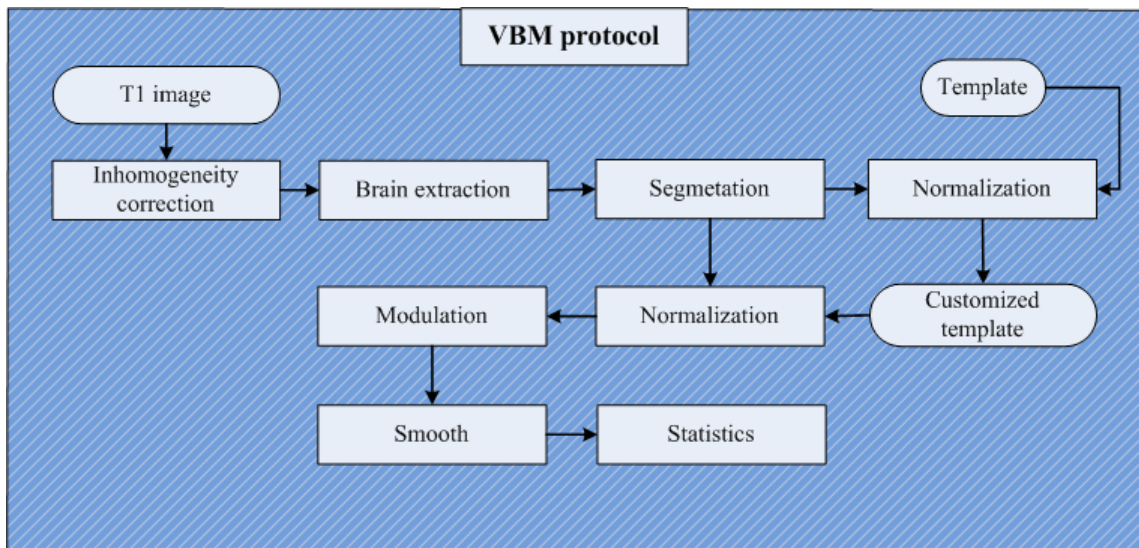


Figure 2.6: **Flowchart of VBM implementation.** Our implementation of VBM uses several tools and can be described in eight steps: (1) Bias correction, (2) non-brain exclusion of T1 images with HWA, (3) segmentation and extraction of brain T1 images with FAST, (4) normalization of segmented GM, WM and CSF images, (5) creation of customized GM, WM and CSF templates, (6) normalization of segmented GM, WM and CSF images to customized template, (7) correction for volume changes, (8) smoothing and voxel-based morphometric statistical analysis.

usually due to poor radio frequency (RF) field uniformity. Raw images are first corrected by nonparametric nonuniform intensity normalization (N3) [21] which is a non-parametric method for correction of intensity non-uniformity in MRI data and minimize the within-class variance of GM, WM and CSF. Bias correction will also improve the image quality for segmentation. Figure 2.7 is an example of bias correction.

2. Non-brain exclusion of T1 images with HWA

The T1 corrected images are secondly skull-stripped using a hybrid watershed algorithm (HWA) [22]. Hybrid Watershed algorithm is a relatively more sensitive tool that often results in a conservative strip that rarely removes any brain tissue. It is a fully automatic, robust and efficient algorithm which removes non-brain tissue, and does not unduly influence the outcome. All images are segmented to remove

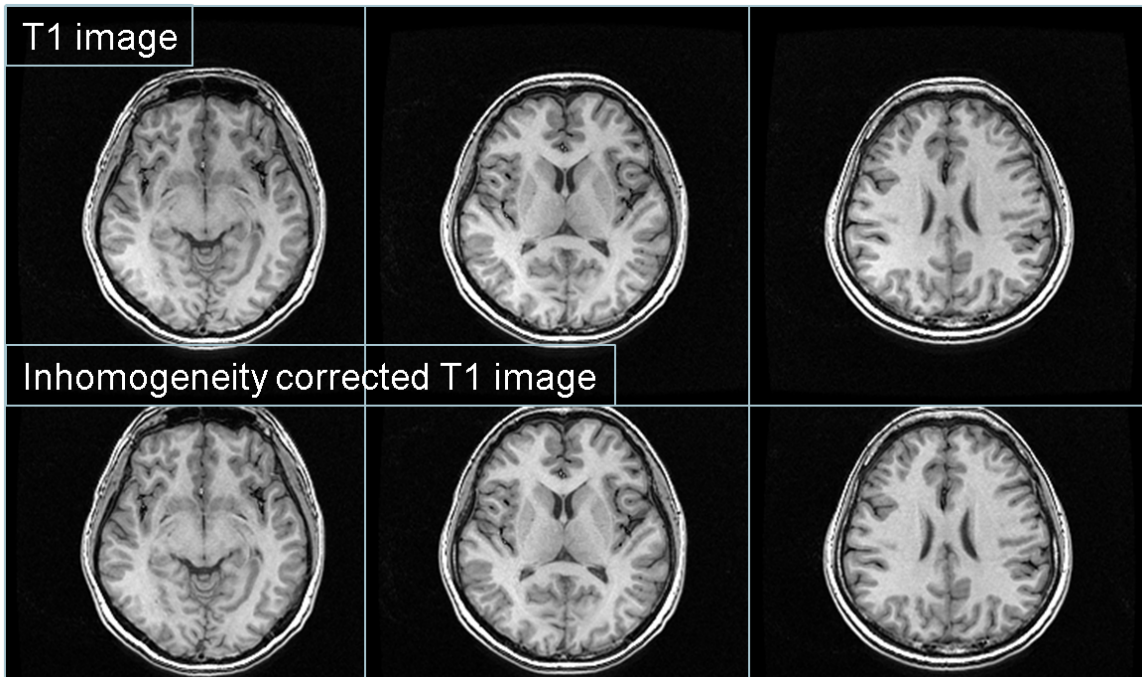


Figure 2.7: **Bias correction with N3.** The figure shows that the result of bias correction done by N3 tool is clear between GM and WM. The image is shown in different three slices and first row is the raw image, and second row is done by N3. It can see that WM in the down left corner is brighter than top right corner.

non-brain parts in native space with HWA. The default parameters were utilized for automated processing. On average, HWA required less than 8 min of processing time per dataset. Figure 2.8 is an example of non-brain exclusion.

3. Segmentation and extraction of brain T1 images with FAST

All T1 inhomogeneity corrected images without non-brain tissues derived from the previous step are segmented into GM, WM and CSF images in native space with FMRIB's Automated Segmentation Tool (FAST) in FSL. Its method is based on a hidden Markov random field model and an associated Expectation-Maximization algorithm [23,24]. The value of a voxel in segmented images represents a probability of belonging to one particular tissue, ranged from 0 to 1. We use this probability to represent the tissue volume of the segmented images.

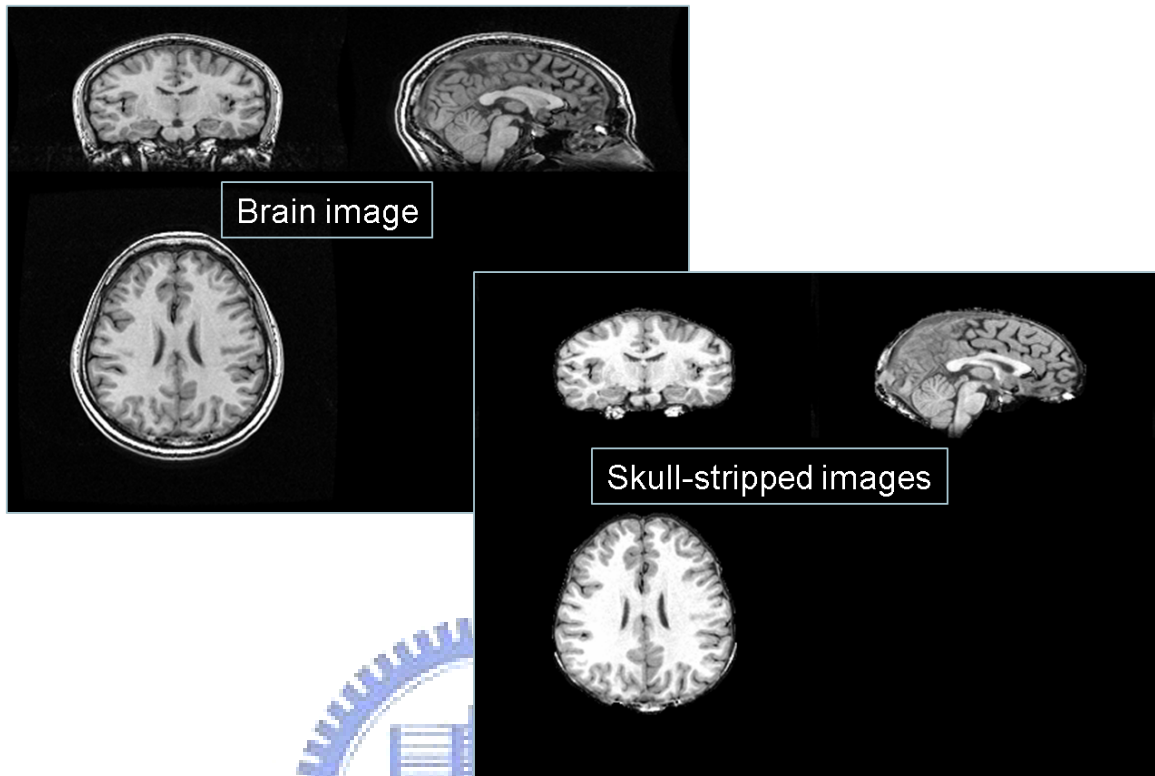


Figure 2.8: **Brain extraction with HWA.** This figure shows non-brain exclusion from a T1 image by using HWA. The left image is T1 images with lower contrast and the right one is an extracted brain image without non-brain materials after segmentation by HWA. The quality of the extracted image has been improved and would make a good segmentation with FAST.

4. Normalization of segmented GM, WM and CSF images

All segmented GM, WM and CSF images are respectively normalized to a template by first an affine-registration and follow a nonlinear registration [25].

5. Creation of customized GM, WM and CSF templates

All segmented normalized GM, WM and CSF images are in a standard space and averaged to create customized GM, WM and CSF templates. The customized templates are more close to the population sample of the study and minimize the distortion caused by normalization in later processes.

6. Normalization of segmented GM, WM and CSF images to customized templates

The segmented GM, WM and CSF images in native space obtained in third step are independently normalized to the corresponding GM, WM and CSF customized templates obtained from the previous step. Then all segmented and normalized GM/WM/CSF images of different subjects are now in the same space that is the voxel in the same position will stand for the same tissue. Moreover, during the normalization of the deformation field are stored in order to correct volume changes in next step.

7. Correction for volume changes (modulation)

Due to the nonlinear spatial normalization, the volumes of certain brain areas may be enlarge or atrophy. In order to preserve the volume of a certain region within a voxel, a correction for volume changes, usually called as modulation. A multiplying voxel values in the segmented and normalized images by the Jacobian determinants which is obtained in the spatial normalization step. In our analysis, these modulated images are used to analyze the volume discrepancy between different groups.

8. Smoothing and voxel-based morphometric statistical analysis

The segmented, normalized and modulated images are smoothed to be close to normal distribution by using an isotropic Gaussian kernel, and an 12mm FWHM smoothing kernel is used. Then, a voxel-wise statistical analysis is performed on these segmented, normalized, modulated and smoothed GM/WM/CSF images to characterize regionally discrepancy between different groups. The use of two-sample t test is to calculate the significance of group differences at every voxel. Then a 3D volume with t -test map is stored to make inferences in group differences.

In this work, we applied preprocessing of the VBM protocol to deal with MR images. We maintain concepts of the VBM protocol and implement it with N3 (IDeA Lab, UC Davis Center for Neuroscience), HWA (FreeSurfer, <http://surfer.nmr.mgh.harvard.edu>), FSL (Analysis Group, FMRIB, Oxford, UK), SPM2 softwares in Matlab 7.0 (the MathWorks, Inc. Natick, MA, USA).

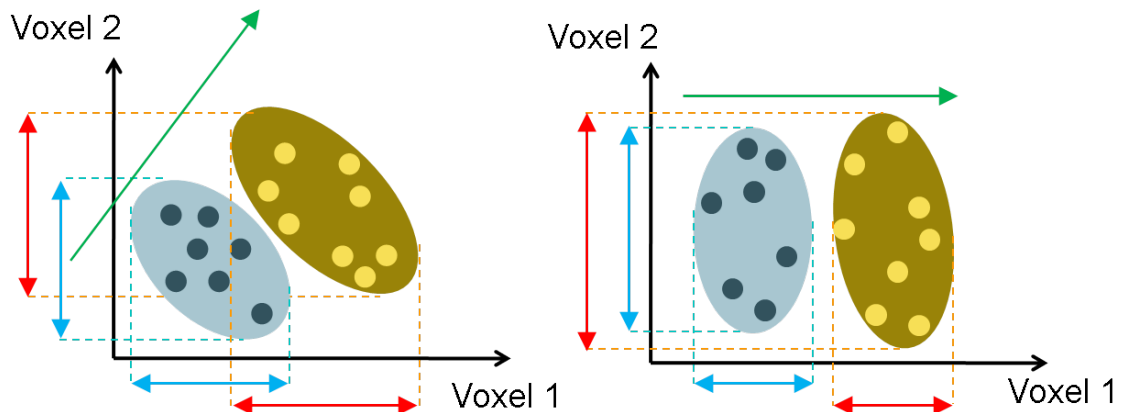


Figure 2.9: **Schematic scatterplots illustrating of significant bias of VBM.** There are two ellipse which stands for two different morphological groups. For example, one is normal control group the other is affected group. In the right case, there is no overlay along the voxel 1 axis. it is easy for VBM to detect group difference depending at the voxel 1 even with a small number of samples, but detect no difference at the voxel 2. In the left case, VBM may fail to find group difference along each axis because of the high overlay. This is a significant bias of VBM analysis which is very limited in detecting group differences.

2.4 Drawbacks of VBM

Each of subjects can form a person's morphological profile by collecting voxel-wise morphological measurements which consist of every voxel in volume data. These measurements can be placed into a high-dimensional space, each dimension representing a voxel. That is, if spatial normalization is perfect, we can say that each voxel in different MR image stands for the same tissue, the orientation of group differences in a high-dimensional space consists of every voxel in a MR image. Then the group differences are then reflected by the degree of separation of the respective morphological profiles. Figure 2.9 is a schematic scatterplots in two dimension. The normal morphological profiles and the affected morphological profiles will form two distributions in two-dimension space. The dimensionality of the space is much higher and equal to the number of voxels being interrogated, but here we use 2D examples for display purposes.

Davatzikos [12] points out that VBM determines structural differences directly from

the data in an bias way, it is fundamentally limited in making inference of group differences. Two cases are shown in figure 2.9. The orientation of group differences in a high-dimensional space in practice, here in our case, 2-dimensional space is used. Owing to the voxel-based morphometry analysis detect group differences in a voxel-wise manner, VBM considers only one dimension at a time. That is on the right of figure 2.9, in which the group difference will be detected along dimension 1 (voxel 1), even with very small number of samples. Because there is a significant difference at voxel 1. VBM may detect no group difference along voxel 2. In another case, on the left of figure 2.9, VBM may detect no group difference along each axis because diseased and normal groups might have different means, but the overlap is high. This is a significant bias of VBM analysis which is very limited in detecting group differences. In summary, the two cases, show that voxel-based morphometry analysis will detect group differences easily at one axis in morphological profile. However, the dimension in MR images is always high and there are subtle and complex differences in brain structures, may not be easy for VBM to detect the significance of group differences.

Although voxel-based morphometry analysis in group differences is of great worth. But the bias of VBM limits the power of detecting subtle and complex structures. This bias is an fundamental limitation of voxel-based morphometry, because the ways of VBM in detecting group differences is voxel-by-voxel manner rather than the consideration of nearby voxels or several structures in brain. In the above two cases, it is clear that there is a group different between two distribution at voxel 1 and voxel 2. If two voxels are in consideration, It is easy to differentiate between two different distribution of morphological profiles. That is the more voxels we consider, the more subtle or complex structures we may detect. Therefore, in this thesis, we proposed another unbiased method using a region-based multivariate analysis approach which is also automatic to overcome this fundamental limitation.

Chapter 3

Parcellation-Based Multivariate Morphometry



3.1 Introduction

According to the drawbacks of voxel-based morphometry analysis method, we use a multivariate morphometry analysis method which characterizing the group differences of brain structures. The multivariate morphometry method is an unbiased method that we can compare voxels in a multivariate manner to overcome the drawbacks of voxel-based morphometry analysis. Before the multivariate analysis is adopted, the preprocessing of the raw MR images is also similar with VBM analysis. The main difference of this thesis is the multivariate analysis.

In multivariate analysis, all voxels in MR images are features simultaneously taken into consideration in a high-dimensional space. The more voxels this multivariate method analysis the higher dimension it forms. The goal of the multivariate analysis is to detect the most discriminative hyper-plane which separates the two different groups in the high-dimensional space. That is the most discriminative hyper-plane is a linear combination of features which best separate two or more groups of MR images. Each features are projected onto this discriminative hyper-plane which best separates two different groups. Further, each parameters of this discriminative vector is a weight which stands for the discrimination of each dimensions, features or voxels. That means, once we find a discriminative projection vector, each weights of the vector is a discrimination of characterizing group differences and it is also an image called discriminant map. The discriminant map can be visualized to identify the location in brain.

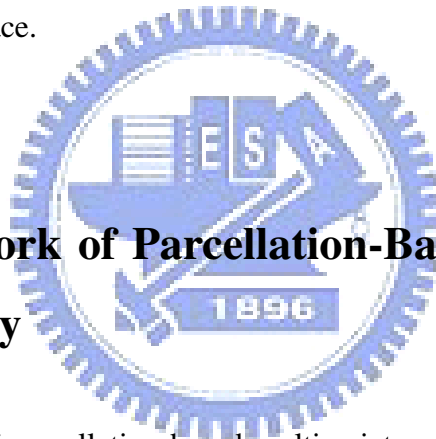
From the previous work of our group [16], a multivariate whole brain analysis is proposed. The use of whole brain images and linear multivariate classification technique demonstrated that the method has a good sensitivity to subtle and complex brain structural differences. Somehow, taking all features into consideration may be redundant in our experience. And voxel-based analysis method which considers only one voxel at a time without nearby voxels is also a drawbacks. Thus a parcellation-based approach is needed.

The concept of the parcellation-based analysis method is proposed. That every voxel in the same regions are taken into account simultaneously for characterizing group differences

in each regions. The brain will be parcellated into several different regions especially based on brain structures. The interaction of every voxel in the same region can be sufficiently analyzed by a multivariate method. The relation between disease and brain structures is quite close but the relation between disease and undefined-regions is relatively small. Moreover, several voxels or predefined regions which are more important in characterizing in group differences can be taken into consideration if they were known in advanced. In brief, the related information of each voxel in same regions are in consideration, it contradicts to the voxel-based morphometry analysis in characterizing group discrepancy.

In consequence, a parcellation-based multivariate morphometry method is proposed for characterizing differences of brain structures. we can quantified differences of each regions through the parcellation-based manner by a linear multivariate classification technique in a high-dimensional space.

3.2 Framework of Parcellation-Based Multivariate Morphometry



The procedure of parcellation-based multivariate morphometry is similar with voxel-based morphometry. The first seven steps of the implementation of voxel-based morphometry is used. The preprocessing includes bias correction, brain extraction, segmentation, normalization, template creation, normalization to customized template and modulation. Smoothing step is not included because of the subtle differences of brain structures may be reduced by smoothing data, more details will be listed in chapter 5, discussion. After the preprocessing, the segmented, normalized and modulated gray/white matter images are all in the same space. Subsequently, parcellation-based multivariate morphometry analysis will be adopted to find group differences of brain structures.

The parcellation-based multivariate morphometry analysis can be divided into three parts. First of all, we extract regions of brain by Anatomical Automatic Labeling (AAL)



Figure 3.1: **Schematic of the Anatomical Automatic Labeling template.** The AAL template is in three different views which is obtained in MRICron software. An official site for Anatomical Automatic Labeling (AAL) freeware: <http://www.cyceron.fr/freeware/>

which is a software package and digital atlas of the human brain [26]. The definition of 45 anatomical volumes of interest (AVOI) in each hemisphere were delineated with the Montreal Neurological Institute (MNI) single-subject main sulci. The procedure was performed using a dedicated software which allowed a 3D following of the sulci on the brain. Regions of interest were then drawn manually with the same software every 2 millimeter on the axial slices of the high-resolution MNI single subject figure 3.1 is a schematic of AAL template. There are 116 regions defined by AAL and all of the regions will be extracted by using this AAL template.

Secondly, the main part of the multivariate analysis, each of the regions will adopt a modified LDA-based method, the discriminative common vector method [27] to find the most discriminant projection vector. It is simultaneously minimizes the scatter within each individual group and maximizes the scatter between groups without the small sample size problem. The resulting projection vector forms a spatial map, whose image size is the same with each regions, containing the regions which are most representative of group differences. That is, each parameters of this discriminative projection vector is a representative of the discrimination of each groups, features or voxels. Details of the method will be interpreted in the next section.

Thirdly, combining each regions back into original brain, the resulting projection vector containing the most representative of group differences of each extracted regions. It

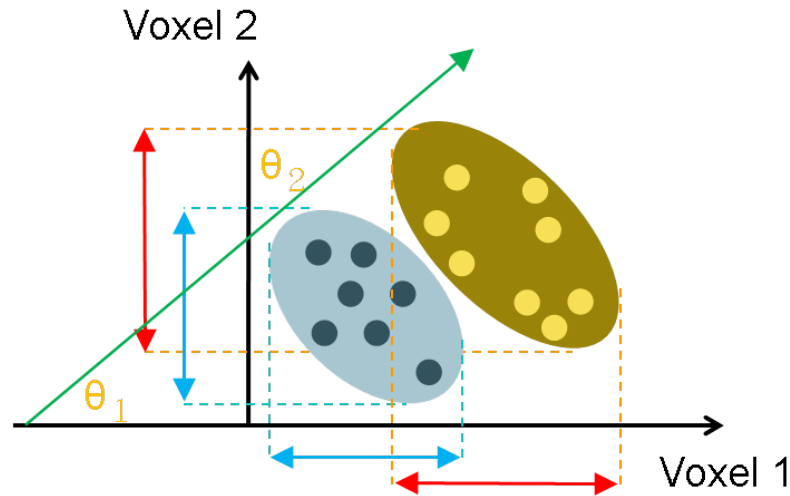


Figure 3.2: Concept of the relation between projection vector with each standard bases.

is a most discriminant map of each regions that the weight of each feature represents the degree of importance for characterizing group differences. The resulting projection vector will form an angle with each standard basis. The angle Θ_i is computed by the formula $\Theta_i = \arccos \frac{P_{lda} \cdot \hat{e}_i}{|P_{lda}| |\hat{e}_i|}$. Where P_{lda} is the projection vector and \hat{e}_i is the standard basis. That is each of the weight w_i is the same with $\cos \Theta_i$. Even the weights are in different regions we can combine them all together. Figure 3.2 is the concept of the relation between projection vector and each standard basis. Before we combine each parameters of the resulting projection vectors back into original brain, there will be a problem of representing the degree of importance for characterizing group differences. The resulting projection vector will be a unit vector which is computed by modified linear discriminant method. The more dimension the unit vector has, the smaller parameters it gets with the same atrophy. The correction is done before combining each results. Details of the method of the combination of each results will also be interpreted in the next section. After the combination, we will get the most discriminant projection vector of two different groups. The weight of projection vector represents the degree of importance for characterizing group differences.

Finally, for the purpose of displaying each regions of the significance level which is the weight of the discriminant map. There are two map we will illustrate. One is the t map

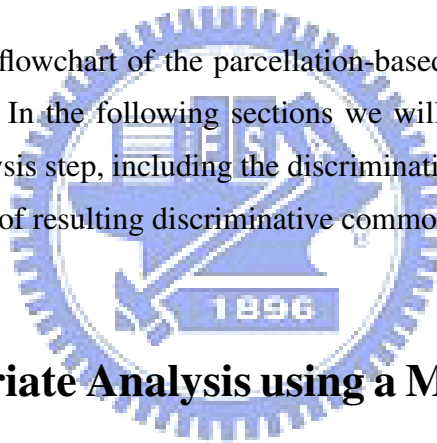
of each regions the other is weights of the discriminant map itself. A t -test map is calculated by projecting all the subject onto the projection vector. That is a high-dimensional space reduce to an one dimensional space, a value, which represent a subject from different groups. A two-sample t test is adopted to these values to calculate t value of each regions. That means, we can obtain a whole brain confidence to demonstrate the significance level of each regions by calculating T-statistic. Each voxel in the same regions will have same t statistic value. Once we know the important regions by T-statistic value, we may be interested not only in the regions we found but also the more precise location of this region. Therefore, weights of the discriminant map is shown with a smoothing and thresholding (optional). Each parameter of the discriminating map denotes the discrimination of characterizing the group discrepancy, the changes of the weight of neighboring parameters should be slight. However, in practice, it does not often look smooth because of the error produced during the preprocessing of a bad image registration or tissue segmentation or because of the noise or the variation within groups. Some errors may be produced by an imperfect image registration. To overcome these problems, the smoothness is used with a 6 millimeter FWHM gaussian kernel. The smoothing and thresholding are used for visualization of discriminant map to show the location of the group differences.

In summary, the parcelation-based multivariate morphometry contains the following steps:

1. Bias correction of T1 images
2. Brain extraction
3. Segmentation of the brain only images into GM, WM, and CSF
4. Spatial normalization of all images to the same stereotactic space
5. Creation of customized template
6. Spatial normalization of all segmented images to the customized template space
7. Modulation

8. Multivariate analysis
 - (a) Extraction of regions of brain
 - (b) Discriminative common vector method to obtain the most discriminant projection vector
 - (c) Combination of resulting discriminant projection vector
9. Visualization of the discrepancy pattern
 - (a) Smoothing
 - (b) Thresholding

Figure 3.3 is the flowchart of the parcellation-based multivariate analysis without the preprocessing steps. In the following sections we will introduce the techniques used in the multivariate analysis step, including the discriminative common vector method and the combination method of resulting discriminative common vector.



3.3 Multivariate Analysis using a Modified LDA-Based Method

3.3.1 Conventional Linear Discriminant Analysis and Its Potential Problem

Fisher's Linear discriminant analysis (LDA) is one of the most popular linear classification techniques which is invented in 1936 and the methods has been used in statistics and machine learning to find the linear combination of features which best separate two or more classes of objects or events. The objective of this method is to find the most discriminant projection vector \mathbf{P} , in which different groups can be separated with the maximum between-class scatter matrix and the minimum within-class scatter matrix. The most projection matrix \mathbf{P}_{lda} that maximizes the Fisher's linear discriminant criterion, which is

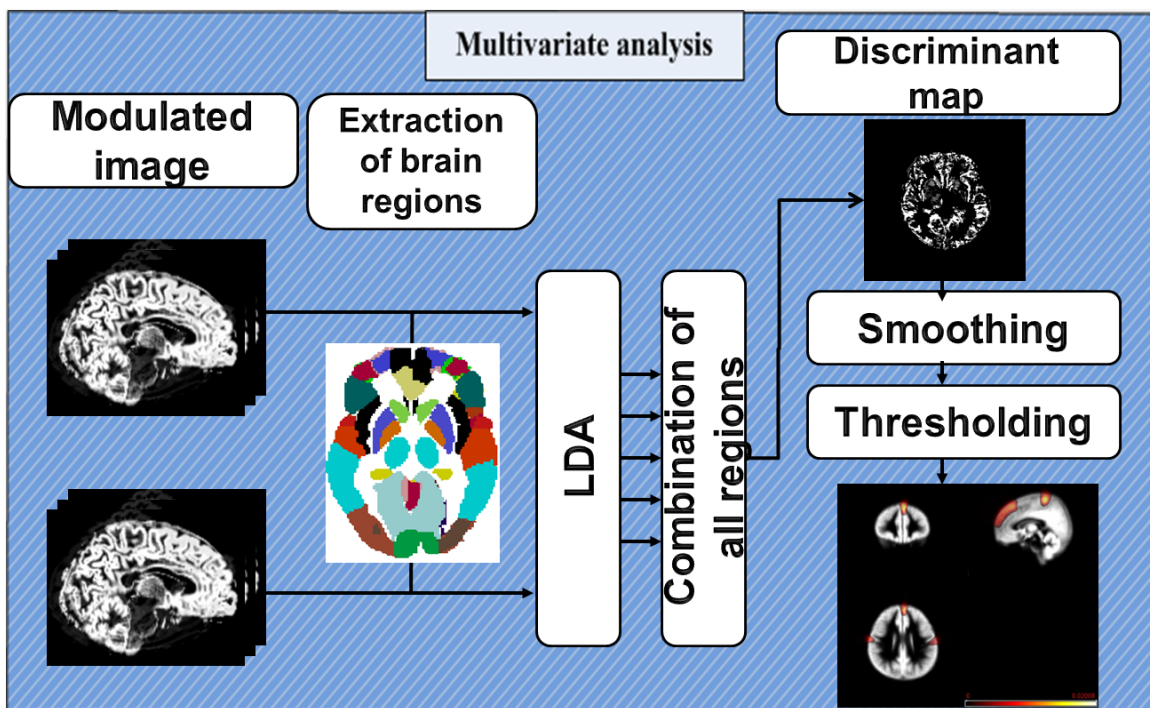


Figure 3.3: **Flowchart of parcellation-based multivariate analysis.** After the preprocessing, in the parcellation-based multivariate analysis we first extract the regions of brain, and then we apply the discriminative common vector method to each region and the correction is done before combination. Finally, we combine all the results of every region in brain back to original brain.

defined as

$$\mathbf{P}_{\text{lda}} = \arg \max_{\mathbf{P}} F(\mathbf{P}) = \arg \max_{\mathbf{P}} \frac{|\mathbf{P}^T \mathbf{S}_b \mathbf{P}|}{|\mathbf{P}^T \mathbf{S}_w \mathbf{P}|}. \quad (3.1)$$

and the between-class scatter matrix and the within-class scatter matrix are defined as following. Let the training set (subjects) be composed of C classes (groups), where each classes (i th class) contain S_c samples, and let \mathbf{x}_j^i be a d -dimensional column vector which denotes the j th sample of the i th class. There will be a total $M = \sum_{i=1}^C \sum_{j=1}^{S_c} x_j^i$ samples. The within-class scatter matrix \mathbf{S}_w is defined as

$$\mathbf{S}_w = \sum_{i=1}^C \sum_{j=1}^{S_c} (\mathbf{x}_j^i - \mu^i)(\mathbf{x}_j^i - \mu^i)^T, \quad (3.2)$$

and the between-class scatter matrix \mathbf{S}_b is defined as

$$\mathbf{S}_b = \sum_{i=1}^C S_c (\mu^i - \mu)(\mu^i - \mu)^T, \quad (3.3)$$

where $\mu^i = 1/S_c \sum_{j=1}^{S_c} \mathbf{x}_j^i$ is the mean of samples in the i th class, and $\mu = 1/M \sum_{i=1}^C \sum_{j=1}^{S_c} \mathbf{x}_j^i$ is the mean of all samples.

According to Lagrange multiplier, the ratio is maximized when the column vectors of \mathbf{P}_{lda} are the eigenvectors of $\mathbf{S}_w^{-1} \mathbf{S}_b$. And there are only two classes (groups) in our study case. Therefore, we can obtain the most discriminant projection vector \mathbf{P} by the formula $\mathbf{P} = \mathbf{S}_w^{-1}(\mu^1 - \mu^2)$.

However, in group analysis of MR images, FLDA cannot be applied directly. It is because of the dimension (voxels) of the sample space is larger than the number of the samples of training set. The within-class scatter matrix S_w will be singular in this case that is \mathbf{S}_w^{-1} can not be calculate. This problem is also known as the small sample size (SSS) problem [28]. Therefore we introduce another method called discriminative common vector method [27] based on the variation of Fisher's Linear Discriminant Analysis for solving the small sample size problem.

3.3.2 Discriminative Common Vector Method

The discriminative common vector method is based on a modification of the LDA method by maximizing the modified Fisher's linear discriminant criterion to solve the small sample size (SSS) problem. The basic idea of the common vector is extracting the common properties of classes in the training set by eliminating the differences of the samples in each class. That is, a common vector for each individual class is obtained by removing all the features that are in the direction of the eigenvectors corresponding to the nonzero eigenvalues of the scatter matrix of its own class. After getting each individual common vector of every class, The principal components analysis (PCA) is used to find the principal components which actually equate the most discriminant projection vectors of LDA.

Let us use all previous definitions then the total scatter matrix be defined as

$$\mathbf{S}_t = \sum_{i=1}^C \sum_{j=1}^{S_c} (\mathbf{x}_j^i - \mu)(\mathbf{x}_j^i - \mu)^T = \mathbf{S}_w + \mathbf{S}_b. \quad (3.4)$$

The modified Fisher's linear discriminant criterion will be

$$\hat{F}(\mathbf{P}) = \frac{|\mathbf{P}^T \mathbf{S}_b \mathbf{P}|}{|\mathbf{P}^T \mathbf{S}_t \mathbf{P}|} = \frac{|\mathbf{P}^T \mathbf{S}_b \mathbf{P}|}{|\mathbf{P}^T \mathbf{S}_w \mathbf{P} + \mathbf{P}^T \mathbf{S}_b \mathbf{P}|} \quad (3.5)$$

The modified Fisher's criterion is exactly equivalent to the original Fisher's criterion which has been proved by Liu et al. [29], that is in formula:

$$\arg \max_{\mathbf{P}} \hat{F}(\mathbf{P}) = \arg \max_{\mathbf{P}} F(\mathbf{P}). \quad (3.6)$$

To solve the small sample size problem, the modified Fisher's criterion will attain a maximum in the special case, where $\mathbf{p}^T \mathbf{S}_w \mathbf{p} = 0$ and $\mathbf{p}^T \mathbf{S}_b \mathbf{p} \neq 0$, for all $\mathbf{p} \in \mathbb{R}^N \setminus \{0\}$. Then the projection vector \mathbf{p} does not necessarily maximize the between-class scatter matrix \mathbf{S}_b , and a better criterion will be

$$\arg \max_{|\mathbf{P}^T \mathbf{S}_w \mathbf{P}|=0} |\mathbf{P}^T \mathbf{S}_b \mathbf{P}| = \arg \max_{|\mathbf{P}^T \mathbf{S}_w \mathbf{P}|=0} |\mathbf{P}^T \mathbf{S}_t \mathbf{P}|. \quad (3.7)$$

That is to say, the special case is when all samples are projected onto the null space of \mathbf{S}_w to make the the projected within-class scatter matrix to be a zero matrix, $|\mathbf{P}^T \mathbf{S}_w \mathbf{P}| = 0$.

Then we can obtain the optimal projection vectors by performing PCA. The method solving the small sample size problem is called the null space method which is proposed by Chen et al. [28]. However the computation of the null space method can be very large because of the large dimension in null space. Another efficient way to calculate in a lower dimensional space is by using the orthogonal complement of the null space of S_W .

The transformation matrix from the original sample space to the null space of S_W is $\bar{Q}\bar{Q}^T$, where the column vectors of \bar{Q} are the vectors spanning the null space of S_W . And the transformation matrix from the original sample space to the rang space of S_W is QQ^T , where the column vectors of Q are the vectors spanning the range space of S_W . Cevikalp and Wilkes [27] have proved that, the projections of the samples \mathbf{x}_j^i (which denotes the j th sample of the i th class) of the class i onto the null space of S_W produce a unique common vector $\mathbf{x}_{\text{com}}^i = \bar{Q}\bar{Q}^T \mathbf{x}_j^i$, in addition, because of

$$\mathbf{x}_j^i = \bar{Q}\bar{Q}^T \mathbf{x}_j^i + QQ^T \mathbf{x}_j^i \quad (3.8)$$

then the common vector $\mathbf{x}_{\text{com}}^i$ of the i th class can be calculated without \bar{Q} by using

$$\mathbf{x}_{\text{com}}^i = \mathbf{x}_j^i - QQ^T \mathbf{x}_j^i, \quad (3.9)$$

We can figure out that, instead of computing the common vector $\mathbf{x}_{\text{com}}^i = \bar{Q}\bar{Q}^T \mathbf{x}_j^i$, we compute the common vector $\mathbf{x}_{\text{com}}^i = \bar{Q}\bar{Q}^T \mathbf{x}_j^i$. which the number of columns in \bar{Q} is about $d - M$ (d is the total number of dimension of the sample size and M is the total sample size) but the number of columns in Q is about M . Thus the size of Q is much smaller than \bar{Q} . The method greatly reduce the computational rather than the null space method.

After obtaining the common vectors $\mathbf{x}_{\text{com}}^i$, optimal projection vectors will be those that maximize the total scatter of the common vectors,

$$\arg \max_{\mathbf{P}^T S_W \mathbf{P} = 0} |\mathbf{P}^T S_t \mathbf{P}| = \arg \max_{\mathbf{P}} |\mathbf{P}^T S_{\text{com}} \mathbf{P}|. \quad (3.10)$$

where S_{com} is the scatter matrix of the common vectors,

$$S_{\text{com}} = \sum_{i=1}^C (\mathbf{x}_{\text{com}}^i - \mu_{\text{com}})(\mathbf{x}_{\text{com}}^i - \mu_{\text{com}})^T, \quad (3.11)$$

where μ_{com} is the mean of all common vectors, $\mu_{\text{com}} = 1/S_c \sum_{i=1}^C \mathbf{x}_{\text{com}}^k$.

In this case, optimal projection vectors can be found by an eigenanalysis of S_{com} . In particular, all eigenvectors corresponding to the nonzero eigenvalues of S_{com} will be the optimal projection vectors.

$$\mathbf{A}_{\text{com}} = \sum_{i=1}^C (\mathbf{x}_{\text{com}}^i - \mu_{\text{com}})(\mathbf{x}_{\text{com}}^i - \mu_{\text{com}})^T, \quad (3.12)$$

In our practice, samples are divided into only two groups, there will be one optimal projection vectors since the rank of S_{com} is $C - 1$ ($C = 2$) if all common vectors are linearly independent. These principal components of the common vectors are called the discriminative common vectors. We obtain the most discriminant projection vector \mathbf{P} by computing the eigenvectors of S_{com} , corresponding to the nonzero eigenvalues. There are at most $C - 1$ ($C = 2$) eigenvectors that correspond to the nonzero eigenvalues which is the most discriminant projection vector.

So the steps of the discriminative common vector method are as follows:

1. Compute the eigenvectors $\alpha_1, \alpha_2, \dots, \alpha_r$ corresponded to the nonzero eigenvalues of \mathbf{S}_W , where r is the rank of \mathbf{S}_W , and set $\mathbf{Q} = [\alpha_1 \ \alpha_2 \ \dots \ \alpha_r]$.
2. Obtain the common vectors for each class by choosing any sample from each class and projecting it onto the null space of \mathbf{S}_W , those are

$$\mathbf{x}_{\text{com}}^1 = \mathbf{x}_j^1 - \mathbf{Q}\mathbf{Q}^T \mathbf{x}_j^1, \quad j \in \{1, \dots, S_1\}, \quad (3.13)$$

and

$$\mathbf{x}_{\text{com}}^2 = \mathbf{x}_j^2 - \mathbf{Q}\mathbf{Q}^T \mathbf{x}_j^2, \quad j \in \{1, \dots, S_2\}. \quad (3.14)$$

3. Compute the eigenvectors of S_{com} , corresponding to the nonzero eigenvalues, by using the matrix $\mathbf{A}_{\text{com}}^T \mathbf{A}_{\text{com}}$, There are at most $C - 1$ eigenvectors that correspond to the nonzero eigenvalues which is the most discriminant projection vector.

3.3.3 The Problem of Combining The Unit Projection Vector

Once, we get the most projection vector, the weights of this projection vector which represents the discrimination level for characterizing group differences is an unit vector. There is a problem that weights of a unit vector with a highly dimensional space will be smaller than of a unit vector with a low dimensional space. That is, if there are two different regions with same variation of brain tissues, the weight of two different regions should be the same with each other. But the weight of the unit projection vector is much smaller in a high-dimensional space. For example, assume region 1 has n voxels and region 2 has m voxels with the same atrophy level a , after analysis we will get

$$P_{\text{lda}}^1 = [w_1 \cdots w_n], w_1 = \cdots = w_n = \frac{1}{\sqrt{n}}, \quad (3.15)$$

and

$$P_{\text{lda}}^2 = [w_1 \cdots w_m], w_1 = \cdots = w_m = \frac{1}{\sqrt{m}}, \quad (3.16)$$

where P_{lda}^1 is the projection vector in first region and P_{lda}^2 is the projection vector in second region. According to the same atrophy level, the weight of two projection vector should be same. but it is not because of the unit vector. Thus we project two regions onto the most projection vector, there will form two distance in two different regions which is calculus by two different means. we can have formula

$$P_{\text{dist}}^1 = P_{\text{lda}}^1 GM^1 = a\sqrt{n}, \quad (3.17)$$

and

$$P_{\text{dist}}^2 = P_{\text{lda}}^2 GM^2 = a\sqrt{m}, \quad (3.18)$$

where P_{dist}^i is the distance of projected group mean in region i , GM^i is the group mean in region i $i = 1, 2$. The correction of the P_{lda}^1 and P_{lda}^2 is

$$P_{\text{correct}}^1 = P_{\text{lda}}^1 P_{\text{dist}}^1 = [a \cdots a]^T, \quad (3.19)$$

and

$$P_{\text{correct}}^2 = P_{\text{lda}}^2 P_{\text{dist}}^2 = [a \cdots a]^T. \quad (3.20)$$

Therefore, we let the two projection vector in different region with the same weight for characterizing group differences when the atrophy level is identical.



Chapter 4

Experiment Results



4.1 Simulation Analysis

In this section we provide experiments that demonstrate the performance of parcellation-based multivariate approach by using simulated atrophy data. The validation is that the proposed method can detect more subtle differences between different groups. The simulation data is generated by an atrophy simulation package which is proposed by Bilge Karacali in 2006 [30]. The reason why we use the simulation data is to get the ground truth to compare the group differences. The method of data generation, accuracy evaluation and experiment results will be described.

4.1.1 Simulation Data Generation

The atrophy simulation data set is generated by using atrophy simulation package [30] and the normal data set is selected from real data set. In normal group, normal subjects are selected and the preprocessing is done in advance including inhomogeneity correction, brain extraction and tissue segmentation. All normal T1 images are segmented into GM/WM/CSF and subsequently spatially normalized into a customized template. This image data set in the same space are taken to be simulated normal group and there are 28 normal subjects is selected.

In the simulated atrophy data set, we use atrophy simulation package which simulate atrophy and growth within a spherical region of an input image. That is we generate the patient group from simulated normal control. The approach of atrophy simulation package is to seek a deformation that produces volumetric changes or volumetric loss. In order to make the simulation realistic, there are three conditions is considered. Firstly, the warping transformation of the atrophy should be obtained with no volumetric restrictions over the cerebrospinal fluid. That is to say, letting the brain-cerebrospinal fluid boundary move freely through the simulation. Secondly, the deformation over the skull should be zero since it does not get affected by the atrophy of the brain tissue. In the last, to constrain the solution to within a class of deformations for which topology is preserved. With these

conditions, we use atrophy simulation package to generate the simulated atrophy data from the simulated normal group one by one. The generated deformation fields are used to modulate the normal groups to get the patient groups. There will be 28 simulated atrophy images generated from the other 28 normal data set in the patient group.

In summary, we have generated 28 patients from 28 normal controls, and all of them are in the same space. The atrophy simulation package produces a simulated atrophy deformation which is used to modulate the normal groups to get the patient groups. The atrophy scale is from 1 millimeter to 4 millimeter respectively. The location of the center voxel of the spherical region is at voxel (187, 141, 124) which is in the left precentral gyrus, all images are normalized to a template space that the voxel size is $1 \times 1 \times 1\text{mm}^3$ and the size of the images is $259 \times 259 \times 185$.

4.1.2 Accuracy Evaluation

In the accuracy evaluation, we have to know the ground truth of the simulation data. By the use of the simulation atrophy package, we control the simulation parameters such as atrophy scale, location and rate. That is, the simulation data is controlled by us. Ground truth refers to information that contains the discrepancy between simulated normal and patient groups. It is obtained by subtracting patient groups, which is generated by simulation package, from normal groups. In practice, we subtract average of the patient groups from average of the normal groups to get the ground truth of each simulation data set. The positive value in the ground truth represent the atrophy location and the negative values is the enlarge location.

Once we know the ground truth and the analysis results of the simulation data which is the discriminant map of parcellation-based multivariate morphometry analysis or t-test map of VBM analysis. We can classify every voxels into 4 category which is true-positive (TP), false-positive (FP), true-negative (TN) and false-negative (FN). The four terms TP, FP, TN and FN is described in order:

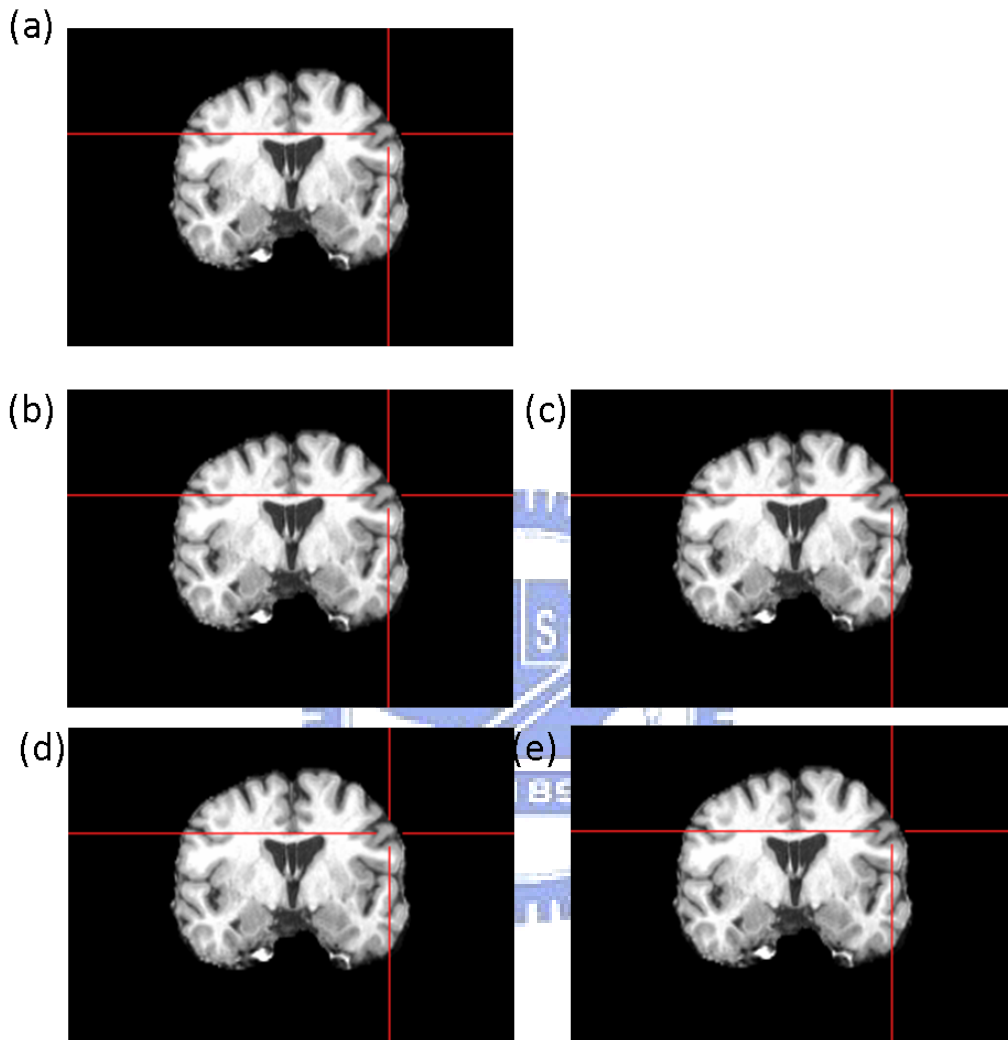


Figure 4.1: **The normal and the simulated atrophy images by Atrophy Simulation Package.** (a) is a normal image which is also a source for the package to generate the simulated atrophy image. (b),(c),(d),(e) are the simulated patient images with atrophy scale of 1mm, 2mm, 3mm, 4mm respectively. The images are for display only, actually we use the GM images with the Atrophy Simulation Package to obtain the atrophy deformation fields respectively. The size of these images are all $259 \times 259 \times 185$ with a voxel size $1 \times 1 \times 1\text{mm}^3$. The red cross is place on the voxel (187,141,124).

Table 4.1: Definitions of TP, FP, TN, and FN.

Actual value	Predicted outcome	
	Yes	No
Yes	TP	FN
No	FP	TN

- True-positive (TP): voxels in the analysis result reveal that it is in the atrophy area, and voxels in the ground truth reveal that it is also in the atrophy area;
- False-positive (FP): voxels in the analysis result reveal that it is in the atrophy area, and voxels in the ground truth reveal that it is **not** in the atrophy area;
- True-negative (TN): voxels in the analysis result reveal that it is **not** in the atrophy area, and voxels in the ground truth reveal that it is **not** in the atrophy area;
- False-negative (FN): voxels in the analysis result reveal that it is **not** in the atrophy area, and voxels in the ground truth reveal that it is in the atrophy area;

Table 4.1 shows the definitions of TP, FP, TN and FN. There are four possible outcomes from a binary classifier. If the outcome from a prediction is yes and the actual value is also yes, then it is called a true positive (TP); however if the actual value is no then it is said to be a false positive (FP). Conversely, a true negative has occurred when both the prediction outcome and the actual value are no, and false negative is when the prediction outcome is no while the actual value is yes. Moreover, the rates of TP, FP, TN and FN are defined as:

$$TPrate = \frac{TP}{TP + FN}, \quad (4.1)$$

$$FPrate = \frac{FP}{TN + FP}, \quad (4.2)$$

$$TNrate = \frac{TN}{TN + FP}, \quad (4.3)$$

$$FNrate = \frac{FN}{TP + FN}. \quad (4.4)$$

These regions can be shown to compare two morphometric analysis methods after labeling each voxels with TP, FP, FN and TN. Under the same FP rate, we compare the result of TP rate and FN rate with each other. The result with more TP regions and fewer FP regions indicate a high accuracy or performance.

Another evaluation method is receiver operating characteristic (ROC) curve [31]. It measures the performance of the method and is a graphical plot of the sensitivity and (1 - specificity) for a binary classifier system as its discrimination threshold is varied. The ROC curve can also be represented equivalently by plotting the fraction of true positives (TPR = true positive rate) and the fraction of false positives (FPR = false positive rate). The sensitivity is the TPR which means that the ability of an analysis method to detect voxels with actually atrophy; and the specificity is the TNR which means the ability of an analysis method to detect voxels without actually atrophy. We can obtain these rate by varying the parameter (threshold) of the analysis results, which are refer to the discriminant map of multivariate analysis or *t*-test map of VBM. That is, the sensitivity and the 1-specificity can be plotted with various threshold of discriminative map. Any system that appears in the lower right triangle performs worse than random guessing in ROC curve. That is, any method on the diagonal may be said to have no information about the method and the method above the diagonal is said to have information about the method. However, we may want to reduce ROC performance to a single scalar value representing the performance to compare methods. One of the common method is to calculate the area under the ROC curve (AUC). The AUC is a portion of the area of the unit square, its value will always be between 0 and 1.0. In this work, we look at a specific region of the ROC Curve rather than at the whole curve by using the partial area under the curve (PAUC) to compare different ROC curves. The reason is that the curve is not long enough, and we could only focus on the region of the curve with a same false positive rate. The concept of the AUC and PAUC is similar that the AUC/PAUC with a larger area will have a better performance to the method we use. Figure 4.2 gives an example of a ROC curve.

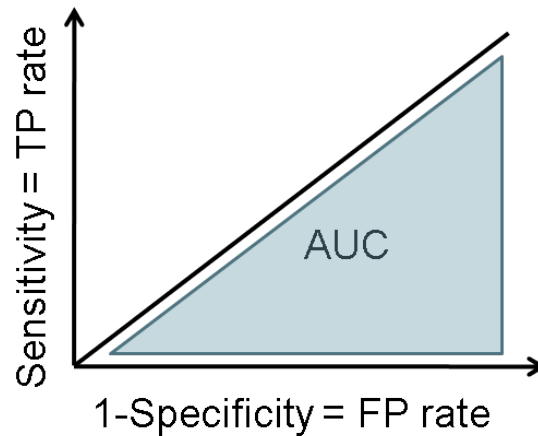


Figure 4.2: **Example of a ROC curve.** It measures the performance of the method and is a graphical plot of the sensitivity and (1 - specificity) for a binary classifier system as its discrimination threshold is varied. Any method that appears in the upper left triangle performs better than random guessing in ROC curve. To compare methods, we calculate the (partial) area under the ROC curve (AUC), which indicates better performance with a larger AUC/PAUC.

4.1.3 Comparisons of Proposed Method and VBM

Both of the parcellation-based multivariate morphometry method (PBM) and VBM method is used to analyze the simulation data. The simulation data is smoothed with a $12mm$ FWHM isotropic gaussian kernel before the VBM analysis. Subsequently, we applied a voxel-wise two sample t -test to form a discriminant t -test map which can identify the significance level of each voxel by judging t statistics value. Although the smoothed simulation data is used, Data smoothing is omitted in proposed method that the information of each voxel may be damaged by smoothing them. We first parcellate all simulated images into several regions by a template which is defined by Anatomical Automatic Labeling (AAL). And then we applied the discriminative common vector method to each region to obtain the most discriminant map of each region. Finally, we combine these resulting discriminant map back into original brain rather than a parcellated map.

After we obtain the discriminant map of two method, the ROC curve is formed with simulation data which is atrophied in the scale of $1mm$ to $4mm$ respectively. Thus there

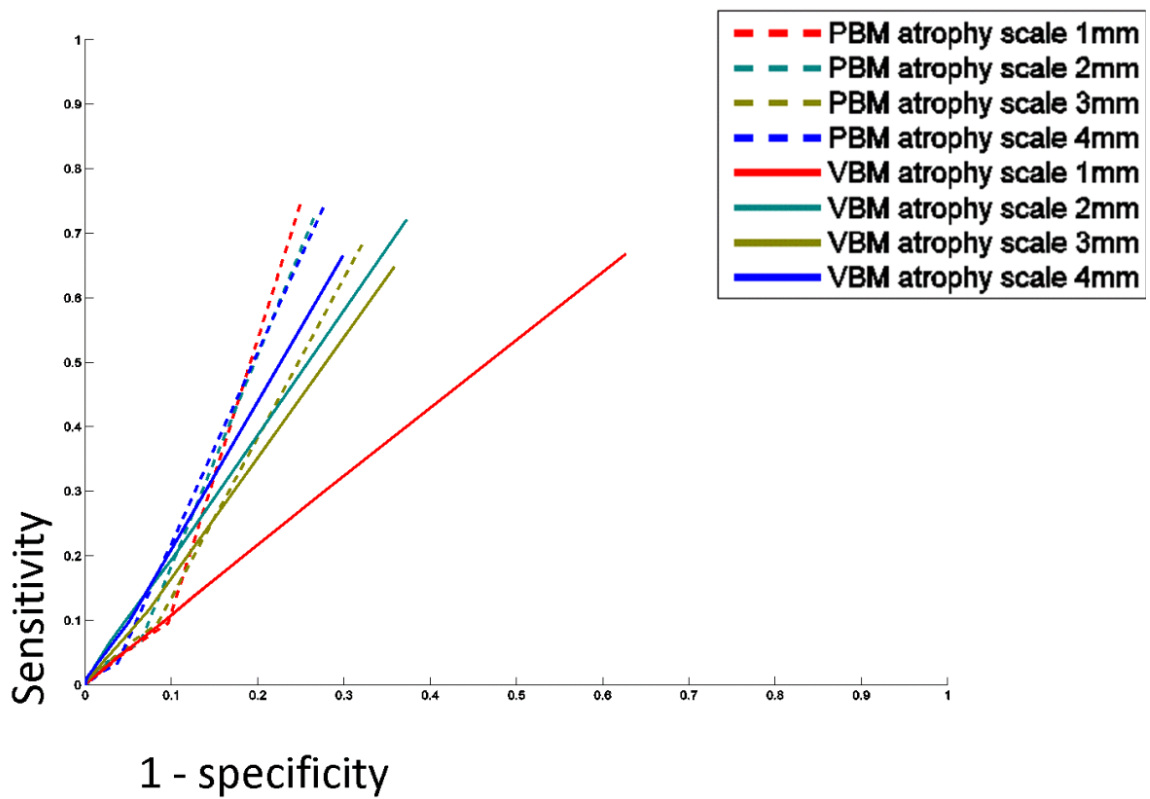


Figure 4.3: ROC curves of PBM and VBM results with the simulation data. Notice that both horizontal axes are limited from 0 to 1 and both vertical axes are limited from 0 to 1 for more specific display.

Table 4.2: PAUC indices for ROC curves of parcellation-based multivariate morphometry (PBM) and VBM results with the simulation data. The partial area was calculated in a specific region where the TP rate ranges form 0 to 1 and the FP rate ranges form 0 to 1. As this specific region denotes 1, we have $0 \leq \text{PAUC} \leq 1$. It is manifest that PBMM PAUC indices are greater than VBM ones in the same analysis data, especially when the simulated atrophy scale is small. Comparisons of each ROC curve between each atrophy scale, that with the increase of the atrophy scale, the performance of both method is also increased.

Atrophy scale = 1 mm		Atrophy scale = 2 mm	
PBM	VBM	PBM	VBM
0.2592	0.2263	0.2694	0.2075

Atrophy scale = 3 mm		Atrophy scale = 4 mm	
PBM	VBM	PBM	VBM
0.20185	0.1916	0.28583	0.24055

will be 4 simulation data sets for detecting simulated group difference by our proposed method and VBM analysis. Figure 4.3 graphically summarizes each result and the TPR and FPR range from 0 to 1 and 0 to 0.25 and the corresponding PAUC is listed in Table 4.2. The comparisons of PBM and VBM in Figure 4.3 is clear that the ROC curve of PBM is above the ROC curve of VBM in each result. which means the result of PBM method can detect more subtle and distributed patterns than VBM method. Besides, with the increase of the atrophy scale from 1 mm to 4 mm, although the resulting ROC curve of VBM becomes more and more accurate, the resulting ROC curve of PBM method is always better than VBM method, as we can see in Figure 4.3. The partial area under the curve (PAUC) is calculated according to TPR and FPR which is also shown that PBM has greater PAUC than VBM in the result within a specific atrophy scale. Moreover, the PAUC is increasing with the atrophy scale from 1mm to 4mm, 6mm and 8mm. That means with the increase of the atrophy scale, the performance of both method is also increased. Figure 4.3 and Table 4.2 illustrate a better performance of our method.

4.2 Real Data Analysis

4.2.1 Materials

The study involved 89 subjects. The subjects suffering from bipolar disorder I (BDI) is consisted of 10 and 7 female (*age* : 20 – 55, *mean* \pm *SD*, 37.29 ± 10.29); the subjects suffering from bipolar disorder II (BDII) is consisted of 4 male and 15 female (*age* : 20 – 61, *mean* \pm *SD*, 37.58 ± 10.79); the subjects suffering major depressive disorder (MDD) is consisted of 9 male and 16 female (*age* : 23 – 56, *mean* \pm *SD*, 36.76 ± 9.91); the healthy subjects is consisted of 11 male and 17 female (*age* : 21 – 57, *mean* \pm *SD*, 37.35 ± 11.68). The clinical data is summarized in Table 4.3.

	Male	Female	Age	Education
BDI	10	7	37.29 ± 10.29	13.8 ± 2.14
BDII	4	15	37.58 ± 10.79	14.94 ± 1.95
MDD	9	16	36.76 ± 9.91	14.28 ± 1.88
Healthy control	11	17	37.35 ± 11.68	15.35 ± 2.31

Table 4.3: **Clinical data of each groups.** and all MR images are collected by Integrated Brain Research Unit (IBRU) of Taipei Veterans General Hospital.

4.2.2 MRI acquisition

All subjects were scanned on the same 1.5 Tesla GE MR scanner, using a 3-dimensional-FSPGR pulse sequence (TR = 8.67 ms, TE = 1.86 ms, TI = 400 ms, NEX = 1, flip angle = 15° , bandwidth = 15.63 kHz, matrix size = $256 \times 256 \times 124$, voxel size = $1.02 \times 1.02 \times 1.5\text{mm}^3$). All MR scans were collected by Integrated Brain Research Unit (IBRU) of Taipei Veterans General Hospital.

4.2.3 Results and Comparisons of PBM and VBM

In the VBM analysis, according to the implementation of VBM, all images were pre-processed before the voxel-wise statistics analysis including inhomogeneity correction with N3, brain extraction with HWA, tissue segmentation with FAST, two spatial normalization and modulation. ALL of the steps were perform on a linux server. These images were spatial normalized to a customized template without changing the voxel size that is the normalized images had a high resolution with the voxel size unchanged. And then the smoothing is perform with a 12 mm FWHM isotropic Gaussian kernel. Subsequently, we applied a two-sample t -test, and set the significance level at $p < 0.005$ uncorrected (i.e. t value > 2.69 as degree of freedom = 44 in MDD analysis) for the final t -test map. In the PBM analysis, it is similar with the preprocessing of the VBM analysis, the differences is that we eliminate the smoothing steps for the PBM analysis. Then we parcelled brain into several regions to calculate the most discriminant map respectively in each region. Finally, after we have obtained the most discriminant map of each region, we combine them back into original brain. An 6 mm FWHM isotropic Gaussian kernel was used for the visualization of the PBM result. In the visualization of the discriminant map, a threshold is chosen by statistics t value which has a significant level at $p < 0.005$ uncorrected in VBM analysis, but the threshold in PBM can not be chosen in this way. However, we choose a compatible threshold of PBM by t -test map of VBM analysis result. That is by choosing a range of t value in VBM then search the regions whose t value are within the range, and finally we choose the mean threshold of the same regions found in PBM for analysis. Thus we can have a compatible threshold for visualization of PBM result. A minimum cluster size is used with the size set in 200 voxels. Finally, there will be a discriminant map and a t -test map of each regions in PBM analysis. Only a discriminant t test map is shown in VBM analysis. Figure 4.4 is the concept of choosing the threshold.

Figure 4.5 illustrates statistic t value of each region in MDD patients by PBM analysis method. The significant level of t value is listed in Table 4.4, As we can see, comparing the variety of regions of MDD patients to normal controls. Regions with a high significant level were in frontal lobe (left and right middle frontal gyrus, left and right superior frontal

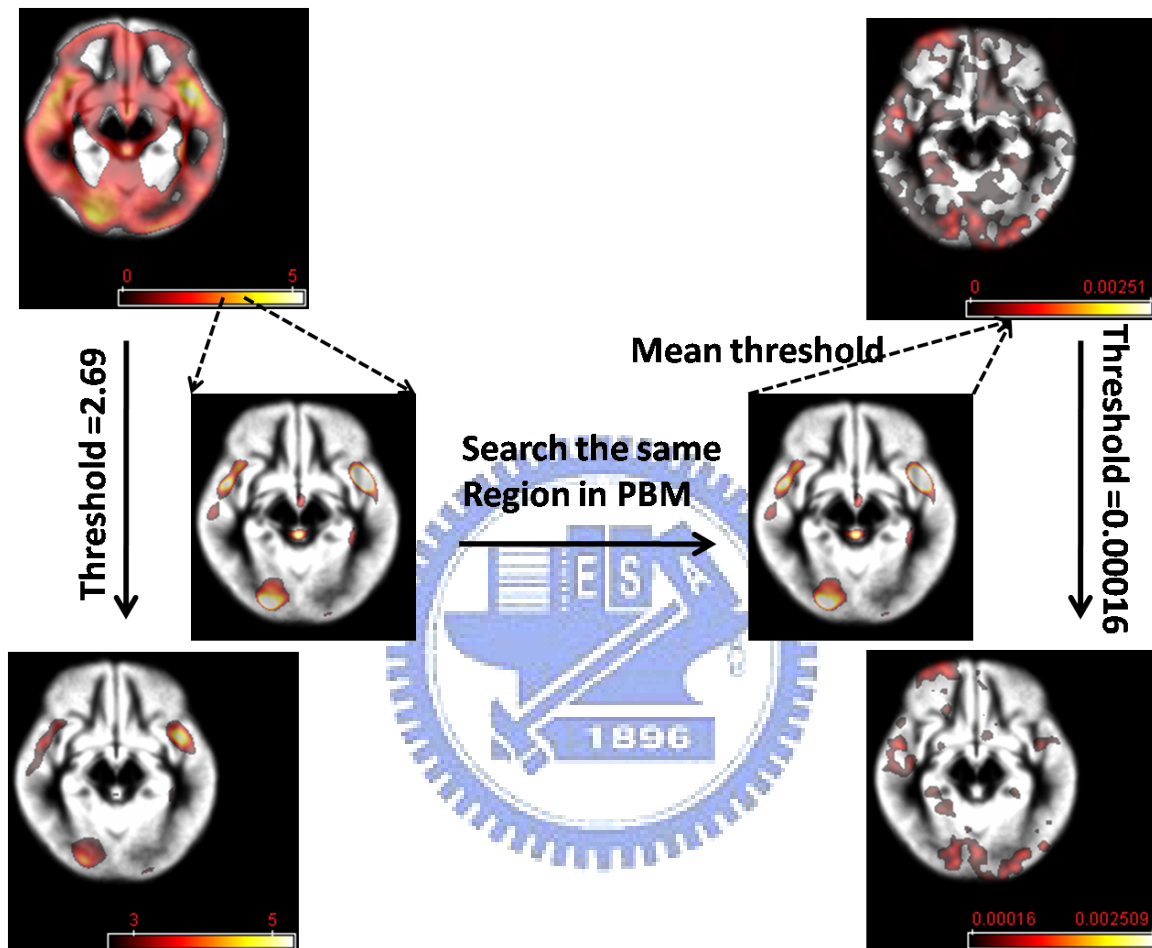


Figure 4.4: Concept of choosing a compatible threshold of PBM by t -test map of VBM analysis result. First we choose a range of t value in VBM then search the regions whose t value are within the range, and finally we choose the mean threshold of the same regions found in PBM for analysis. For examples, we choose t value within 2.69 and 3.69. Search regions whose t value are in this range. And then we map these regions to the PBM result and calculate the mean weight of these regions to be the threshold in PBM analysis.

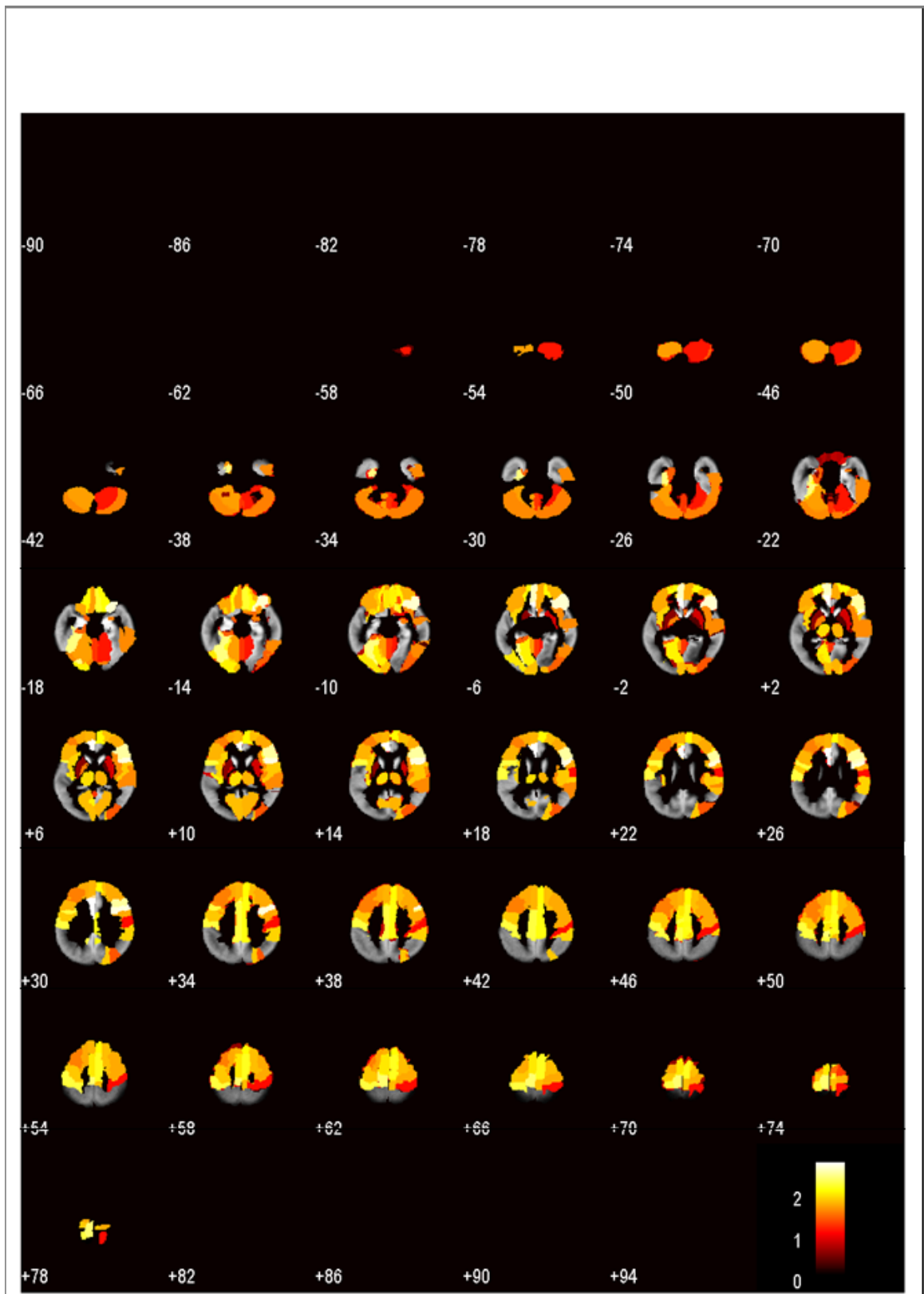


Figure 4.5: Statistics t value within each region in MDD patients by PBM analysis method is shown. Each statistics t value information within each region is listed in Table 4.4.

Table 4.4: Statistics t value within each region in MDD patients by PBM analysis method in MDD. These statistic t values are arranged in order by the t value of each region, and the corresponding locations in AAL labeling are listed.

AAL label side	t value	AAL label side	t value
AMYGDD Amygdala R 4202	2.694	T3D Temporal Inf R 8302	1.9445
F3TD Frontal Inf Tri R 2312	2.6208	F2G Frontal Mid L 2201	1.9256
F3OPD Frontal Inf Oper R 2302	2.5236	CERCRO1G Cerebellum Crus1 2 R 9997	1.9153
F1OD Frontal Sup Orb R 2112	2.4482	HESCHLG Heschl L 8101	1.8961
LPCD Paracentral Lobule R 6402	2.4119	T1G Temporal Sup L 8111	1.8815
PQD Precuneus R 6302	2.3934	O3D Occipital Inf R 5302	1.8776
V1D Calcarine R 5002	2.3149	FMD Frontal Sup Medial R 2602	1.8753
O3G Occipital Inf L 5301	2.2902	FMOG Frontal Med Orb L 2611	1.8354
V1G Calcarine L 5001	2.2712	PAG Postcentral L 6001	1.8318
FMOD Frontal Med Orb R 2612	2.2697	F1D Frontal Sup R 2102	1.794
FAD Precentral R 2002	2.2595	F1G Frontal Sup L 2101	1.7522
ORD Rolandic Oper R 2332	2.245	T1AD Temporal Pole Sup R 8122	1.7491
LINGG Lingual L 5021	2.23	COBD Olfactory R 2502	1.741
HESCHLD Heschl R 8102	2.2298	F2D Frontal Mid R 2202	1.6967
COBG Olfactory L 2501	2.159	CERCRO1G Cerebellum Crus1 2 L 9996	1.6647
CIPG Cingulum Post L 4021	2.1531	P2D Parietal Inf R 6202	1.5805
F3TG Frontal Inf Tri L 2311	2.1322	FAG Precentral L 2001	1.5734
GSMD SupraMarginal R 6212	2.1247	CER Cerebellum R 9998	1.515
PARA HIPPOD ParaHippocampal R 4112	2.1184	FMG Frontal Sup Medial L 2601	1.5107
CIAG Cingulum Ant L 4001	2.1151	CER Cerebellum L 9999	1.4532
SMAD Supp Motor Area R 2402	2.0814	PAD Postcentral R 6002	1.4437
T1AG Temporal Pole Sup L 8121	2.0678	GRG Rectus L 2701	1.3462
LINGD Lingual R 5022	2.052	VER Vermis all 9995	1.2895
CINMG Cingulum Mid L 4011	2.0448	ORG Rolandic Oper L 2331	1.2541
IND Insula R 3002	2.0116	PARA HIPPOG ParaHippocampal L 4111	1.2282
F3OPG Frontal Inf Oper L 2301	2.0026	THAG Thalamus L 7101	1.1801
T1D Temporal Sup R 8112	1.982	NCG Caudate L 7001	0.66337
F2OD Frontal Mid Orb R 2212	1.9721	CIPD Cingulum Post R 4022	0.50429
NLD Putamen R 7012	1.9636	PALLG Pallidum L 7021	0.44813
F2OG Frontal Mid Orb L 2211	1.961	NLG Putamen L 7011	0.42948

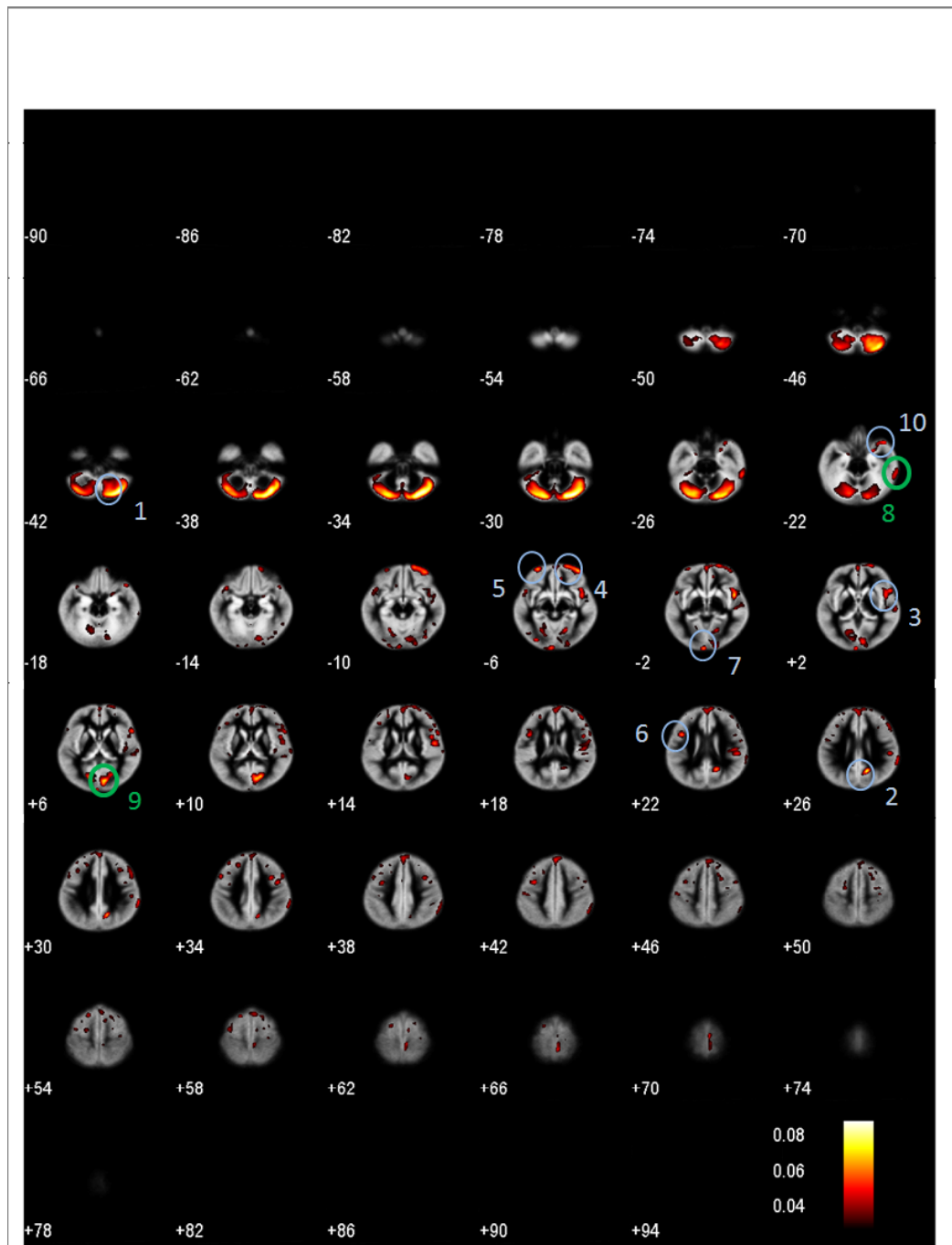


Figure 4.6: Volumetric atrophy of gray matter in MDD patients by PBM analysis method. Regions detected as significant group differences are marked with circles. One marked with a green circle is also found in the VBM analysis result; one marked with a blue circle is only revealed in the PBM result. Numbers of these circles represent the importance of characterizing volume loss in MDD patients. More information of each region is listed in Table 4.5.

Table 4.5: Atrophy of gray matter in MDD patients by PBM analysis method. These atrophy regions are arranged in order by their peak discrimination weights of each cluster, and the numbers denote the sequence of peak discrimination weights. The serial numbers are informative for revealing the significance of gray matter atrophy in MDD.

Location	BA	Side	Talairach coordinate			Peak discrimination	Cluster size	Fig. 4.6 no.
			x	y	z			
Cerebellum Posterior Lobe Pyramis	R	R	28.8471	-74.3515	-34.6086	0.0835	45257	1
Cerebrum Limbic Lobe Cingulate Gyrus	31	R	8.4718	-55.6847	27.6268	0.07	1251	2
Cerebrum Sub-lobar Insula	13	R	40.3298	5.5766	-4.7088	0.0655	9315	3
Cerebrum Frontal Lobe Superior Frontal Gyrus	11	R	33.2776	52.6233	-14.0448	0.064	9854	4
Cerebrum Frontal Lobe Middle Frontal Gyrus	11	L	-34.7413	56.3315	-12.5322	0.0585	559	5
Cerebrum Frontal Lobe Inferior Frontal Gyrus	44	L	-48.5911	13.5689	17.4811	0.0579	675	6
Cerebrum Occipital Lobe Cuneus	L	L	-13.8885	-99.3842	3.5755	0.0557	1150	7
Cerebrum Temporal Lobe Fusiform Gyrus	20	R	53.7814	-40.0059	-20.9259	0.0524	1064	8
Cerebrum Occipital Lobe Cuneus	30	L	-25.7484	-72.5119	10.3815	0.0508	1958	9
Cerebrum Temporal Lobe Superior Temporal Gyrus	38	R	37.2571	21.4833	-23.7627	0.0504	1197	10
Cerebellum Anterior Lobe Culmen	9	R	10.8073	-64.0117	-1.0662	0.0466	539	
Cerebrum Frontal Lobe Precentral Gyrus	9	L	-41.4675	6.7216	37.4873	0.0457	567	
Cerebrum Occipital Lobe Inferior Occipital Gyrus	18	L	-40.2202	-85.0376	-0.3781	0.0456	211	
No Gray Matter found			30.3335	15.5125	31.6105	0.045	442	
Cerebrum Parietal Lobe Inferior Parietal Lobule	40	R	58.4531	-33.7749	27.8275	0.0436	1616	
Cerebrum Frontal Lobe Superior Frontal Gyrus	8	L	-23.8241	28.1729	49.3901	0.0427	253	
Cerebrum Frontal Lobe Paracentral Lobule	6	L	-1.4681	-35.6515	65.3171	0.0411	1107	
Cerebrum Frontal Lobe Middle Frontal Gyrus	9	L	-56.6577	17.5451	30.6433	0.0409	394	
Cerebrum Temporal Lobe Superior Temporal Gyrus	38	L	-47.1569	16.6937	-15.3457	0.0405	951	
Cerebrum Frontal Lobe Middle Frontal Gyrus	46	R	40.6301	46.9065	8.5930	0.0403	577	
Cerebrum Occipital Lobe Middle Occipital Gyrus	18	R	31.4926	-79.3517	-5.0549	0.0373	443	
Cerebrum Frontal Lobe Middle Frontal Gyrus	6	L	-43.2563	1.3634	53.8648	0.0368	338	
Cerebrum Frontal Lobe Middle Frontal Gyrus	9	L	-25.7992	38.6552	26.0373	0.0366	305	
Cerebrum Frontal Lobe Middle Frontal Gyrus	6	L	-28.5588	-0.6377	48.1311	0.0356	324	
Cerebrum Frontal Lobe Middle Frontal Gyrus	46	L	-43.0841	43.2446	26.1357	0.0354	235	
Cerebrum Frontal Lobe Middle Frontal Gyrus	10	L	-30.7225	47.6949	9.0201	0.0347	321	
Cerebrum Parietal Lobe Postcentral Gyrus	3	L	-55.6938	-14.6022	43.0603	0.0342	314	
Cerebrum Frontal Lobe Middle Frontal Gyrus	46	L	-42.3639	29.0472	23.1151	0.0315	379	

gyrus, left inferior frontal gyrus), temporal lobe (left and right superior temporal gyrus), occipital lobe (inferior occipital gyrus, calcarine fissure), parietal lobe (inferior parietal lobe, supramarginal gyrus) and Cerebellum whose t value is relatively small. Figure 4.6 illustrate gray matter volume reduce in MDD patients by PBM analysis method. The detected significant atrophy is marked with a circle and number in Figure 4.6. The information of each marked circle is also listed in Table 4.5. Regions marked with green circle is found by both VBM and PBM method. Regions marked with blue circle is only found by PBM method.

Figure 4.6 illustrate gray matter volume reduce in MDD patients by VBM analysis method. The detected significant atrophy is marked with a circle and number in Figure 4.7. The information of each marked circle is also listed in Table 4.6. As we can see, comparing brain structures of MDD patients to normal controls, the reduction of GM is detected in the regions of temporal lobe (left and right superior temporal gyrus, inferior temporal gyrus), frontal lobe (middle frontal gyrus, superior frontal gyrus, left and right precentral gyrus), occipital lobe (middle occipital gyrus, lingual gyrus) and parietal lobe (postcentral gyrus). Regions marked with green circle is found by both VBM and PBM method. Regions marked with blue circle is only found by VBM method.

To compare the differences of brain structures of MDD and BD patients, there are several findings of volume loss of gray matter in dorsolateral prefrontal cortex (DL-PFC or DLPFC). The DLPFC is the area to develop myelinate in the human cerebrum and it is roughly consist of lateral portions of Brodmann areas 9 - 12, of areas 45, 46, and the superior part of area 47. DL-PFC is connected to the orbitofrontal cortex, and to a variety of brain areas, which include the thalamus, parts of the basal ganglia (the dorsal caudate nucleus), the hippocampus, and primary and secondary association areas of neocortex. This brain region has been implicated in planning complex cognitive behaviors, personality expression, decision making and moderating correct social behavior. The orbitofrontal cortex (OFC) is a region of association cortex of the human brain involved in cognitive processes such as decision-making. The name of this region is based upon the region's location within the frontal lobes, resting above the orbits of the eyes. It is defined as the part

of the prefrontal cortex and a more restricted definition of this area describes it as roughly equivalent to Brodmann areas 11 and 12. The basal ganglia (BG) which is made up of the caudate, putamen, globus pallidus (GP) subthalamic nucleus (STN), and substantia nigra (SN), were traditionally conceptualized as a center of motoric integration. The result of the PBM method in MDD patients detects several regions which is reasonable and consistent such as middle frontal gyrus and superior frontal gyrus both in OFC. The bilateral volume reduction is also reported by Lai et al. [32]. This. It plays an important role of cognitive processes. The detection of the thalamus is also reasonable that thalamus is believed to both process and relay sensory information selectively to various parts of the cerebral cortex and it is highly associated with BG. In the VBM analysis of MDD patients, it is also several finding is associated with middle frontal gyrus and superior frontal gyrus which is the same with our result. A report by Chen et al.(2008) [33] also detects reduction of insula and amygdala with MDD patients, however, insula is only detected by PBM method.

Figure 4.9 illustrates statistic t value of each region in BD2 patients by PBM analysis method. The significant level of t value is listed in Table 4.7, As we can see, comparing the variety of regions of BD2 patients to normal controls. Regions with a high significant level were in frontal lobe (left and right middle frontal gyrus, left and right superior frontal gyrus, left inferior frontal gyrus, precentral), temporal lobe (superior temporal gyrus), occipital lobe, and insula whose t value is relatively small. Figure 4.10 illustrate gray matter volume reduce in MDD patients by PBM analysis method. The detected significant atrophy is marked with a circle and number in Figure 4.10. The information of each marked circle is also listed in Table 4.8. Regions marked with green circle is found by both VBM and PBM method. Regions marked with blue circle is only found by PBM method.

Figure 4.10 illustrate gray matter volume reduce in BD2 patients by VBM analysis method. The detected significant atrophy is marked with a circle and number in Figure 4.11. The information of each marked circle is also listed in Table 4.9. As we can see, comparing brain structures of BD2 patients to normal controls, the reduction of GM is detected in the regions of frontal lobe (right middle frontal gyrus, right superior frontal gyrus, left precentral gyrus, paracentral lobule), parietal lobe (supramarginal gyrus) and occipital lobe

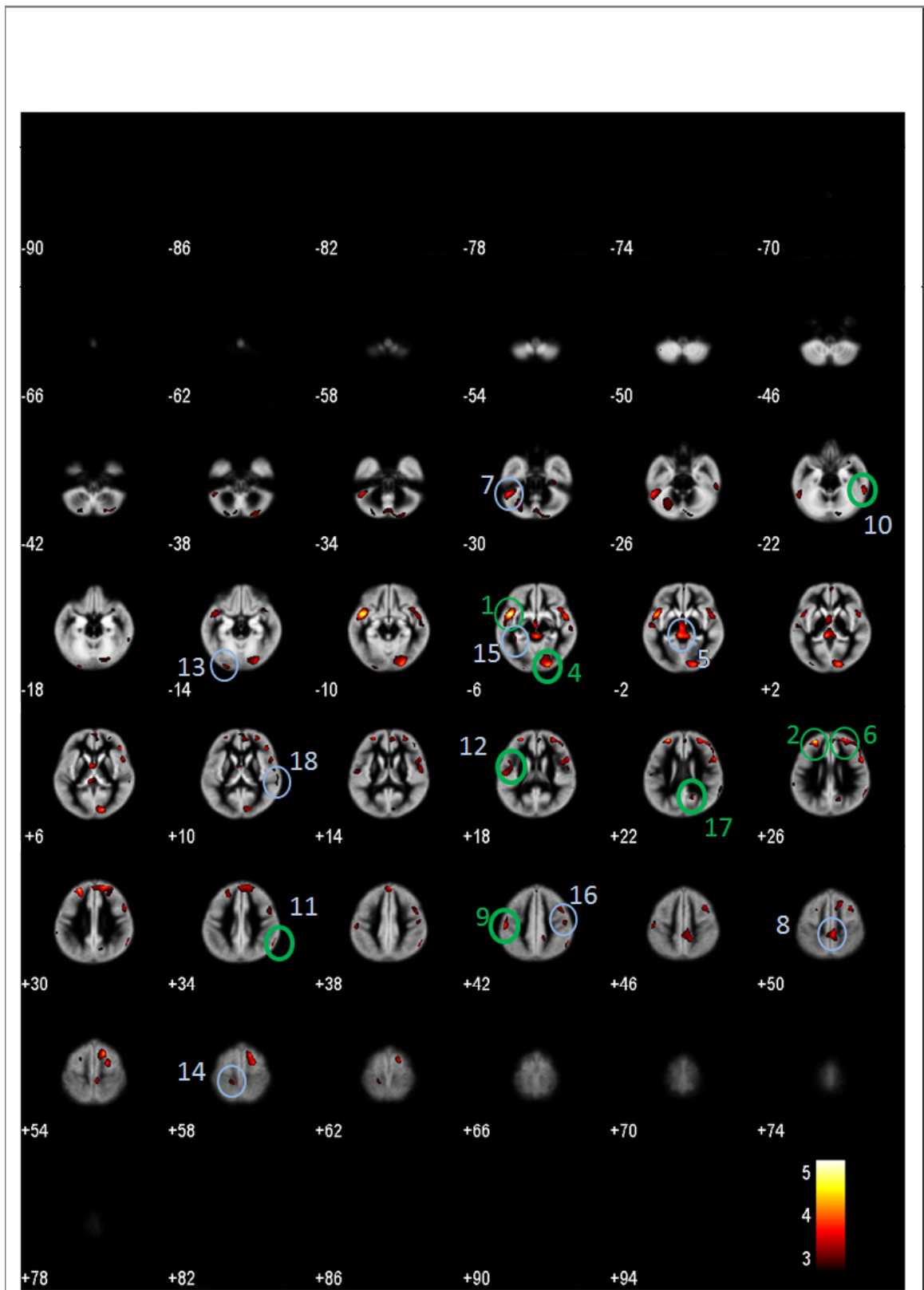


Figure 4.7: Volumetric atrophy of gray matter in MDD patients by VBM analysis method. Regions detected as significant group differences are marked with circles. One marked with a green circle is also found in the PBM analysis result; one marked with a blue circle is only revealed in the VBM result. Numbers of these circles represent the importance of characterizing volume loss in MDD patients. More information of each region is listed in Table 4.6.

Table 4.6: Atrophy of gray matter in MDD patients by VBM analysis method. These atrophy regions are arranged in order by their peak discrimination weights of each cluster, and the numbers denote the sequence of peak discrimination weights. The serial numbers are informative for revealing the significance of gray matter atrophy in MDD.

Location	BA	Side	Talairach coordinate			Peak t value	Cluster size	Fig. 4.7 no.
			x	y	z			
Cerebrum, Temporal Lobe, Superior Temporal Gyrus	38	L	-44.1852	6.2306	-10.4225	5.294	3374	1
Cerebrum, Frontal Lobe, Middle Frontal Gyrus	10	L	-28.4769	49.697	17.3044	4.9652	1836	2
Cerebrum, Frontal Lobe, Superior Frontal Gyrus	8	R	15.8211	-22.6336	49.4896	4.3549	2362	3
Cerebrum, Occipital Lobe, Middle Occipital Gyrus	18	R	24.0962	-88.8226	-0.8206	4.3325	9504	4
Brainstem Midbrain, Red Nucleus	10	L	-4.7304	-16.042	-4.4852	4.1341	4287	5
Cerebrum, Frontal Lobe, Superior Frontal Gyrus	10	R	18.3944	52.9055	19.932	3.9822	13084	6
Cerebellum, Anterior Lobe, Culmen	6	L	-49.2229	-46.2464	-24.8077	3.8798	2150	7
Cerebrum, Frontal Lobe, Paracentral Lobule	6	R	5.4166	-28.5791	50.0615	3.7583	1805	8
Cerebrum, Parietal Lobe, Postcentral Gyrus	3	L	-53.3074	-16.3475	39.7631	3.6602	731	9
Cerebrum, Temporal Lobe, Inferior Temporal Gyrus	20	R	59.0377	-38.9876	-17.4631	3.5457	667	10
Cerebrum, Parietal Lobe, Supramarginal Gyrus	40	R	57.2897	-51.3743	36.2443	3.4867	755	
Cerebrum, Parietal Lobe, Postcentral Gyrus	43	L	-52.5017	-10.5864	15.8207	3.3493	914	
Cerebrum, Occipital Lobe, Lingual Gyrus	18	L	-25.0234	-93.1901	-7.9937	3.2414	400	
Cerebrum, Frontal Lobe, Precentral Gyrus	4	L	-18.2245	-24.1098	58.8354	3.202	333	
Cerebrum, Limbic Lobe, Parahippocampal Gyrus	37	L	-36.1239	-37.0811	-5.2696	3.1602	213	
Cerebrum, Frontal Lobe, Precentral Gyrus	4	R	50.1181	-11.0995	38.5752	3.1382	338	
Cerebrum, Limbic Lobe, Cingulate Gyrus	31	R	18.0091	-56.8861	24.8263	3.064	437	
Cerebrum, Temporal Lobe, Superior Temporal Gyrus	42	R	61.5597	-31.7629	9.8118	2.8983	216	

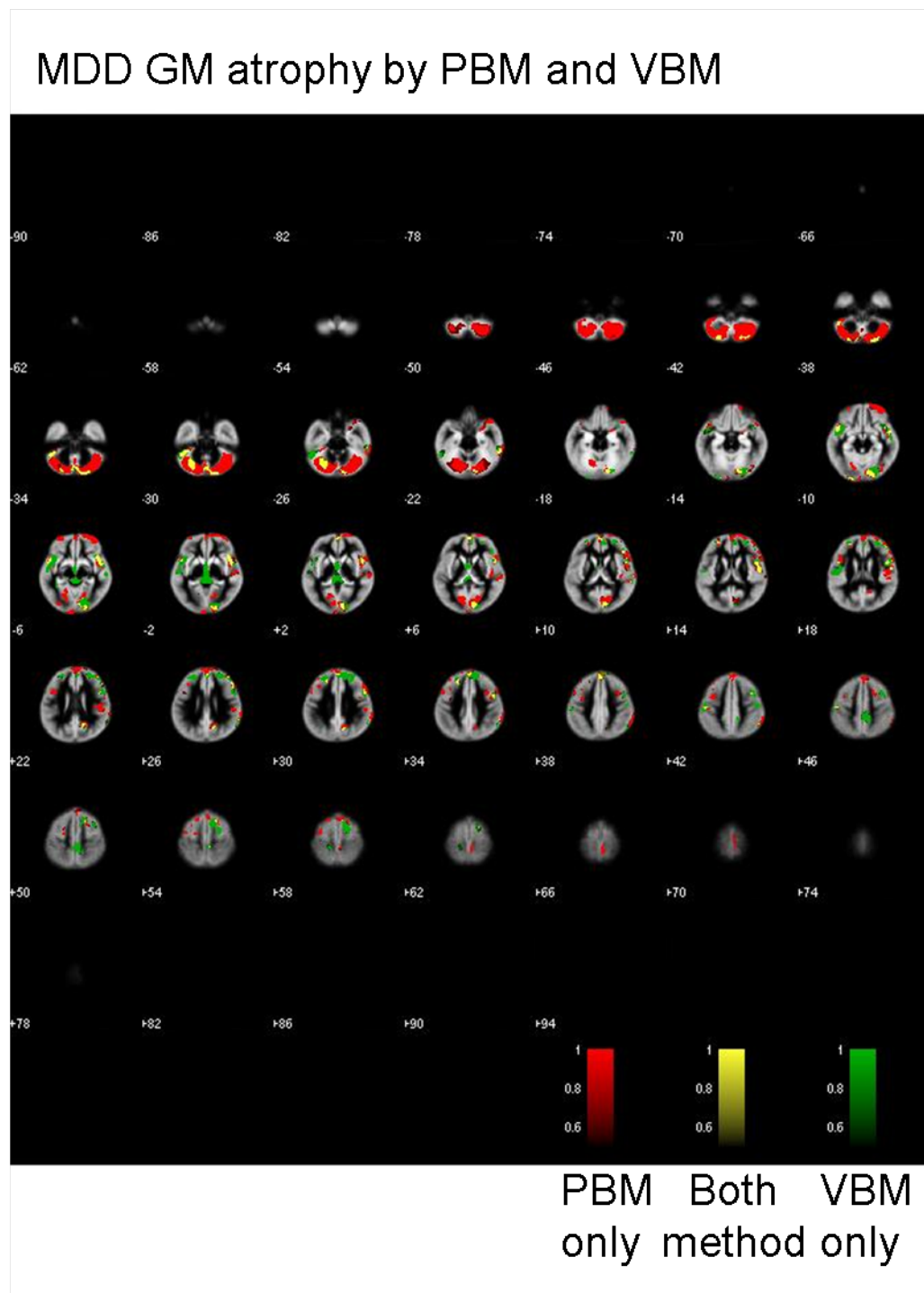


Figure 4.8: Volumetric atrophy of gray matter in MDD patients by PBM method only is labeled with red color; both method is labeled with yellow color; vbm method only is labeled with green color.

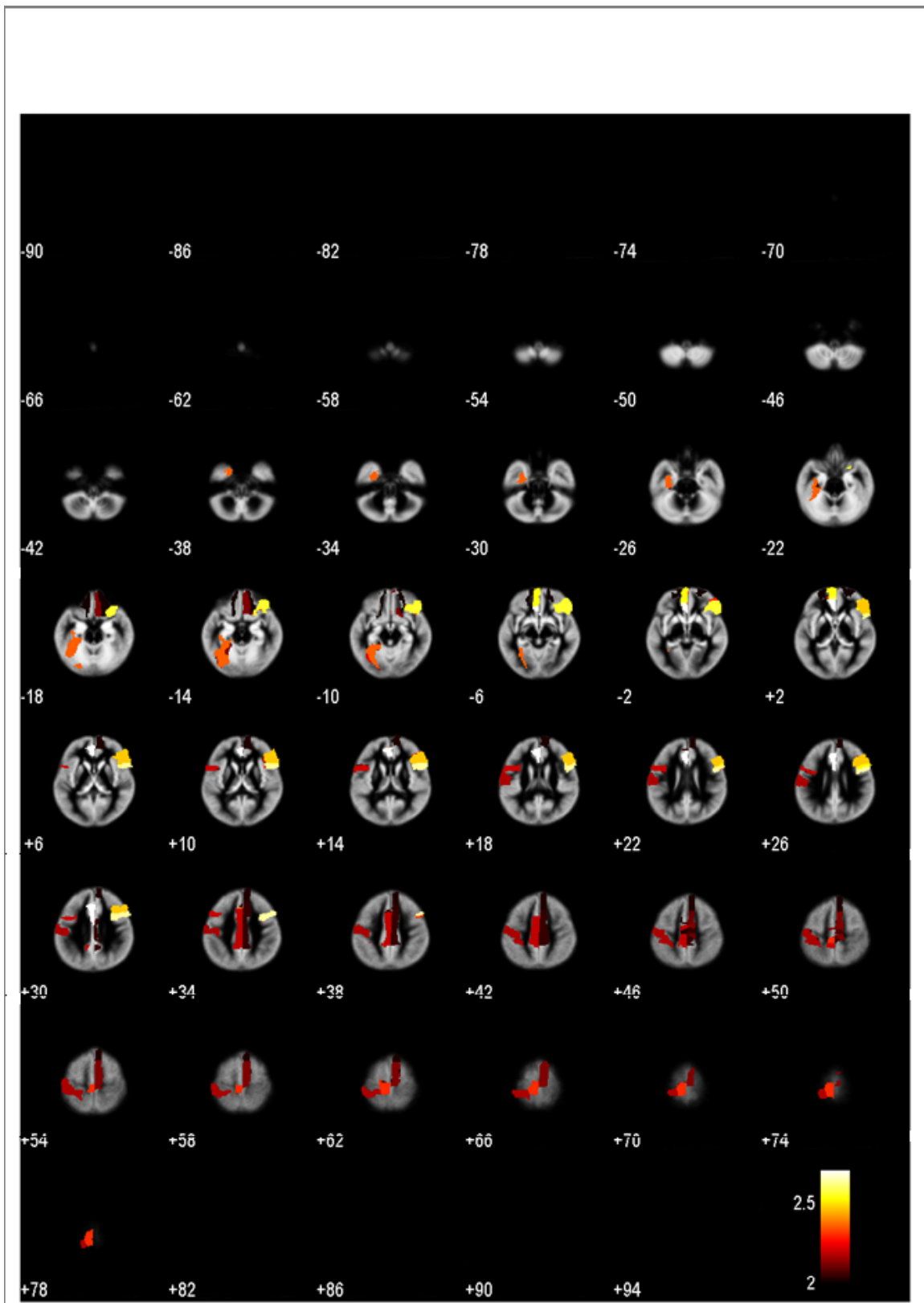


Figure 4.9: Statistics t value within each region in BD2 patients by PBM analysis method is shown. Each statistics t value information within each region is listed in Table 4.7.

Table 4.7: Statistics t value within each region in BD2 patients by PBM analysis method in BD2. These statistic t values are arranged in order by the t value of each region, and the corresponding locations in AAL labeling are listed.

AAL label side	t value	AAL label side	t value
CIAG Cingulum Ant L 4001	2.706	F3TG Frontal Inf Tri L 2311	1.7143
F3OPD Frontal Inf Oper R 2302	2.6332	F2OD Frontal Mid Orb R 2212	1.7081
F3OD Frontal Inf Orb R 2322	2.5594	THAD Thalamus R 7102	1.7073
FMOG Frontal Med Orb L 2611	2.5327	FMG Frontal Sup Medial L 2601	1.7048
F3TD Frontal Inf Tri R 2312	2.4669	F2OG Frontal Mid Orb L 2211	1.6895
FUSIG Fusiform L 5401	2.3628	F1G Frontal Sup L 2101	1.68
LPCG Paracentral Lobule L 6401	2.3025	FAD Precentral R 2002	1.6784
F3OPG Frontal Inf Oper L 2301	2.2057	FMOD Frontal Med Orb R 2612	1.6761
CINMG Cingulum Mid L 4011	2.191	F2D Frontal Mid R 2202	1.6717
PAG Postcentral L 6001	2.1699	F3OG Frontal Inf Orb L 2321	1.6717
GRD Rectus R 2702	2.1279	CER Cerebelum L 9999	1.6396
SMAD Supp Motor Area R 2402	2.1244	GRG Rectus L 2701	1.6148
CINMD Cingulum Mid R 4012	2.0459	T3D Temporal Inf R 8302	1.5648
FMD Frontal Sup Medial R 2602	2.0234	CERC1G Cerebelum Crus1 2 L 9996	1.5564
F1OG Frontal Sup Orb L 2111	2.0137	T1D Temporal Sup R 8112	1.5522
F1OD Frontal Sup Orb R 2112	2.0127	IND Insula R 3002	1.5262
HESCHLG Heschl L 8101	1.9748	F2G Frontal Mid L 2201	1.5224
LINGG Lingual L 5021	1.9636	AMYGDD Amygdala R 4202	1.5055
O3G Occipital Inf L 5301	1.9438	CERC2G Cerebelum Crus1 2 R 9997	1.4962
SMAG Supp Motor Area L 2401	1.9424	PALLG Pallidum L 7021	1.482
THAG Thalamus L 7101	1.9083	COBD Olfactory R 2502	1.4171
GSMD SupraMarginal R 6212	1.84	O3D Occipital Inf R 5302	1.3959
ING Insula L 3001	1.8317	PARA HIPPOG ParaHippocampal L 4111	1.3797
HESCHLD Heschl R 8102	1.825	O2D Occipital Mid R 5202	1.3135
ORD Rolandic Oper R 2332	1.8217	VER Vermis all 9995	1.2067
O1D Occipital Sup R 5102	1.8107	CER Cerebelum R 9998	1.0803
FAG Precentral L 2001	1.7997	PAD Postcentral R 6002	1.0415
F1D Frontal Sup R 2102	1.7656	NLD Putamen R 7012	0.8109
V1G Calcarine L 5001	1.7605	NLG Putamen L 7011	0.51612
LPCD Paracentral Lobule R 6402	1.7482	PALLD Pallidum R 7022	0.29064
V1D Calcarine R 5002	1.7323		

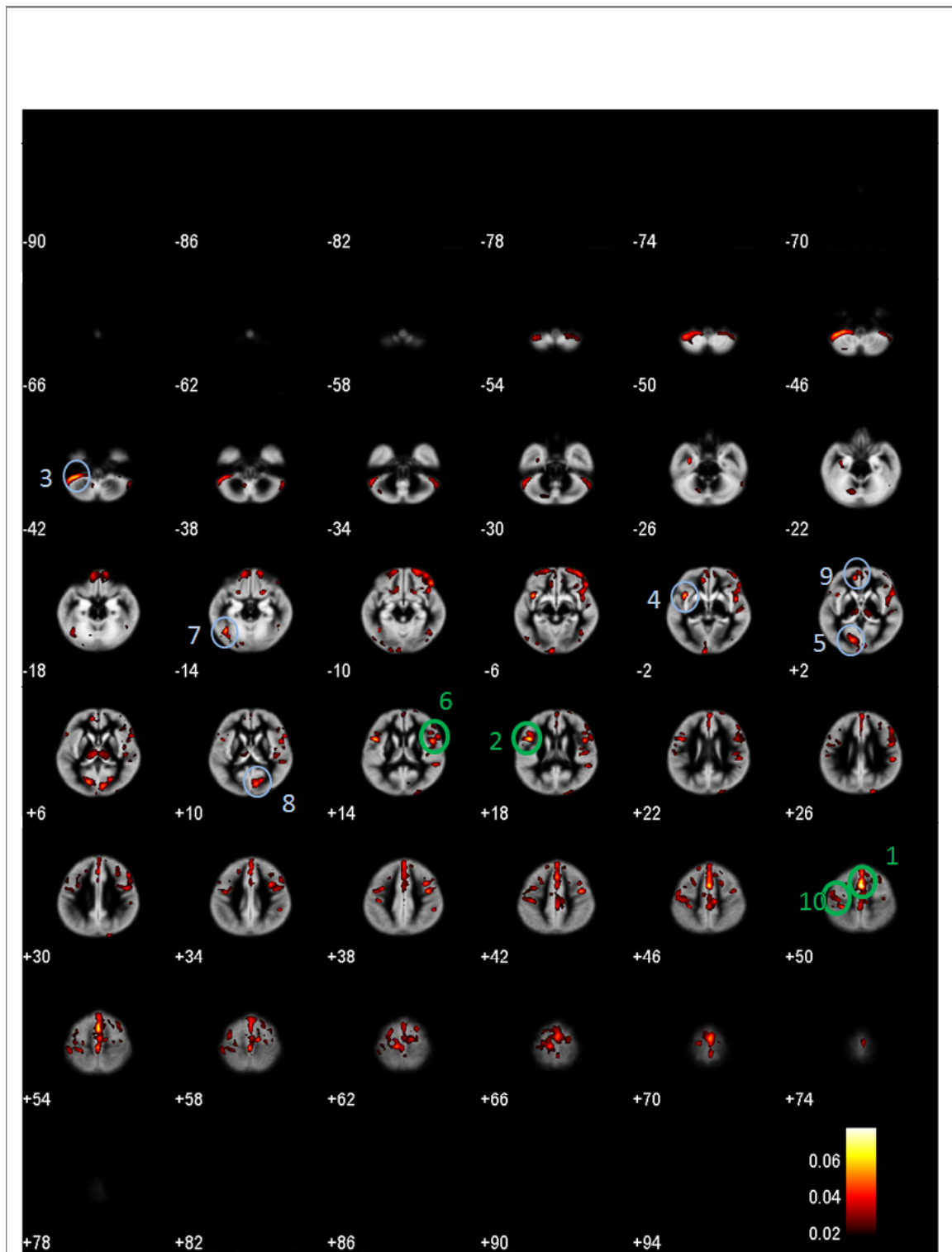


Figure 4.10: Volumetric atrophy of gray matter in BD2 patients by PBM analysis method. Regions detected as significant group differences are marked with circles. One marked with a green circle is also found in the VBM analysis result; one marked with a blue circle is only revealed in the PBM result. Numbers of these circles represent the importance of characterizing volume loss in BD2 patients. More information of each region is listed in Table 4.8.

Table 4.8: Atrophy of gray matter in BD2 patients by PBM analysis method. These atrophy regions are arranged in order by their peak discrimination weights of each cluster, and the numbers denote the sequence of peak discrimination weights. The serial numbers are informative for revealing the significance of gray matter atrophy in BD2.

Location	BA	Side	Talairach coordinate			Peak discrimination	Cluster size	Fig. 4.10 no.
			x	y	z			
Cerebrum Frontal Lobe Medial Frontal Gyrus	6	L	-5.6951	13.3972	46.0184	0.078	18289	1
Cerebrum Frontal Lobe Inferior Frontal Gyrus	44	L	-52.5001	12.6182	13.2329	0.0684	1491	2
Cerebellum Posterior Lobe Cerebellar Tonsil		L	-49.3212	-45.4035	-36.6494	0.0618	4441	3
Cerebrum Temporal Lobe Superior Temporal Gyrus	22	L	-46.2603	11.6459	-5.6307	0.0617	717	4
Cerebrum Occipital Lobe Cuneus	30	L	-22.8093	-73.7706	8.9323	0.0581	1743	5
Cerebrum Sub-lobar Insula	13	R	42.865	9.5307	11.2699	0.0557	10705	6
Cerebrum Occipital Lobe Middle Occipital Gyrus	19	L	-47.9059	-59.4915	-8.317	0.0556	711	7
Cerebrum Occipital Lobe Cuneus	17	R	2.0869	-79.4899	12.1488	0.0504	1490	8
Cerebrum Frontal Lobe Medial Frontal Gyrus	10	L	-16.3892	46.8298	-5.3699	0.0488	1050	9
Cerebrum Parietal Lobe Postcentral Gyrus	3	L	-37.4095	-28.6098	48.762	0.0481	3396	10
Cerebrum Frontal Lobe Superior Frontal Gyrus	11	L	-14.32	49.2216	-21.5981	0.0476	1749	
Cerebrum Sub-lobar Insula	13	R	46.4141	-24.2297	24.668	0.0462	415	
Cerebrum Temporal Lobe Fusiform Gyrus	20	L	-38.6575	-9.3312	-23.8167	0.0457	346	
Cerebrum Frontal Lobe Medial Frontal Gyrus	25	R	14.62	15.2813	-16.0062	0.0432	292	
Cerebrum Sub-lobar Insula	13	R	40.9705	-13.2856	17.4962	0.0415	660	
Cerebrum Temporal Lobe Superior Temporal Gyrus	41	R	46.2236	-37.7275	15.1578	0.0413	568	
Cerebrum Parietal Lobe Inferior Parietal Lobule	40	R	42.821	-35.3562	36.1182	0.0409	211	
Cerebrum Occipital Lobe Cuneus	19	R	11.6614	-87.5703	31.9194	0.0405	574	
No Gray Matter found			35.4144	-60.6931	-4.2064	0.0396	257	
Cerebellum Anterior Lobe Culmen		R	40.3348	-46.066	-29.2029	0.0384	1931	
Cerebrum Sub-lobar Thalamus		L	-13.9046	-18.0469	2.5833	0.0383	790	
Cerebrum Frontal Lobe Superior Frontal Gyrus	6	R	16.5824	16.8723	56.491	0.0361	321	
Cerebrum Parietal Lobe Postcentral Gyrus	2	L	-52.825	-29.783	54.3731	0.0354	426	
Cerebrum Frontal Lobe Medial Frontal Gyrus	10	L	-7.0215	56.1742	-6.0781	0.0339	330	
Cerebrum Sub-lobar Thalamus		L	-0.924	-16.6505	3.8245	0.0333	681	
Cerebrum Limbic Lobe Cingulate Gyrus	32	R	16.1034	18.3387	41.518	0.0329	281	
Cerebrum Frontal Lobe Middle Frontal Gyrus	8	L	-30.3524	17.1095	39.2285	0.0326	328	

(lingual gyrus). Regions marked with green circle is found by both VBM and PBM method. Regions marked with blue circle is only found by VBM method.

There are lot of findings in middle frontal gyrus and superior frontal gyrus by both PBM and VBM methods. They are all highly associated with the cognitive processes which is mentioned before. Most of the findings in VBM result are also detected by PBM except two regions: supramarginal gyrus and lingual gyrus which detects no differences by PBM.

Figure 4.13 illustrates statistic t value of each region in BD1 patients by PBM analysis method. The significant level of t value is listed in Table 4.10, As we can see, comparing the variety of regions of BD1 patients to normal controls. Regions with a high significant level were in frontal lobe (right middle frontal gyrus, left precentral gyrus, left superior frontal gyrus) and thalamus whose t value is relatively small. Figure 4.14 illustrate gray matter volume reduce in BD1 patients by PBM analysis method. The detected significant atrophy is marked with a circle and number in Figure 4.14. The information of each marked circle is also listed in Table 4.11. Regions marked with green circle is found by both VBM and PBM method. Regions marked with blue circle is only found by PBM method.

Figure 4.14 illustrate gray matter volume reduce in BD1 patients by VBM analysis method. The detected significant atrophy is marked with a circle and number in Figure 4.15. The information of each marked circle is also listed in Table 4.12. As we can see, comparing brain structures of BD1 patients to normal controls, the reduction of GM is detected in the regions of temporal lobe (left superior temporal gyrus), frontal lobe (left superior frontal gyrus, right inferior frontal gyrus, paracentral lobule), occipital lobe (lingual gyrus) and limbic lobe (parahippocampal gyrus). Regions marked with green circle is found by both VBM and PBM method. Regions marked with blue circle is only found by VBM method.

Both of the methods detect superior frontal gyrus (and paracentral lobule which is a more medial part of the superior frontal gyrus) in the analysis of BD1 patients. The findings in middle frontal gyrus and thalamus is also in consistent with previous studies. Parahippocampal gyrus which is known as memory encoding and retrieval is also detected

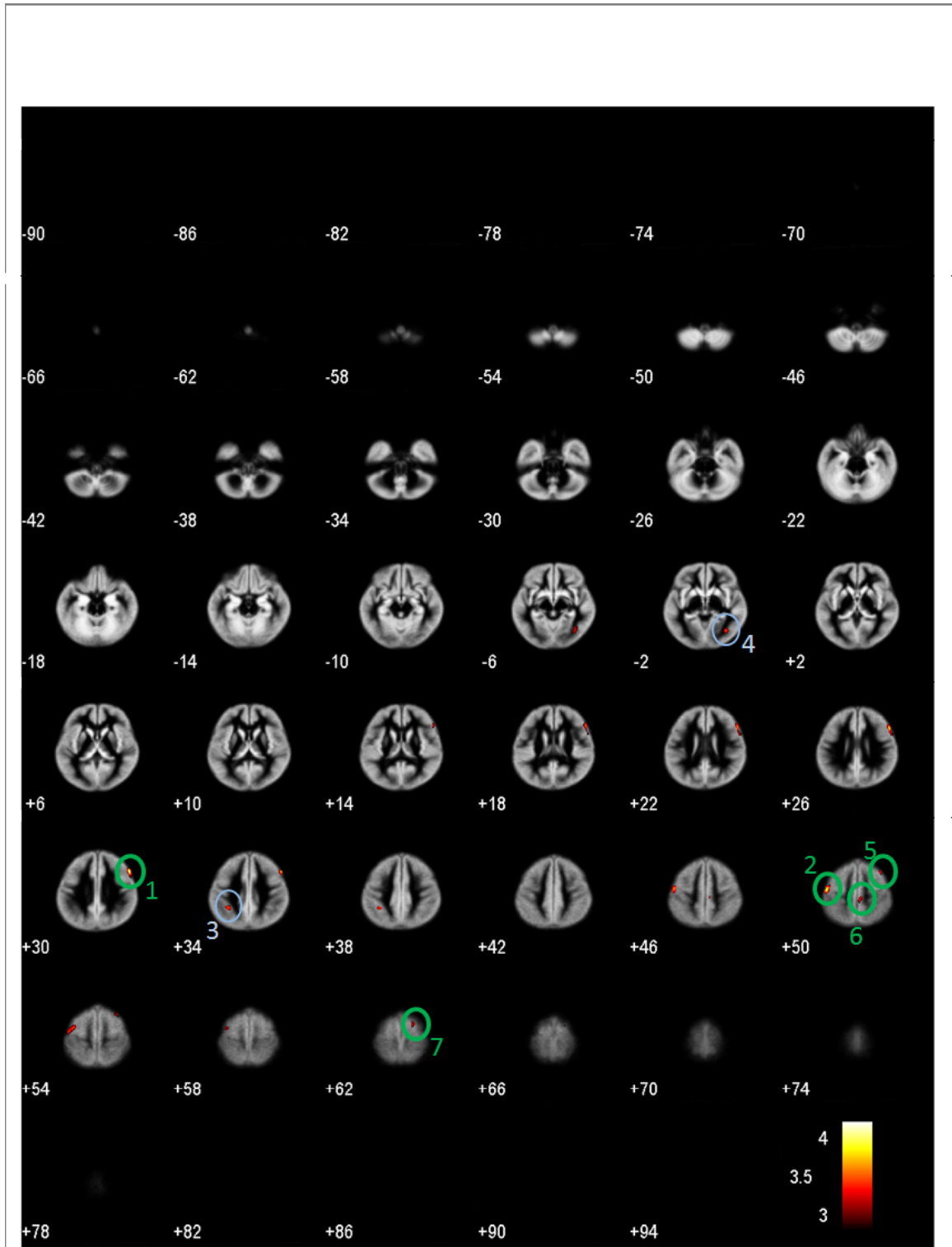


Figure 4.11: Volumetric atrophy of gray matter in BD2 patients by VBM analysis method. Regions detected as significant group differences are marked with circles. One marked with a green circle is also found in the PBM analysis result; one marked with a blue circle is only revealed in the VBM result. Numbers of these circles represent the importance of characterizing volume loss in MDD patients. More information of each region is listed in Table 4.9.

Table 4.9: Atrophy of gray matter in BD2 patients by VBM analysis method. These atrophy regions are arranged in order by their peak discrimination weights of each cluster, and the numbers denote the sequence of peak discrimination weights. The serial numbers are informative for revealing the significance of gray matter atrophy in BD2.

Location	BA	Side	Talairach coordinate			Peak t value	Cluster size	Fig. 4.11 no.
			x	y	z			
Cerebrum, Frontal Lobe, Middle Frontal Gyrus	46	R	49.0372	27.1320	24.0700	4.1218	1338	1
Cerebrum, Frontal Lobe, Precentral Gyrus	6	L	-56.9541	-4.7021	46.9413	3.8918	1171	2
Cerebrum, Parietal Lobe, Supramarginal Gyrus	40	L	-42.2206	-42.9692	37.1545	3.5639	386	3
Cerebrum, Occipital Lobe, Lingual Gyrus	19	R	28.1500	-65.5593	0.4888	3.478	376	4
Cerebrum, Frontal Lobe, Middle Frontal Gyrus	8	R	32.9872	30.4887	44.7022	3.2758	292	5
Cerebrum, Frontal Lobe, Paracentral Lobule	31	L	-0.0415	-22.3390	48.2255	3.2739	287	6
Cerebrum, Frontal Lobe, Superior Frontal Gyrus	6	R	14.6703	14.7121	56.7135	3.0974	322	7

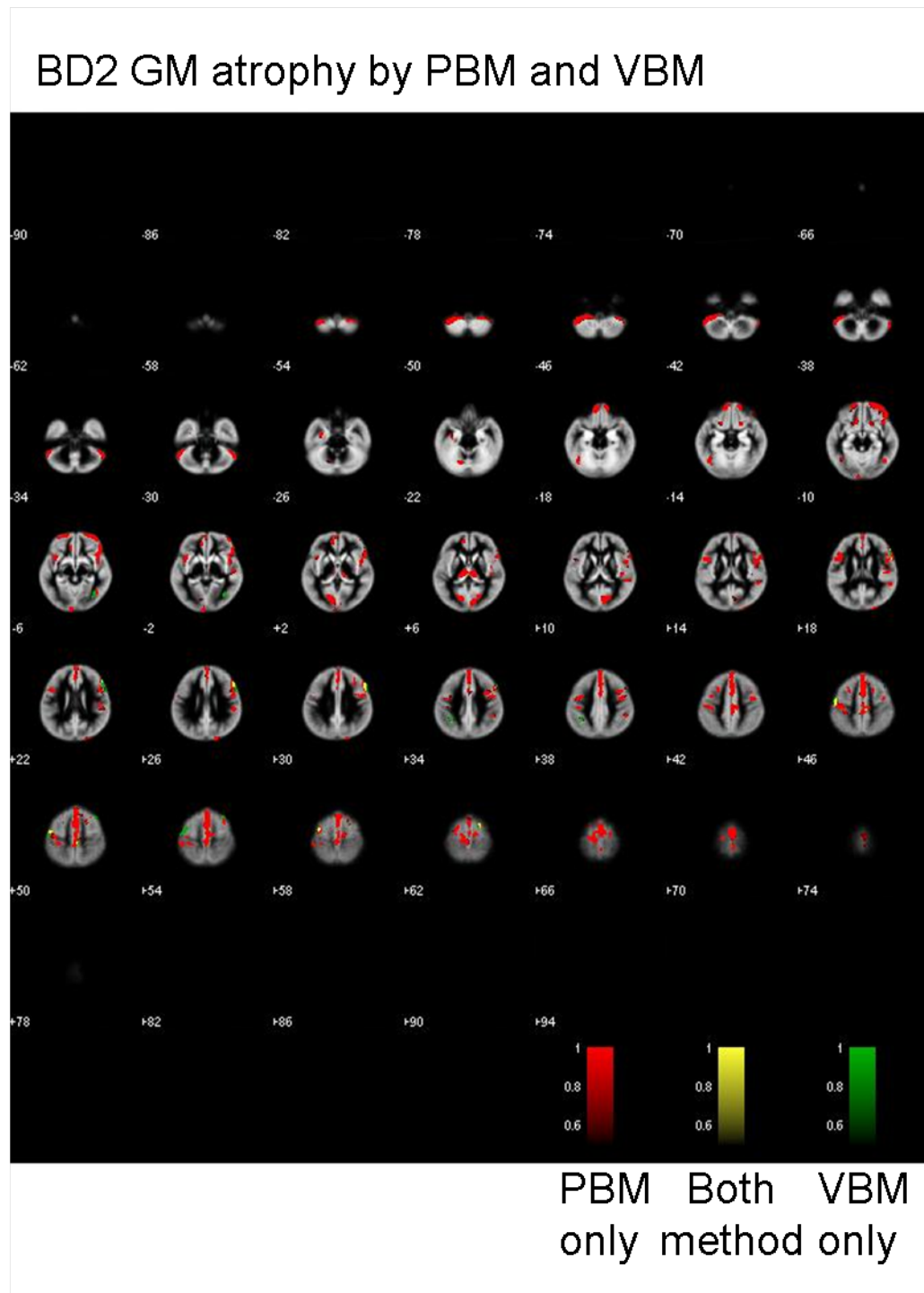


Figure 4.12: Volumetric atrophy of gray matter in MDD patients by PBM method only is labeled with red color; both method is labeled with yellow color; vbm method only is labeled with green color.

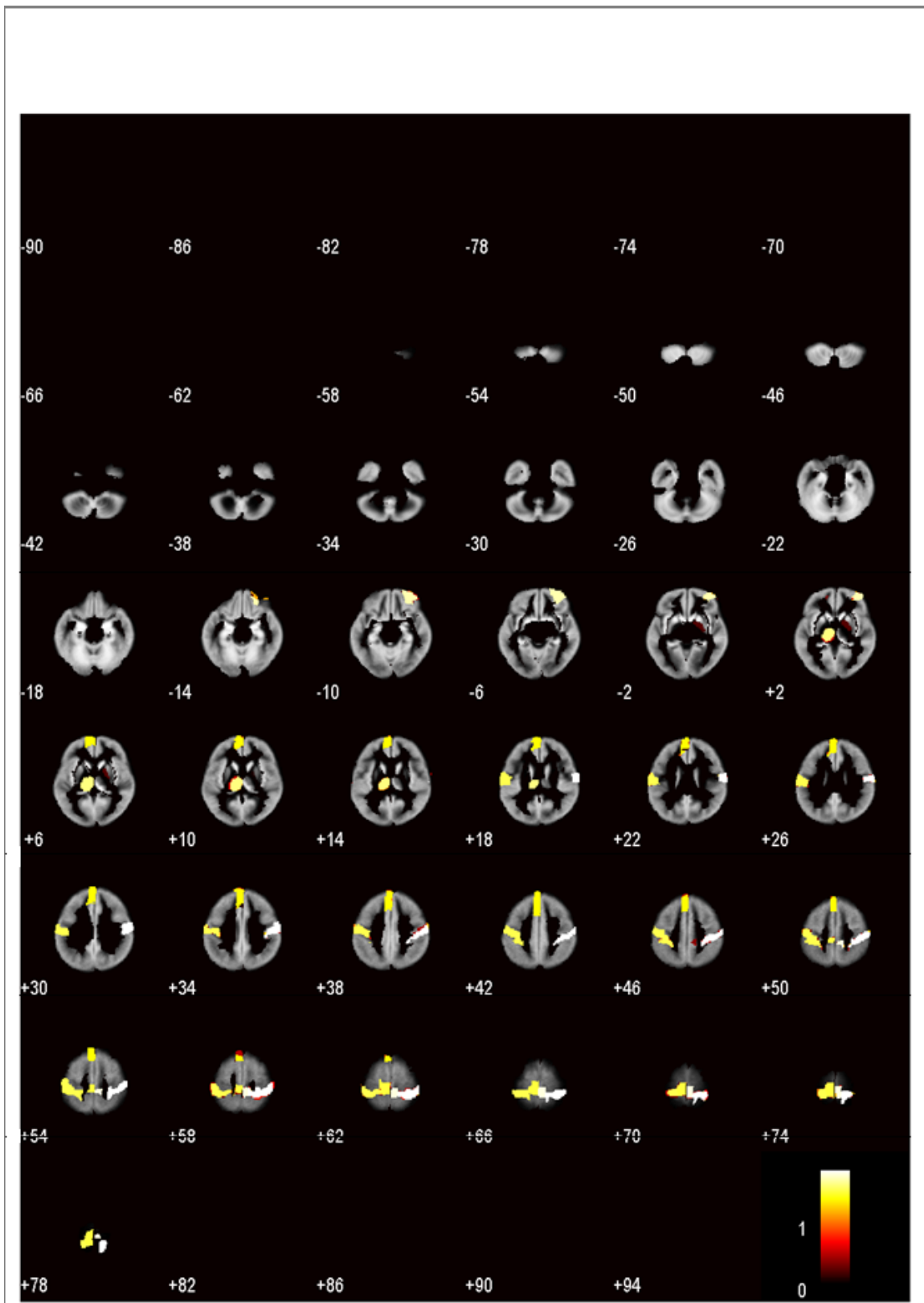


Figure 4.13: Statistics t value within each region in BD1 patients by PBM analysis method is shown. Each statistics t value information within each region is listed in Table 4.10.

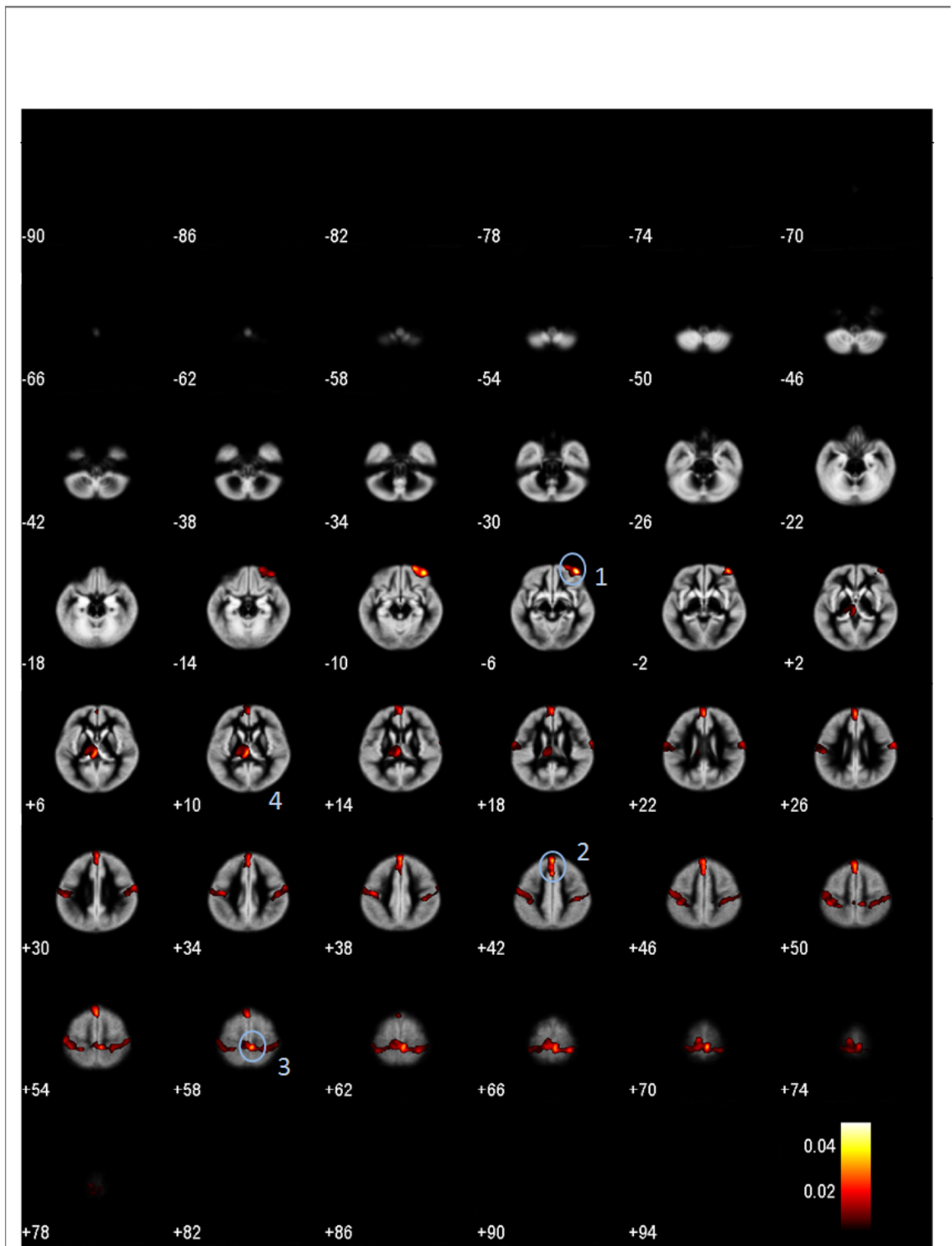


Figure 4.14: Volumetric atrophy of gray matter in BD1 patients by PBM analysis method. Regions detected as significant group differences are marked with circles. One marked with a green circle is also found in the VBM analysis result; one marked with a blue circle is only revealed in the PBM result. Numbers of these circles represent the importance of characterizing volume loss in BD1 patients. More information of each region is listed in Table 4.11.

by VBM and PBM method with BD2 patients. There are findings with decrease in volume of parahippocampal gyrus by Lochhead et al. (2004) [34].



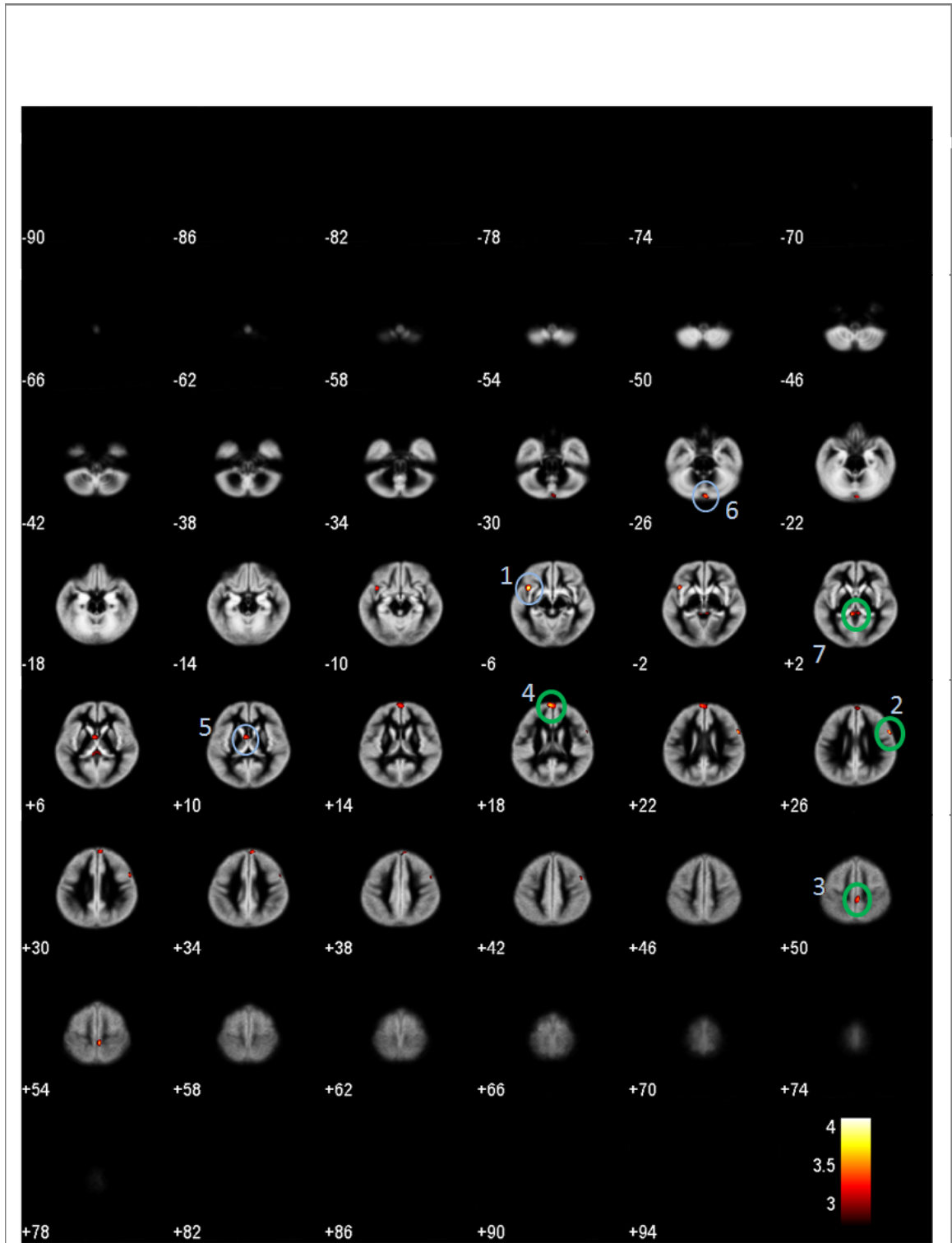


Figure 4.15: Volumetric atrophy of gray matter in BD1 patients by VBM analysis method. Regions detected as significant group differences are marked with circles. One marked with a green circle is also found in the PBM analysis result; one marked with a blue circle is only revealed in the VBM result. Numbers of these circles represent the importance of characterizing volume loss in BD1 patients. More information of each region is listed in Table 4.12.

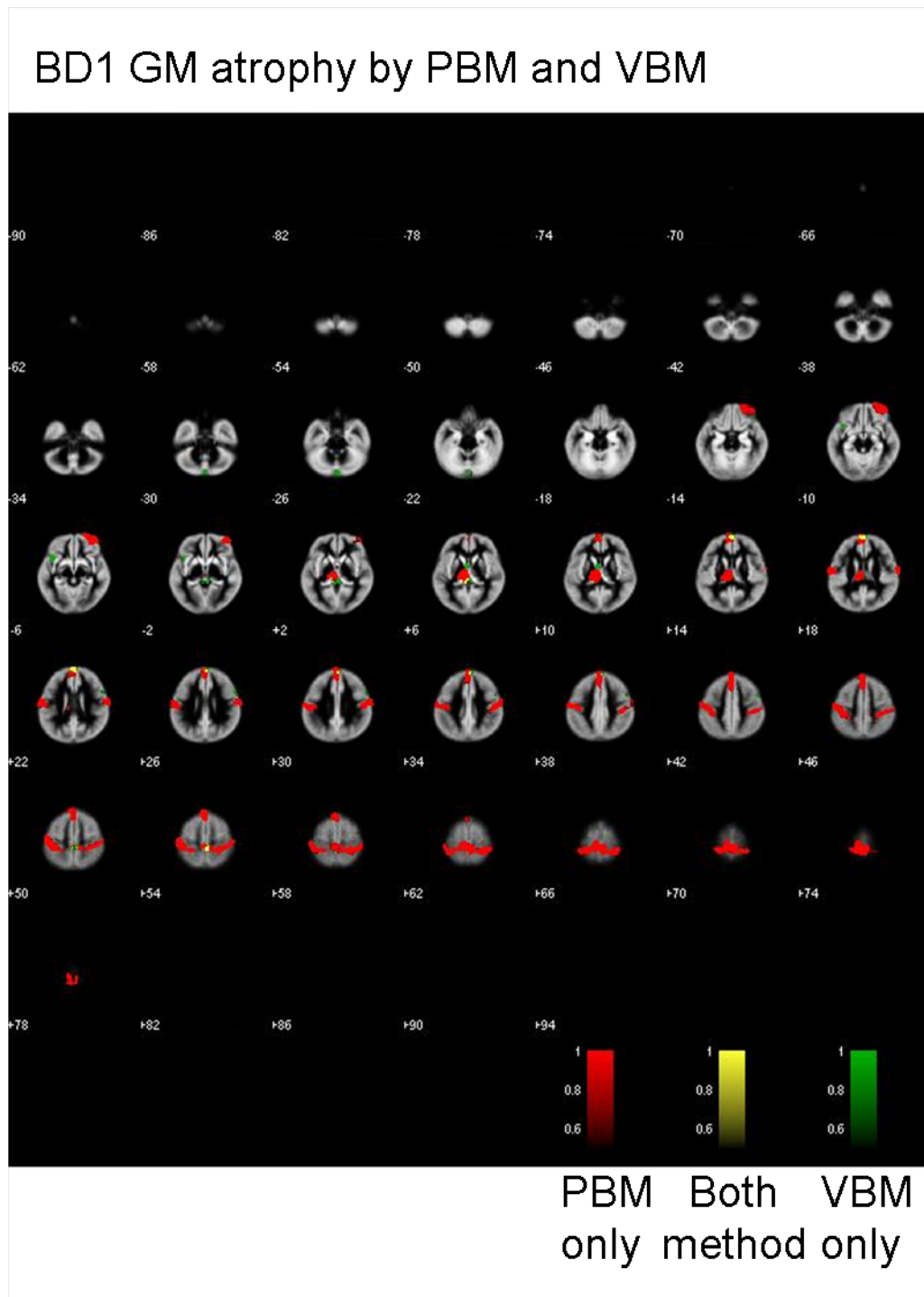


Figure 4.16: Volumetric atrophy of gray matter in MDD patients by PBM method only is labeled with red color; both method is labeled with yellow color; vbm method only is labeled with green color.

Table 4.10: Statistics t value within each region in BD2 patients by PBM analysis method in BD1. These statistic t values are arranged in order by the t value of each region, and the corresponding locations in AAL labeling are listed.

AAL label side	t value
PAD Postcentral R 6002	1.8056
LPCD Paracentral Lobule R 6402	1.7599
F2OD Frontal Mid Orb R 2212	1.6642
THAG Thalamus L 7101	1.562
PAG Postcentral L 6001	1.4787
LPCG Paracentral Lobule L 6401	1.4595
FMG Frontal Sup Medial L 2601	1.3473
PALLD Pallidum R 7022	0.19076

Table 4.11: Atrophy of gray matter in BD1 patients by PBM analysis method. These atrophy regions are arranged in order by their peak discrimination weights of each cluster, and the numbers denote the sequence of peak discrimination weights. The serial numbers are informative for revealing the significance of gray matter atrophy in BD1.

Location	BA	Side	Talairach coordinate			Peak discrimination	Cluster size	Fig. 4.14 no.
			x	y	z			
Cerebrum Frontal Lobe Middle Frontal Gyrus	11	R	35.3649	52.9592	-12.7518	0.0502	4543	1
Cerebrum Frontal Lobe Superior Frontal Gyrus	9	L	-5.2878	50.3165	33.3028	0.0358	10476	2
Cerebrum Frontal Lobe Paracentral Lobule	6	L	0.1068	-29.3435	57.5671	0.0347	34284	3
Cerebrum Sub-lobar Thalamus		L	-8.8946	-21.6497	5.7670	0.0345	5481	4

Table 4.12: Atrophy of gray matter in BD1 patients by VBM analysis method. These atrophy regions are arranged in order by their peak discrimination weights of each cluster, and the numbers denote the sequence of peak discrimination weights. The serial numbers are informative for revealing the significance of gray matter atrophy in BD1.

Location	BA	Side	Talairach coordinate			Peak t value	Cluster size	Fig. 4.15 no.
			x	y	z			
Cerebrum, Temporal Lobe, Superior Temporal Gyrus	38	L	-46.2590	13.1310	-8.4300	4.1119	550	1
Cerebrum, Frontal Lobe, Inferior Frontal Gyrus	44	R	51.5954	14.7574	19.4365	4.0652	569	2
Cerebrum, Frontal Lobe, Paracentral Lobule	5	L	-2.2288	-29.3261	51.7070	3.7555	516	3
Cerebrum, Frontal Lobe, Superior Frontal Gyrus	10	L	-8.8806	65.0677	8.6466	3.7201	1604	4
Cerebrum, Sub-Iobar, Lentiform Nucleus		L	-11.2348	0.6100	4.5168	3.5515	462	5
Cerebrum, Occipital Lobe, Lingual Gyrus	18	L	-4.3471	-87.1453	-17.6287	3.5445	508	6
Cerebrum, Limbic Lobe, Parahippocampal Gyrus	27	L	-13.0328	-35.3014	1.4200	3.5042	743	7



Chapter 5

Discussion



5.1 Using the Parcellation-Based Approach

In this study, A method of parcellation-based multivariate approach is proposed. The reason is that regions of the brain structures are always correlated to diverse functions and regions defined by Korbinian Brodmann are also defined by organization. Therefore, we should take all the voxels within the same region in consideration simultaneously. There are several advantages of using the parcellation-based approach.

At first, it is more flexible for the analysis. if we can know the region which is not important in characterizing group differences in advance, then it can be without consideration. Also, it could be a whole-brain analysis in characterizing group differences, that is to define a whole-brain region without parcellating the brain. Occasionally, regions are concerned only in several organization with patients suffering certain disease. We can just analyze regions which are important to characterizing the group differences. Secondly, using this region-based approach method can help the analysis with collecting the voxels which may cause by wrong segmentation of the tissues, an imperfect registration or a bad brain extraction. Thus, the voxel with wrong information or noise may not influence the result. At last, the most important point is, by using parcellation-based approach all the information of each voxel are in the same region to analyze brain anatomy with different disease simultaneously. The parcellation-based approach is used to analyze the neighbor voxels together instead of smoothing the data.

5.2 Different Size of Each Region

In the proposed method, we have to define the regions before we analyze. There are several way in defining the region, such as by voxel (which is the VBM), a cube, sulci and gyri or organization. The size of every region may or may not be the same with each other. Therefore, there may be some issues when comparing results under different size of regions.

One is that regions are in different size with an identical atrophy size. In an ideal case, voxels which produce no variation between two groups can have no effect to the discriminant map. That is only the voxels with atrophy will be detected, others will have no contributions to the discriminant projection vector. Thus it may not influence the result with same atrophy size but different region. The other is that regions and the atrophy size are both different. According to the discriminative common vector method, the discriminant projection vector is a unit vector. The weights of the projection vector which represent the discrimination for characterizing group discrepancy may be diminished by being a normalized (unit) vector. Thus we adopt a correction to the projection vector which we have mentioned and proved in section 3.3.3. Therefore, with the correction, the weight of the projection vector may not be diminished and can denote the discrimination for characterizing group discrepancy in an unbiased way.

5.3 Limitations of the Atrophy Simulation Package

The atrophy simulation package simulates atrophy and growth within a spherical region of an input image that is to produce the volumetric changes or volumetric loss. It is fast and realistic to simulate, but the limitations of this simulation package is that it can only simulate one area for volumetric changes at a time. As we know that in reality, the MDD or BD patient may not have only one area with gray matter atrophy or enlarge. It always has more than one area with gray matter atrophy or enlarge. Therefore the simulation data may not represent as patient in reality. Another limitation is that the atrophy simulation package can freely move the CSF boundary to produce the volumetric changes. That is we can only simulate our data with the CSF boundary. In consequently, the simulation area is highly correlated with CSF boundary.

Moreover, the results of the simulation data have shown that the parcellation-based multivariate (PBM) method is better than VBM in ROC curve. Once if we can simulate the gray matter atrophy with more than one area, it may improve the results of the PBM method and also the simulation will be more close to the MDD or BD patient in reality.

5.4 Why the Smoothing is Eliminated

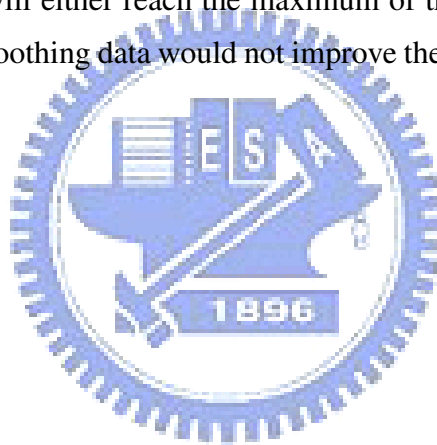
In the parcellation-based morphometry (PBM) analysis, the smoothing step which is used in the preprocessing of the VBM method is eliminated from the preprocessing of our method for characterizing group differences. The reason is that it is redundant and needless to our proposed method. However, there are several advantages in smoothing data for VBM analysis, but in other point of view, the advantage is also associated with some drawbacks especially to our PBM analysis.

Several advantages of smoothing data for VBM analysis are not taken by our method, but these are still good for VBM analysis. The advantages of smoothing are listed below:

1. The effect of rendering the data set more normally distributed
2. The consideration of neighbor voxels
3. The elimination of errors within spatial normalization

First of all, the effect of rendering the data set more normally distributed is that to increase the validity of voxel-by-voxel parametric statistical test. By central limit theorem, the sum of many independent random variables (voxels), will be approximately normally distributed and it guarantees the validity of the test even if the populations are nonnormal. Secondly, owing to the voxel-wise analysis, VBM analysis considers only one voxel at a time without any other nearby voxels. The smoothness can let each voxel containing other voxel information around them. Last advantage is to eliminate errors within spatial normalization. Which means, the registration errors may influence the statistics test in voxel-wise analysis. By the use of the smoothness can eliminate the variation produce by registration error and also increase the correctness of the VBM result. However, in our method, we have already considered each voxel within a region during analysis. That is, the region information of each voxel is taken into consideration simultaneously. Therefore, we eliminate the smoothness during the multivariate analysis. It is necessary for voxel-wise analysis instead of an multivariate method.

In another point of view, the advantage we mentioned above tends to be drawbacks during the analysis. First of all, the consideration of neighbor voxels may be bad when voxels are near the borders of GM WM and CSF. We may sum up the wrong voxel information with each other, which are not in the same tissue, that is smoothing can always sum all information to be together without checking them and it reduces the correctness of the VBM result. The other is the subtle difference may be weakened during smoothing the data. The small variance of brain structures may not be detected with smoothed data. In the last, it is hard for every of us to decide the smoothing kernel size. It is always a problem with the size of the kernel. However, it is recommended that the size of the smoothing kernel should be comparable to the size of the expected regional differences between the groups. In our previous work [16], we have proved that the result of using the smoothed data or non-smoothed data will either reach the maximum of the Fisher's criterion, which means that the use of the smoothing data would not improve the discrimination of the discriminant map.





Chapter 6

Conclusions



In this study, we proposed a reformatory method which is a parcellation-based multivariate method for characterizing brain discrepancy of different populations. The procedures of parcellation-based multivariate morphometry are similar to one of the most popular morphometry method which is called voxel-based morphometry (VBM), it includes image preprocessing and parcellation-based multivariate analysis. In image preprocessing, several tools are used to maximize the performance of each step. The main idea of the proposed method is parcellation-based analysis, that is, we divide brain into several pieces before the multivariate analysis. we adopted the discriminative common vector method to detect the most discriminant hyper-plane which represents the discrimination of each region or voxel. Finally, we combine each region back into the original brain to identify group discrepancy in an unbiased way. According to our experiment, we have demonstrated that the performance of the parcellation-based multivariate method is better than VBM. The multivariate result is shown that it detects more subtle and widely distributed pattern of brain structures which are often not detectable by VBM.

There are several important characters of parcellation-based multivariate method. First of all, the most important point is, all voxels in same region are simultaneously taken into consideration with multivariate analysis by using parcellation-based approach rather than using all features in brain. Obviously, features may be redundant especially for those region which is not important in group difference. Moreover, with an imperfect registration may cause some regions failed to spatial normalize to a template, these regions may also reduce the ability of characterizing group differences. Another important character is that feature reduction is omitted owing to the discriminative common vector method which can deal with plenty of features simultaneously. Therefore, the information of each voxel may not loss with feature reduction, every voxel will be in analysis instead. That enables the proposed method superior to other multivariate analysis which uses feature reduction within analysis. At last, the smoothness is not included in the preprocessing of the proposed method since the smoothness may mix up or reduce the information of each voxel. It has been proved that the maximums of Fisher's criterion is equivalent with smoothing or not.

These are still some defects within the proposed method. In VBM analysis, that the ef-

fect of spatial normalization is different between each subject. Therefore, the global mean voxel value is included as a confounding covariate in an analysis of covariance (ANCOVA). Different from VBM analysis, the proposed method take no consideration with this effect. Another defect is about the discriminant map. The resulting discriminant map of VBM analysis provides a t -test map, which means the value of each voxel represent a significant level by a t statistic value. The discriminative map of our proposed method is a discrimination weight which is lack of statistic result. Although, we still provide a result with two-sample t test which is calculated by projecting all subjects onto the most projection vector we have found, then all the subjects will be indicated by a value for two sample t test. However, our proposed method has shown that the parcellation-based multivariate morphometry analysis has a good performance on subtle and widely-distributed structural difference and it is more flexible within analysis.





Bibliography

- [1] Korbinian Brodmann. *Vergleichende Lokalisationslehre der Grosshirnrinde in ihren Prinzipien dargestellt auf Grund des Zellenbaues*. Johann Ambrosius Barth Verlag, Leipzig, 1909.
- [2] J. L. Lancaster, M. G. Woldorff, L. M. Parsons, M. Liotti, C. S. Freitas, L. Rainey, P. V. Kochunov, D. Nickerson, S. A. Mikiten, and P. T. Fox. Automated talairach atlas labels for functional brain mapping. *Hum Brain Mapp*, 10(3):120–31, 2000.
- [3] J. Talairach and P. Tournoux. *Co-planar stereotaxic atlas of the human brain*. Thieme Medical Publishers, New York, 1988.
- [4] P. C. Lauterbur. Image-formation by induced local interactions - examples employing nuclear magnetic-resonance. *Clinical Orthopaedics and Related Research*, (244):3–6, 1989.
- [5] C. Davatzikos, A. Genc, D. R. Xu, and S. M. Resnick. Voxel-based morphometry using the ravens maps: Methods and validation using simulated longitudinal atrophy. *Neuroimage*, 14(6):1361–1369, 2001.
- [6] C. Davatzikos. Measuring biological shape using geometry-based shape transformations. *Image and Vision Computing*, 19(1-2):63–74, 2001.
- [7] M. Chen, T. Kanade, D. Pomerleau, and J. Schneider. 3d deformable registration of medical images using a statistical atlas. *Medical Image Computing and Computer-Assisted Intervention, Miccai'99, Proceedings*, 1679:621–630, 1999.

- [8] P. A. Freeborough and N. C. Fox. Modeling brain deformations in alzheimer disease by fluid registration of serial 3d mr images. *Journal of Computer Assisted Tomography*, 22(5):838–843, 1998.
- [9] P. M. Thompson, D. MacDonald, M. S. Mega, C. J. Holmes, A. C. Evans, and A. W. Toga. Detection and mapping of abnormal brain structure with a probabilistic atlas of cortical surfaces. *Journal of Computer Assisted Tomography*, 21(4):567–581, 1997.
- [10] C. D. Good, I. S. Johnsrude, J. Ashburner, R. N. A. Henson, K. J. Friston, and R. S. J. Frackowiak. A voxel-based morphometric study of ageing in 465 normal adult human brains. *Neuroimage*, 14(1):21–36, 2001.
- [11] J. Ashburner and K. J. Friston. Voxel-based morphometry - the methods. *Neuroimage*, 11(6):805–821, 2000.
- [12] C. Davatzikos. Why voxel-based morphometric analysis should be used with great caution when characterizing group differences. *Neuroimage*, 23(1):17–20, 2004.
- [13] D. J. Pettey and J. C. Gee. Sexual dimorphism in the corpus callosum: A characterization of local size variations and a classification driven approach to morphometry. *Neuroimage*, 17(3):1504–1511, 2002.
- [14] Z. Q. Lao, D. G. Shen, Z. Xue, B. Karacali, S. M. Resnick, and C. Davatzikos. Morphological classification of brains via high-dimensional shape transformations and machine learning methods. *Neuroimage*, 21(1):46–57, 2004.
- [15] C. E. Thomaz, F. L. S. Duran, G. F. Busatto, D. F. Gillies, and D. Rueckert. Multivariate statistical differences of mri samples of the human brain. *Journal of Mathematical Imaging and Vision*, 29(2-3):95–106, 2007.
- [16] Cheng-Chia Yang. *Multivariate Volumetric Morphometry for Characterizing Anatomical Discrepancy in MR Images of Different Groups*. Master thesis, 2006.
- [17] A. M. McIntosh, D. E. Job, T. W. J. Moorhead, L. K. Harrison, K. Forrester, S. M. Lawrie, and E. C. Johnstone. Voxel-based morphometry of patients with

- schizophrenia or bipolar disorder and their unaffected relatives. *Biological Psychiatry*, 56(8):544–552, 2004.
- [18] A. Anand and Y. Li. Voxel-based morphometry (vbm) analysis in major depression and bipolar disorder. *Biological Psychiatry*, 57(8):188s–188s, 2005.
- [19] E. S. Monkul, M. A. Nicoletti, K. Matsuo, F. G. Nery, M. Sanches, M. A. M. Peluso, P. Najt, and J. C. Soares. Suicide and brain regions underlying decision-making and uncertainty: A voxel based morphometry study of female patients with major depression. *Biological Psychiatry*, 61(8):96s–96s, 2007.
- [20] F. L. Bookstein. "voxel-based morphometry" should not be used with imperfectly registered images. *Neuroimage*, 14(6):1454–1462, 2001.
- [21] John G. Sled., Alex P. Zijdenbos., and Alan C. Evans. A nonparametric method for automatic correction of intensity nonuniformity in mri data. *IEEE TRANSACTIONS ON MEDICAL IMAGING*, 17, 1998.
- [22] A. Bischoff-Grethe, I. B. Ozyurt, E. Busa, B. T. Quinn, C. Fennema-Notestine, C. P. Clark, S. Morris, M. W. Bondi, T. L. Jernigan, A. M. Dale, G. G. Brown, and B. Fischl. A technique for the deidentification of structural brain mr images. *Human Brain Mapping*, 28(9):892–903, 2007.
- [23] Y. Y. Zhang, M. Brady, and S. Smith. A hidden markov random field model for segmentation of brain mr images. *Medical Imaging 2000: Image Processing, Pts 1 and 2*, 1(24):1126–1137 1642, 2000.
- [24] Y. Y. Zhang, M. Brady, and S. Smith. Segmentation of brain mr images through a hidden markov random field model and the expectation-maximization algorithm. *Ieee Transactions on Medical Imaging*, 20(1):45–57, 2001.
- [25] Jia-Xiu Liu., Yong-Sheng Chen., and Li-Fen Chen. Affine and nonlinear spatial normalization techniques using derivatives of brain magnetic resonance images. *14th Annual Meeting of the Organization for Human Brain Mapping*, pages 15–19, 2008.

- [26] N. Tzourio-Mazoyer, B. Landeau, D. Papathanassiou, F. Crivello, O. Etard, N. Delcroix, B. Mazoyer, and M. Joliot. Automated anatomical labeling of activations in spm using a macroscopic anatomical parcellation of the mni mri single-subject brain. *Neuroimage*, 15(1):273–289, 2002.
- [27] H. Cevikalp, M. Neamtu, M. Wilkes, and A. Barkana. Discriminative common vectors for face recognition. *Ieee Transactions on Pattern Analysis and Machine Intelligence*, 27(1):4–13, 2005.
- [28] L. F. Chen, H. Y. M. Liao, M. T. Ko, J. C. Lin, and G. J. Yu. A new lda-based face recognition system which can solve the small sample size problem. *Pattern Recognition*, 33(10):1713–1726, 2000.
- [29] KE LIU, YONG-QING CHENG, JING-YU YANG, and XIAO LIU. An efficient algorithm for foley-sammon optimal set of discriminant vectors by algebraic method. *International journal of pattern recognition and artificial intelligence*, 6:5, 1992.
- [30] B. Karacali and C. Davatzikos. Simulation of tissue atrophy using a topology preserving transformation model. *Ieee Transactions on Medical Imaging*, 25(5):649–652, 2006.
- [31] T. Fawcett. An introduction to roc analysis. *Pattern Recognition Letters*, 27(8):861–874, 2006.
- [32] T. J. Lai, M. E. Payne, C. E. Byrum, D. C. Steffens, and K. R. R. Krishnan. Reduction of orbital frontal cortex volume in geriatric depression. *Biological Psychiatry*, 48(10):971–975, 2000.
- [33] C. H. Chen, J. Suckling, C. Ooi, C. H. Fu, S. C. R. Williams, N. D. Walsh, M. T. Mitterschiffthaler, E. M. Pich, and E. Bullmore. Functional coupling of the amygdala in depressed patients treated with antidepressant medication. *Neuropsychopharmacology*, 33(8):1909–1918, 2008.
- [34] R. A. Lochhead, R. V. Parsey, M. A. Oquendo, and J. J. Mann. Regional brain gray

matter volume differences in patients with bipolar disorder as assessed by optimized voxel-based morphometry. *Biological Psychiatry*, 55(12):1154–1162, 2004.

